TÉCNICO LISBOA

Prediction of pharmaceutical blends flowability using a Schulze Ring Shear Cell tester

Maria Madalena Garcia Caldas de Magalhães Guedes

Thesis to obtain the Master of Science Degree in

Chemical Engineering

Supervisors: Doutora Slavomira Doktorovová da Silva
Prof. Doutor António José Boavida Correia Diogo

Examination Committee

Chairperson: Prof. Doutora Maria Cristina de Carvalho Silva Fernandes
Supervisor: Doutora Slavomira Doktorovová da Silva
Member of the Committee: Prof. Doutor Paulo José Pinto Salústio

March 2022

Declaration

I declare that this document is an original work of my own authorship and that it fulfills all the requirements of the Code of Conduct and Good Practices of the Universidade de Lisboa.

Declaração

Declaro que o presente documento é um trabalho original da minha autoria e que cumpre todos os requisitos do Código de Conduta e Boas Práticas da Universidade de Lisboa.

Acknowledgments

I would like to thank my parents and my brother for their unconditional support and for caring for me when I needed it. Thank you for inspiring me and for the wise words all of you kindly had to offer in the most difficult times. A big thank you also to my family, my cousins especially, for the kind words of encouragement.

A heartfelt thank you to Guilherme Portela, for having been there for me in these past 10 months and for giving me your unconditional love always. Thank you for being there for me when I needed and when I didn't even know I needed.

Thank you to all my friends who accompanied me through this journey and gave me kind words of encouragement, keeping me motivated. Francisca Gusmão, Leonor Ferreira, Rui Gil, Mariana Falcão, Miguel Grincho, João Chicau, Madalena Rocha, Miguel Rocha, Jorge Rocha, Rafael Correia, Maria Cunha, Miguel Ribeiro, Francisca Loureiro, João Costa, Marina Araújo, Miguel Carvalho, Father Bernardo Trocado, Margarida Milhazes, Margarida Ribeiro, Inês Rosa and Marta Saraiva. A special thank you to Rita Correia and Beatriz Soares, for the work sessions and for being there for me during the times when I felt little motivation.

Thank you to all the amazing people I met during this project and who I can now proudly call my co-workers: Cíntia Veiga, Patrícia Nunes, Rute Mota, Susana Farinha, Carolina Lopes, Artur Saramago and others. Thank you for lending me a hand everytime I needed and for showing me the meaning of true companionship. A special thank you to Joana Veríssimo, Beatriz Dias and Sofia Clemente who were my co-workers only temporarily, but who left a big impact on me and were examples of hard work and determination.

A big thank you to Instituto Superior Técnico, to Hovione and to my mentors, Professor António Correia Diogo, Slavomira Doctorovová and Maria Paisana, for your guidance, for always trying to make the best out of this project and for making me be in my best intellectual shape.

Finally, I would like to thank Dr. Dietmar Schulze and Dr. Greg Mehos for their help and availability. Thank you for kindly answering our questions.

Abstract

To properly design equipment that handles bulk solids, it's considerably important to be familiar with their fundamental properties. This thesis has the objective of gaining knowledge on the tests performed with the Schulze ring shear tester RST-XS.s and the results obtained.

In the first part of this work, five pharmaceutical powders (flow function coefficient from 2.2 to 19.5 at pre-consolidation stress of 1kPa) are analyzed by the RST-XS.s using two shear cells (XS-Mr, XS-SV3) and two wall friction cells (XS-MW, XS-WL0). The purpose is to select which cells most accurately predict how these materials flow through different hoppers. The data obtained was treated mathematically according to Mehos [1] and validated by discharging the powders through hoppers with varying wall angles (15° to 45°). Results showed that the most adequate cells to characterize pharmaceutical powders are XS-Mr and XS-WL0.

In the second part, ten more powders with different pharmaceutical functions are analyzed to better understand the output from the RST-XS.s. Results showed that flowability must not be evaluated solely by the FFC ratio and should consider other parameters such as particle shape and size distribution.

Finally, in the third part of this study, five pharmaceutical blends varying in active concentration (0 - 60 %(w/w)) were manufactured. After characterizing the blends, tablets were produced at different tableting conditions (varying feeder and turret speed) and a weight variation test was performed. Results showed small relative standard deviations, suggesting that these formulations are adequate for tableting with the Active Principal Ingredient used.

Keywords

Ring Shear Tester, Flowability, Shear Cell, Wall Friction Cell, Yield Locus, Tableting.

Resumo

As propriedades fundamentais dos sólidos granulares são cruciais quando se dimensiona equipamentos destinados ao seu processamento. Este trabalho tem como objetivo a familiarização com o *Schulze Ring shear tester* (RST-XS.s) e os seus resultados.

Em primeiro lugar, analisaram-se cinco pós farmacêuticos (*flow function coefficient* entre 2.2 e 19.5 a tensões normais de pre-consolidação de 1kPa) com o RST-XS.s, usando células de tensão de corte (XS-Mr, XS-SV3) e de atrito na parede (XS-MW, XS-WL0), de forma a selecionar células mais adequadas à previsão da escoabilidade destes materiais em tremonhas. Trataram-se os dados experimentais matematicamente [1] e validaram-se, descarregando os pós por funis com variados ângulos verticais de parede (15° - 45°). As células mais adequadas são a XS-Mr e a XS-WL0.

Na segunda parte deste trabalho, foram analisados dez pós com diferentes funções farmacêuticas, para melhor compreensão dos resultados obtidos com o RST-XS.s. Estes foram tratados matematicamente como na primeira parte. Concluiu-se que a escoabilidade não deve ser avaliada somente pelo rácio FFC, mas também por outros parâmetros (distribuição de tamanhos de partícula, forma, etc.).

Por fim, fabricaram-se 5 misturas farmacêuticas variando o conteúdo de ativo (0 - 60 %(m/m)), caracterizaram-se com o RST-XS.s e, posteriormente, produziram-se comprimidos com diferentes velocidades de rotação do alimentador e mesa. Realizou-se um teste de variação de massa, com intuito de investigar a influência do escoamento na variação de massa dos comprimidos. No entanto, os desvios-padrão relativos obtidos foram insignificantes, o que sugere que estas formulações são adequadas para compressão direta com o ativo usado.

Palavras-Chave

Ring Shear Tester, Escoamento, Célula de Tensão de Corte, Célula de Atrito na Parede, Limite de Cedência, Tableting.

Contents

List of Figures

List of Tables

Acronyms

API	Active Pharmaceutical Ingredients
ASD	Amorphous Solid Dispersions
BCS	Biopharmaceutical Classification System
ff	Flow Factor
FFC	Flow Function Coefficient
HPMC	Hydroxypropyl Methylcellulose
PC	Principal Component
PCA	Principal Component Analysis
PLS	Partial Least Squares
PSD	Particle Size Distribution
PVP	Polyvinylpyrrolidone
RSD	Relative Standard Deviation
SEM	Scanning Electron Microscopy

List of symbols

Roman symbols

A_0 – Cross-sectional area of the die

B_{min} – Minimum outlet diameter required for mass flow

B – Diameter of the punch outlet

d – Hopper outlet diameter

D_F – Critical rathole diameter

F_1 – Horizontal force measured by the ring shear tester

F_2 – Horizontal force measured by the ring shear tester

f_f – Flow factor

FFC – Flow function coefficient

FF_ρ - Flow function coefficient taking the bulk density into account

F_N – Normal force applied by the ring shear tester

g – Gravitational acceleration

h – Height of the powder in the cylindrical zone of the silo

k – Janssen coefficient

L_f – Length of the feeder exposed to the turret

M_M – Torque

$\dot{m}_s$ – Mass discharge rate

$Q2$ – Predicted variance

r – Turret speed

$R2X$ – Explained Variance

R_4 – Pitch circle radius

R_H – Hydraulic radius of the cylindrical part of a silo

RSD – Relative Standard Deviation

S – Standard deviation

t_{250} – Time necessary to discharge 250mg of blend powder into a die

T_{fill} – Die filling time

$\bar{x}$ – Mean weight

x_{10} – Corresponding particle size when the cumulative percentage reaches 10%

x_{50} – Median particle size

x_{90} – Corresponding particle size when the cumulative percentage reaches 90%

Greek symbols

φ_E – Effective angle of internal friction

φ_{lin} – Slope angle of the linearized yield locus

φ_{SF} – Angle of internal friction at steady-state flow

φ_X – Angle of wall friction

ω – Cell rotating speed

ρ_b – Bulk density

ρ_{b0} – Bulk density at the outlet of the punch

ρ_{bmin} – Bulk density immediately before compaction

ρ_w – Water density (liquid, 0ºC and 1bar)

σ – Vertical normal stress

σ_1 – Major principal stress

σ_2 – Minor principal stress

σ_c – Unconfined yield strength

σ_{crit} – Critical vertical normal stress

σ_{pre} – Vertical normal stress at pre-shear

σ_{sh} – Vertical normal stress at shear

σ_t – Tensile strength

σ_v – Vertical stress

σ_{wi} – Vertical Normal stress at the wall at steady state i.

τ – Shear stress

τ_c – Cohesion

τ_w – Shear stress at the wall

θ' – Vertical wall angle

1

Introduction

Contents

1.1 State of the art

Bulk solids are processed in many industries and the pharmaceutical industry is no exception. In this industry, bulk solids are used on a considerable variety of processes, where ideally they flow due to the intervention of gravity. [1] [2] For this type of natural flow to happen without the aid of external intervention it's necessary to know well the materials used and their properties, so that a high quality design can be accomplished for the equipment that processes these materials.

Designing equipment becomes more complex when dealing with bulk solids than when working with liquids or gases, for which necessary information is readily available everywhere. In fact, for bulk solids, even the simplest properties, such as bulk density for example, strongly depend on the shape and size of the particles and their porosity, thus any data published relative to these properties may not be representative of the material being handled and studied. Even more so, since bulk solids' properties are susceptible to alterations when they are compressed. [2] [3] [4]

A very common example of poor design of equipment is the design of storage silos for bulk solids. This design used to be done by a trial and error method in the past and nowadays it's still done in many factories considering only the lowest cost possible or the ease of manufacture instead of the rheology and behaviour of the material to be processed. This type of design in the pharmaceutical industry may be justified by the fact that the most relevant range of shear stresses in this industry are low shear stresses, which couldn't be measured by the first shear stress testers developed. [5] [6] [7]

As a result of poorly designed silos, many unwanted scenarios can happen (see Figure 1.1), which can be the cause of big financial losses for the company. For example, if the opening of the hopper is too narrow, the particles can interlock and form stable arches right above the opening (a), completely obstructing the flux of matter. Funnel flow (b and c) can also happen if the walls of the hopper have an inappropriate slope or if they are too rough, leading to stagnant zones inside the silo and limiting the flux of matter to the zone right above the opening of the hopper. This can be the source of phenomena like segregation (d), where smaller particles remain close to the axis of the silo while larger particles migrate to its periphery; degradation if the product remains inside the silo for a long period of time; large distributions of residence times inside the silo and even irregular flow of matter, which is undesirable from a final product quality perspective. [1] [8] [9] [10]

In this industry, several other processes get affected by the flowability of bulk solids, such as the way a powder flows into a die in less than a second during compression during pharmaceutical tablets manufacture or the feeding capacity of screw feeders or hot melt extruders, which is a function of the density of the bulk solid and its flowability inside the equipment. [2] [11]

It is then easy to understand the importance of choosing the right properties to assess the flowability of a bulk solid and those to use in the design of equipment.

Many tests have been developed along the years to assess the flowability of bulk solids. [8] For

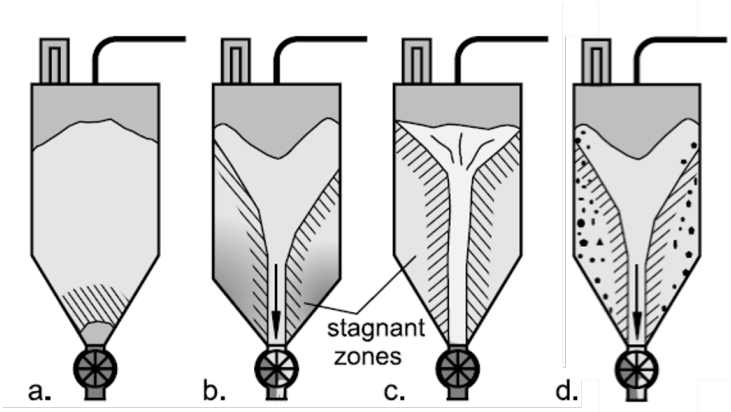

Figure 1.1: Typical problems of a poorly dimensioned silo. a) Formation of a stable bridge; b) formation of stagnant zones; c) funnel flow; d) segregation. Adapted from [8].

example, the angle of repose (see Figure 1.2) test consists in pouring powder through a funnel placed above a plaque, forming a pile of loose powder, and measuring the slope of this pile. This plaque may have a lateral elevation to create a layer of powder and eliminate any possible interference that the plaque could have in the results. This angle can also be determined by measuring the angle of the pile of powder that remains in a container with a small opening on the bottom or by measuring a dynamic angle which is measured in a rotating cylinder. This last method is the least reliable one for materials with worse flowability. For instance, cohesive materials wouldn't flow continuously but in small avalanches. [12]

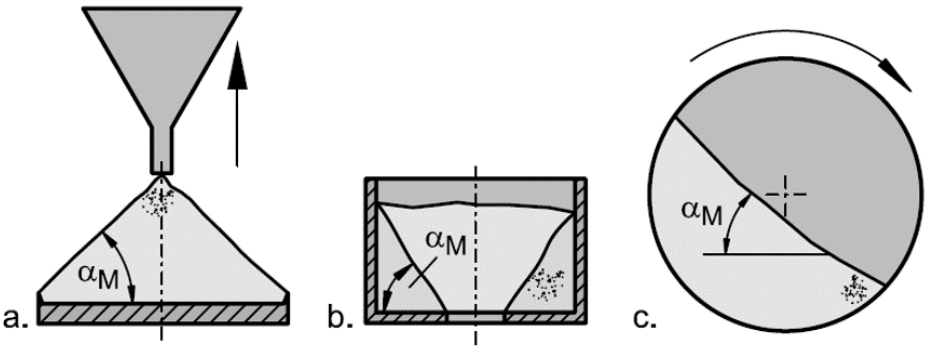

Figure 1.2: Angle of Repose test. Adapted from [8].

Carr's index and Hausner's ratio are indicators for the compressibility of a powder and are based on the influence of adhesive inter-particle interactions on the bulk density, ρ_{b0}, and relate this density with the density of the powder after compaction, ρ_T. Carr's index is given by equation 1.1 and Hausner's ratio is given by equation 1.2. [8] [13] [14]

$$CI = 100\% \cdot \frac{\rho_T - \rho_{b0}}{\rho_T} \tag{1.1}$$

$$HR = \frac{\rho_T}{\rho_{b0}} \tag{1.2}$$

A Carr's index of 0 or a Hausner's ratio of 1 indicate that the bulk solid under study is uncompressible, which corresponds to an excellent flowability. The bigger these values, the worse the powder flows.

Other examples of empirical tests that are done are the measurement of the time of discharge of a bulk solid through a hopper with a small opening or the determination of the minimum size of the opening of the hopper through which there is flow of matter. For the first test, the smaller the discharge time, the better the flowability. For the second test, the minimum diameter of the opening of the hopper becomes an indicator for the flowability. [8] [15]

Indeed, none of these techniques can be used to predict what will happen in practical applications, since they don't simulate the necessary conditions. They may only be used to draw a comparison between samples, ordering them according to their flowability. In this sense, the most useful tests are those that allow the measurement of the fundamental properties of bulk solids while under a consolidation stress that simulates the existing stresses throughout the processing of the material, being these fundamental properties the cohesion, internal friction, compressibility, wall friction and the permeability of the bulk solid. [1] [8]

Some of the greatest contributions to the field of bulk solids were made by two scientists named H. A. Janssen and Andrew W. Jenike.

Janssen was an engineer who lived in Germany at the end of the XIX century who brought to light the notion that unlike what happens with fluids, stress does not increase linearly at the bottom of a silo loaded with bulk solids. Instead, he proposed that stress becomes constant after a certain filling height. [8] [16] [17]

To investigate this property of bulk solids, Janssen used silos with a square cross section made of wood positioned above a balance and with different filling heights inside the silos. By measuring the force acting on the balance and consequently the normal stress, he was able to confirm that the normal stress in fact does not increase linearly with silo depth. Janssen was even able to conclude that this behaviour resulted from the friction between the bulk solid and the silo wall. For this he designed a test that measures the friction coefficient between the wall and the bulk solid and even derived the Janssen equation in 1985, which is used to calculate the stresses in the vertical section of a silo and is still a part of the design codes for silos nowadays in some countries. [8] [16] [17]

Andrew Jenike was an engineer from Poland who spent part of his life in Canada and in the United States of America. His major contribution to the field of bulk solids was the concept of yield locus, which is still used today to determine some of the fundamental properties mentioned above. With this new concept, it was possible to apply the results obtained to practical situations, for example to the design of

hoppers, to make tests more reproducible and to eliminate the influence of external factors such as the aeration state of the sample. [9] [18] [19]

On top of this, Jenike built a theory that describes the existing stresses in silos and specially in the hopper zone, defining the concepts of mass and funnel flow, which became the most important concepts to assess flow in a silo; he developed an algorithm to adequately design silos taking into account the hopper angle and its opening, which is still the main method used today and, to determine the fundamental properties of this type of materials and he developed an equipment named Jenike Shear Tester. [1] [8] [9] [18] [19] Today's equipment for shear testing is based on Jenike's shear tester (see Figure 1.3(a)) and allows the measurement of powders' fundamental properties while the material is under a consolidation stress that simulates the stresses existing in practical applications, unlike the other techniques described above.

1.1.1 Testers

Some other testers used throughout the history worth mentioning are the Warren Spring-Bradford cohesion tester (see Figure 1.3(b)), used to determine a value of cohesion of a powder that can be qualitatively compared to the values obtained for other powders [8] [20] [21] [22]; the uniaxial compression test (see Figure 1.3(c)) in which the powder is pre-consolidated in a confined space and afterwards is compressed again, while being unconfined, until the point of incipient flow (the same as failure for a normal solid) [8] [23]; the monoaxial shear tester (see Figure 1.3(d)), which is similar to the uniaxial compression tester, but after consolidating, a force is applied in the horizontal direction until the point of incipient flow [8] [24]; the torsional shear tester (see Figure 1.3(e), in which the sample is contained in a cylindrical cell and a vertical force is applied to the sample through a round lid with a roughened surface that rotates at a constant speed, allowing the measurement of the torque (M_M). [8] [24] The equipment that will be used throughout this work, the ring shear tester (see Figure 1.5), is a rotational tester, just like the torsional tester.

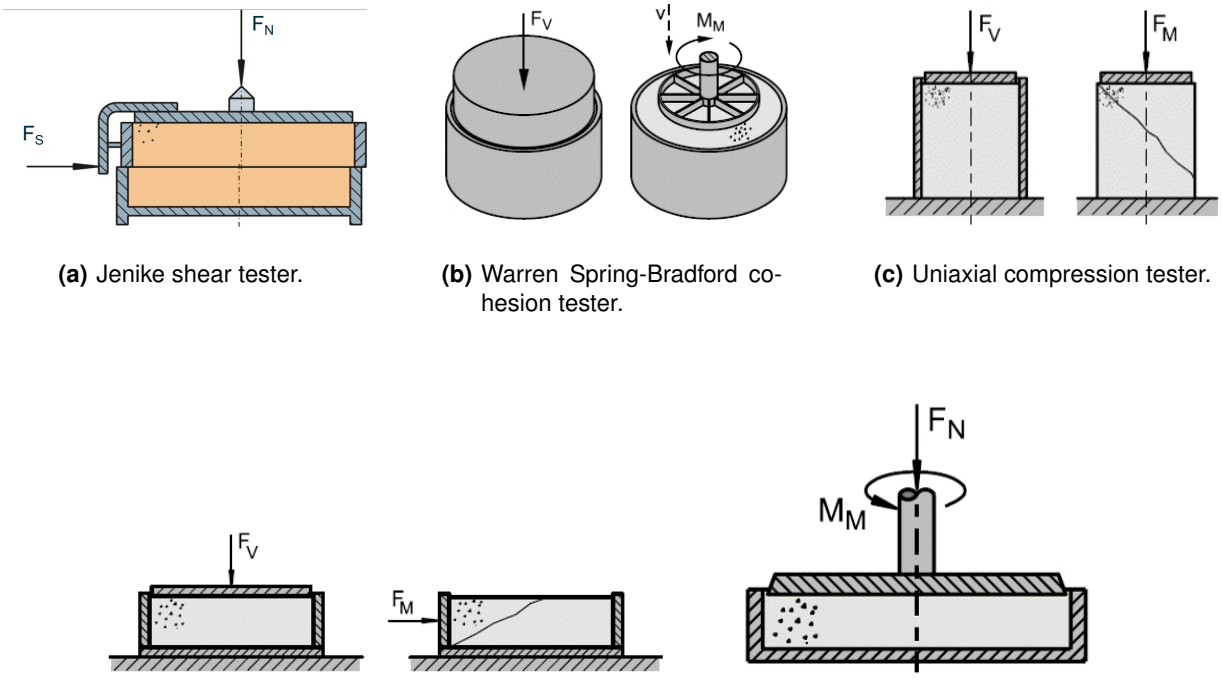

(a) Jenike shear tester.

(b) Warren Spring-Bradford cohesion tester.

(c) Uniaxial compression tester.

(d) Monoaxial compression tester.

(e) Torsional shear tester.

Figure 1.3: Schematic representation of testers used to assess bulk solids' properties. Pictures adapted from [8].

1.2 Motivation

It was mentioned before that the lack of knowledge of powder rheological and physical properties often leads to poor equipment design and equipment malfunction. There are two ways to approach these problems: either re-designing the equipment, which is very expensive, or optimizing the formulations used, so that they are adequate for the equipment used. This second option is the most common and cost-effective. [5] [6] [7]

Shear cell testers have been widely used in the pharmaceutical industry to characterize pharmaceutical powders and guide the development and optimization of formulations.

Throughout this work, a deeper understanding of *Schulze*'s ring shear cell tester *RST-XS.s* will be attained by analyzing different powders belonging to different pharmaceutical functional groups. Different pharmaceutical blends will be manufactured and tested with RSE-XS.s. In order to better understand the relationship between the rheological parameters obtained in shear testing and tablet weight variation, a set of tablets will be produced with these blends and weight variation will be assessed. A mathematical treatment model based on the literature will be be developed to predict whether pharmaceutical powders flow easily or not during their processing stages.

1.3 Literature Review

1.3.1 Ring Shear Tester - Schulze's RST-XS.s

A shear test is performed by subjecting the bulk solid to a vertical normal stress, σ, and then shifting the upper surface of the bulk relative to the lower surface in a direction perpendicular to the normal stress applied. The tester measures the shear stress, τ, created in the bulk due to the deformation. (see Figure 1.4 [8]) [25] Translational shear testers such as the Jenike shear tester, the uniaxial shear tester or the monoaxial shear tester have many limitations, but the most relevant is that the maximum displacement achieved by this testers is of about 6mm, while torsional shear testers have no limitation in this aspect. [26]

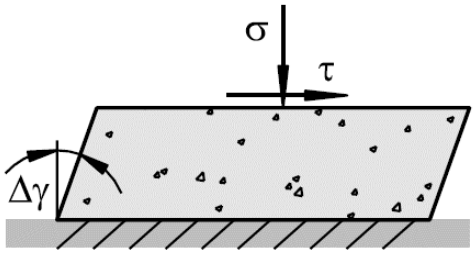

Figure 1.4: Principle of a shear tester.

In a rotational shear tester, the deformation is done by rotating the top of the bulk relatively to the bottom and the shear is measured indirectly by measuring the torque, M_M. In the torsional shear tester, a normal stress is applied to the bulk sample through the round and rough lid and then the powder is sheared by rotation of the lid relative to the cell holding the sample. A limitation of this type of tester is that shear strain at a point depends on the distance to the axis, being zero close to the axis of the cell and increasing linearly with the radius. [8]

In order to lower the influence of the deformation variation, the ring shear cell tester was developed (see Figure 1.5). In this tester, since the cell has an anular shape, the sample deformation is more homogeneous, and investigations have shown that a ratio of inner diameter to outer diameter above 50% allows this variation to be neglected. [8] [27] [28]

The first prototype of a ring shear tester was developed in 1937 for testing of soils by Hvorslev [29], followed by Walker's model, in the 1960's, and some models developed for research purposes in universities. The first model of Schulze's ring shear cell tester was developed in 1992, the RST-01.pc. [8] [24] [30] This first model of Schulze's used samples of 200mL (type S) or 900mL (type M) [31].

In 2012 Schulze developed a smaller model of this tester, the RST-XS.s, which used sample volumes of an order of magnitude lower (3mL to 70mL, depending on the cell used [32]) and this is the model that will be used throughout this investigation.

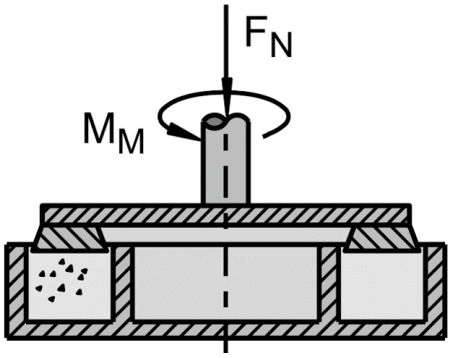

Figure 1.5: Schematic representation of a Ring Shear Tester. Figure adapted from [8].

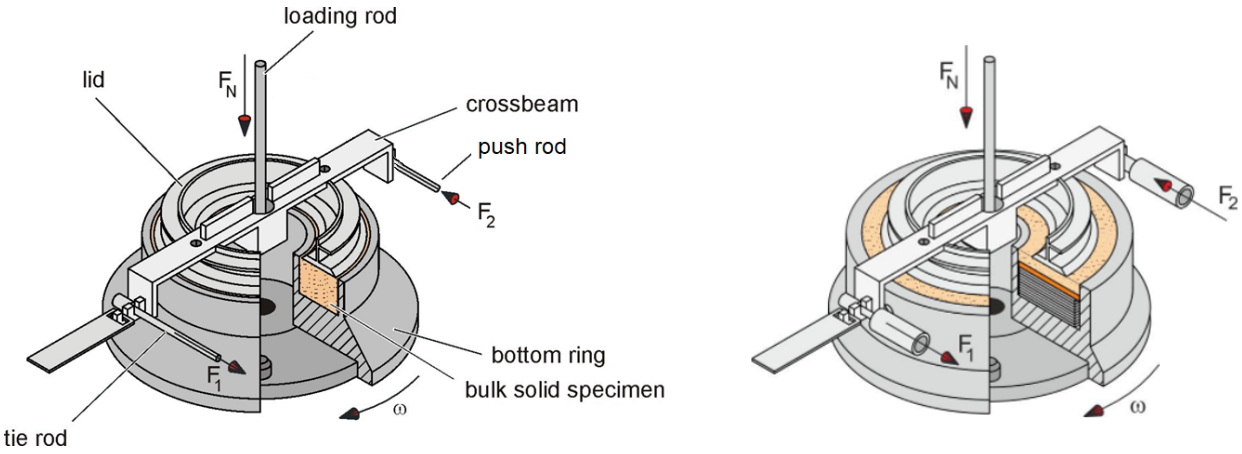

(a) RST-XS.s with a shear cell.

(b) RST-XS.s with a wall friction cell.

Figure 1.6: Schematic representation of a Schulze Ring Shear Tester. Figure adapted from [33].

The most relevant parts of this equipment are a cell, where the powder sample is inserted with due care, a lid that generally has a rough surface to avoid slipping of the powder sample in the powder-lid interface and vertical loading rod that fits in the central axis of the lid, through which a vertical stress, F_N, is applied to the sample. This vertical stress consolidates the bulk solid sample while the basis of the powder cell rotates with a certain rotating speed, ω, causing the bulk displacement associated with shear. The lid is connected to the tie and push rods, which are connected to load sensors, measuring the forces F_1 and F_2 necessary to counteract the lid rotation. These forces F_1 and F_2 are directly proportional to the shear stress, τ. [8] [34] [35]

The geometry of the cell and lid varies according to the type of test to be performed.

1.3.2 Types of cells

There are three types of cells: compressibility cells, shear cells and wall friction cells. [32]

There is only one model of compressibility cells available for the RST-XS.s, called XS-VM. This cell is used to perform compressibility tests where the bulk density is determined in function of stress minimizing the influence from the wall friction as much as possible.

The shear cells are used to perform shear tests, obtaining Yield Locus parameters, as well information on bulk density. There are six cells available for this type of test adequate for RST-XS.s: XS-Sr, XS-Mr, XS-Lr, XS-MV4, XS-SV3 and XS-Lr0 (low stress shear cell). Throughout this study cells XS-Mr and XS-SV3 will be used and compared.

Cell XS-Mr (Figure 2.2(a)) is considered a standard cell and is the cell that is delivered with the equipment. Cell XS-SV3 (Figure 2.2(b)) holds a smaller sample volume and can be used when limited amounts of powder are available.

To perform wall friction tests there are two cells available for the RST-XS.s: cells XS-WM and XS-WL0. Both of these cells will be used and compared in this investigation.

Cell XS-WM (Figure 2.2(c)) is the standard wall friction cell. Cell XS-WL0 (Figure 2.2(d)) is a low stress wall friction cell, where the lid (Figure 2.2(e)) is attached to the loading rod to not take into account its weight in the measurements. In these cells a series of filler rings are used as well as a coupon ring that samples the surface of the equipment where the powder tested is to be processed.

1.3.3 Fundamental concepts

Even though the RST-XS.s is capable of performing three types of tests (compressibility, shear and wall friction tests), only two types of tests will be carried out throughout this investigation: shear tests (also known as Yield Locus tests) and wall friction tests (also known as Wall Yield Locus tests). These tests can also be performed to assess the evolution of powder consolidation with time (Time Yield Locus tests and Time Wall Yield Locus tests), but these two were not performed during this investigation. More information on these tests can be found on [8].

1.3.3.A Shear tests

The following information was processed from [1], [8], [26] and [36].

In a Yield Locus test, the equipment applies a normal force F_N via the loading rod on the crossbeam of the lid, which is transmitted to the powder, consolidating it. The bottom of the cell then rotates clockwise with a rotating speed of ω, generating a shear stress within the bulk powder. The bottom of the cell rotates until the shear stress value is constant, i.e. a steady state has been achieved. This is called the pre-consolidation state, where it is possible to obtain a pair of values of normal (σ) and shear (τ) stress,

called the pre-shear point, where the normal stress is the one applied and the shear stress is the one at steady state. This first pre-consolidation stage is necessary, since bulk solids' history of consolidation influences the state of the powder, because the particles rearrange with every consolidation.

After achieving the steady state for the consolidation tension, all stresses are reduced to zero, meaning that the normal force applied is reduced to zero and the rotation of the bottom of the cell is reversed to the initial state.

From this point on, the second part of the test begins. In this part, a normal force lower than the consolidation tension is applied to the powder until the point of incipient flow. The equipment determines the incipient flow point, which, once again corresponds to a pair of values of shear stress and normal tension, but this time, at incipient flow. This point is called a Yield Locus. The Yield Locus can be measured at various normal tensions (as long as they are lower than the consolidation tension) and a set of yield loci measured at different normal tensions forms a yield locus curve.

RST-XS.s allows the measurement of various Yield Loci per sample (see Figure 1.7), which was a great achievement in collecting experimental data, since prior to this equipment large amounts of samples would be wasted, since only one Yield Locus point could be obtained per sample.

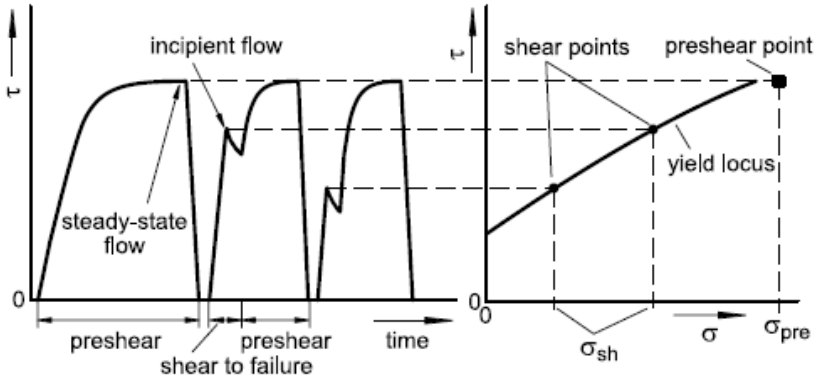

Figure 1.7: Evolution of shear stress with time during a shear test. Figure adapted from [8].

It's worth mentioning that since the consolidation history influences the particles' positions and the state of the bulk solid, each yield locus curve is characteristic of the consolidation tension applied.

To each yield locus correspond two Mohr circles (see Figure 1.8). One corresponding to the unconfined state of the powder and one representing the stress state at the end of consolidation, i.e. at the steady state attained at the end of consolidation, with the powder in the conditions of the test, i.e. inside the cell.

The experimental incipient flow points obtained can be fitted using the Warren-Spring equation (Equation 2.9), from which the values of cohesion and tensile strength can be attained. [37]

With the yield locus curve and the Mohr circles it is possible to obtain a series of results that are useful for the evaluation of powder flowability:

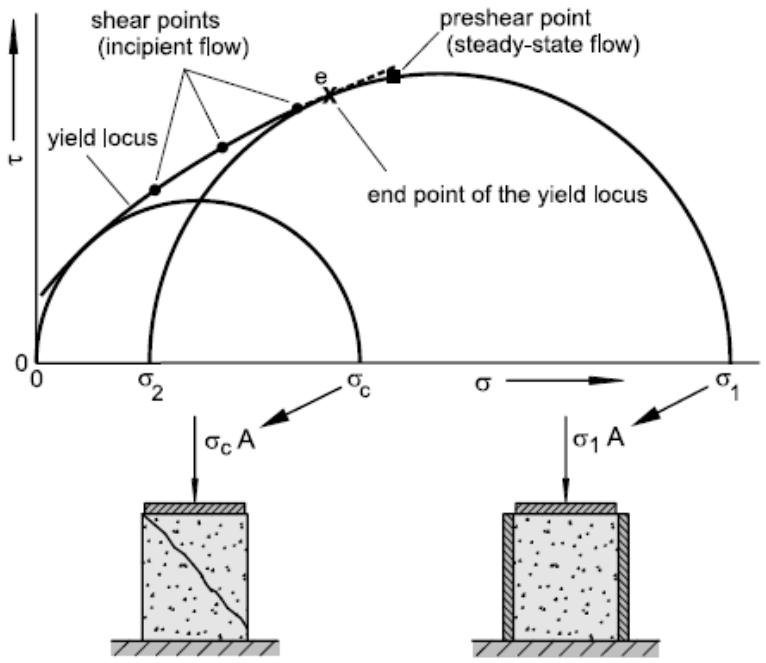

Figure 1.8: Example of a Yield Locus curve and the parameters it yields. Figure adapted from [8].

- Unconfined yield strength, σ_c;
- Major principal stress, σ_1;
- Tensile strength, σ_t;
- Cohesion, τ_c;
- Slope angle of the linearized yield locus, φ_{lin};
- Effective angle of internal friction, φ_E;
- Angle of internal friction at steady-state flow, φ_{SF}.

A set of pairs of values of σ_1 and σ_c obtained at different consolidation tensions form a flow function, which can be used to make a numerical characterization of flowability and to make a comparison between different powders.

1.3.3.B Wall friction tests

The following information was processed from [1], [8], [26] and [36].

The main purpose of the wall friction test is to assess the tensions existing at the interface between the powder and the wall. This 'wall' would be the wall of the powder's container in a real situation, e.g. the internal wall of a storage silo.

In this test, the incipient flow of the powder is not assessed. Only steady-states are obtained. The functioning principle is the same as the Yield Locus test. A normal tension is applied with rotation of the cell until a steady state is reached. The difference is that in this test, this normal tension is reduced by

increments, and for each normal tension applied, a steady state is attained, generating a set of points which will form the wall yield locus curve (see Figure 1.9).

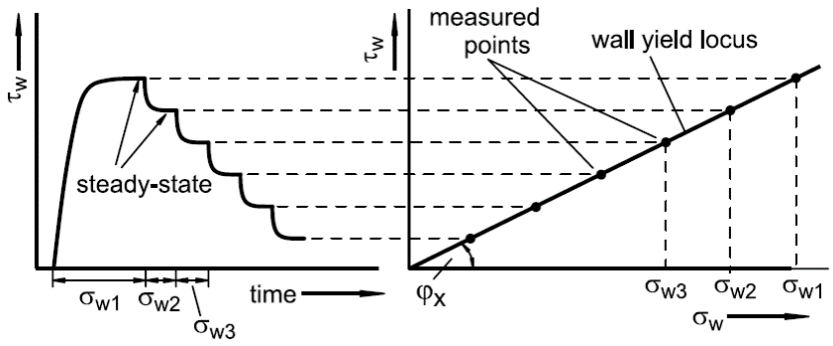

Figure 1.9: Evolution of wall shear stress with time during a wall friction test. Figure adapted from [8].

In this nomenclature, the index 'w' indicates that the normal and shear stresses are measured at the wall.

From the Wall Yield Locus curve it is possible to obtain the wall friction angle, φ_X, which is an important parameter for accurate equipment design.

1.4 Applications

Shear tests can be applied in numerous different fields such as the ceramics industry [37], the food industry [38], the metallurgy industry [39], the pharmaceutical industry [6], among others.

1.4.1 Pharmaceutical powder groups and their functions

As mentioned before, this work's main focus is testing pharmaceutical powders and understanding their rheological behaviour. These powders can be divided into categories according to their function and throughout this work fillers, binders, disintegrants, lubricants and Active Pharmaceutical Ingredients (API) were analysed.

Fillers are inert substances that have the main purpose of increasing the final pharmaceutical product's volume and mass to ease processing and to have a suitable size for consumption. Moreover, an adequate selection of which fillers to use allows the manufacturer to achieve the desired bulk and flow properties in tablet manufacturing, as well as better product stabilization and better compression for tablet manufacture. Common fillers used in the pharmaceutical industry include hydrous or anhydrous lactose and cellulose, among others. [40] [41] [42]

Binders may also be called adhesives, since their main function is to promote cohesiveness, imparting the necessary mechanical strength to the final product. These powders can be divided into two

groups, depending on the way the final product was processed: dry tablet binders, added to the blend either for dry granulation or as a part of direct compression (e.g. cellulose, Polyvinylpyrrolidone (PVP) or Hydroxypropyl Methylcellulose (HPMC) or solution tablet binders, used in the wet granulation process (e.g. polyvinyl pyrrolidone, starch, sucrose, mannitol, etc.) Furthermore, binders can also have a secondary purpose of increasing volume and enhancing mixing performance. [43] [44] [45]

Disintegrants are used in tablets and capsules, promoting the fast break down of the product into small fragments after ingestion, upon contact with a liquid medium. This way, the surface area available for dissolution is increased and drug dissolution and release is accelerated. These can be categorized according to their mechanism of action into traditional disintegrants (starch, alginates or methyl cellulose) or superdisintegrants (croscarmellose sodium, crospovidone or calcium silicate), which are used in the preparation of orally dissolving tablets or fast dissolving tablets due to their enhanced ability to promote disintegration. [46] [47] [48]

Lubricants (e.g. vegetable stearin, magnesium stearate or stearic acid) are added to pharmaceutical formulations to reduce the inter-particle friction and the friction between particles and surfaces, ensuring good processing properties such as flowability. Having good lubrication is important for operations such as blending, roller compaction, tablet compression, and capsule-filling. [49] [50]

Finally, APIs are the primary active compounds of a formulation and are the ingredients that grant the pharmacological effect to the drug product. These compounds are usually present in small quantities in the final product, since only a small amount has a powerful impact. Due to their organic sources, these powders are typically very cohesive and have poor flow properties. [51] [52] [53]

1.4.1.A Spray dried powders

Drug solubility is a major chalenge in the pharmaceutical industry and throughout the decades a series of methodologies have been developed to try to enhance this property. These methods go from optimizing the blend formulations to the use of technologies like spray drying. [54] [55]

Since some of the powders studied in this work are polymers commonly used in spray drying techniques, a brief synthesis of the spray drying methodology is presented.

Spray drying is a well established method that uses the heat of a hot gaseous medium to dry solution droplets into particles with the desired characteristics (size and shape). This is done in three steps: first, the solution is fed to the drying chamber via an atomizer and is broken into fine droplets, then, inside the chamber, the droplets come in contact with the drying gas, vaporizing the moisture, and finally, using the appropriate equipment, the dried particles are separated from the drying medium and collected in a tank. [54] [55]

Depending on the particle shape formed and on the particle size distribution, the flowability of the spray dried particles will either increase or decrease relatively to that of the crystalline particles. [54] [55]

1.4.2 Silo design

Another great application of the data that is obtained with the shear and wall friction tests is an accurate design of equipment that takes into account the properties of the powders being processed.

In this work, a mathematical model is developed to predict whether pharmaceutical powders flow or not through hoppers. Therefore, a brief reference to the methodology for silo designing is made in this section.

Silos are, like any other equipment, designed according to codes. There are many codes developed for the design of Silos, taking into account different aspects (e.g. the action of the wind or seismic loads) and many take into account the loads induced by the stored bulk solid. This last aspect is sometimes neglected, but it is just as important as others, since poorly designed silos can cause a shutdown period in factories due to the potential problems explained before in section 1.1. In this work, the mathematical model developed is based in Andrew Jenike's procedure, which is based on bulk solids' properties. This algorithm is further described in subsection 2.1.2. [8] [9] [18] [56]

1.4.3 Blend formulation

Shear testing can be used to optimize formulations in terms of flowability. A typical blend formulation includes diluents (recommended 20 - 90 %(w/w)), binders (in the desired amount), a disintegrant (recommended 0.5 - 5.0 %(w/w)), a glidant (recommended 0.1 - 0.5 %(w/w)) and a lubricant (recommended 0.5 - 1.0 %(w/w)), API (in the desired amount) among other powders necessary to achieve the desired properties. [57] [58]

1.4.4 Tableting

The flowability of a powder is also an important parameter to evaluate whether tablet compression will be performed smoothly and without problems or whether there will be flow restrictions. Tablet compression, as the name suggests, is a process where powder is dosed and compressed into tablets with uniform API distribution. A basic tablet press has two punches and a die and compression happens due to the high force created by punch movement in the die.

There are two main types of tablet presses: the single punch tablet press and the rotary tablet press. Throughout the third part of this work, a rotary tablet press was used, the Piccola Classica (Riva SA) with module, which has a rotating turret that holds various tooling stations that rotate pressing the powder into tablets. [59] [60]

1.5 Principal Component Analysis

As a complementary analysis, a Principal Component Analysis (PCA) will be applied to compare the blends manufactured and their constituent powders, as well as to better understand the relationship between the variables given by the shear tests performed.

This analysis is useful when there is a high number of variables, discriminating the most relevant ones, while maintaining a variability close to that of the full set of data. This can be done by creating a new smaller set of independent variables via linear transformation.

One of the main features of PCA is the ease in interpreting and classifying the multi-variate data when it is arranged according to uncorrelated principal components. [61] [62] [63]

This tool has been used previously by other authors in the field of powder rheology for powder characterization and comparison. [64] [65] [66]

2

Materials and methods

Contents

The present work is divided in three main parts. In the first part, a selection of the most adequate cells to work with in further studies is made.

Next, a characterization of fifteen pharmaceutical powders is made, which, besides helping to better understand the way the equipment used works, will be used in the future as part of a database for pharmaceutical powders' rheology.

Finally, a characterization of five blends is made, in order to understand how the rheological data obtained for the blends relates with the final tablet attributes.

2.1 Part I - Cell characterization

This stage of the work comprises the comparison between cells XS-Mr and XS-SV3 and cells XS-WM and XS-WL0 (see figures 2.2(a) to 2.2(e)). For this, a method similar to that used by Søgaard, *et al* [6] was applied.

2.1.1 Powder characterization

In order to understand the dependency of the output obtained by each cell on cohesion, five powders of different cohesions (Flow Function Coefficient (FFC) obtained ranging from 2.1 to 19.5 at σ_{pre}=1 kPa) were analyzed using these four cells: filler 1A (FMC Biopolymer), filler 2A (Meggle), filler 3 (Biogrund), binder 1A (Dow) and API 1 (Hovione). The fundamental properties of these powders were assessed through yield locus and wall yield locus tests determined by the *Schulze Ring Shear Tester* model RST-XS.s (see Figure 2.1), with the specifications present on tables 2.1 and 2.2.

Figure 2.1: Schulze Ring Shear tester RST-XS.s.

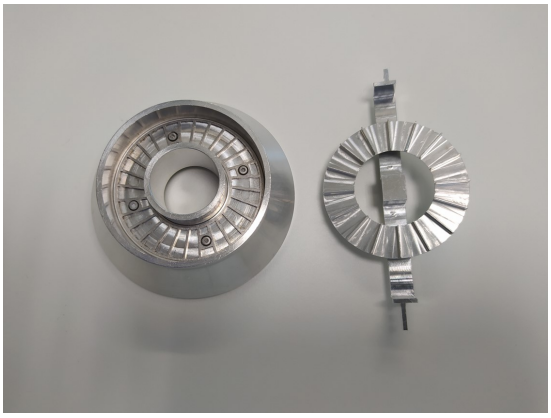

(a) Cell XS-Mr.

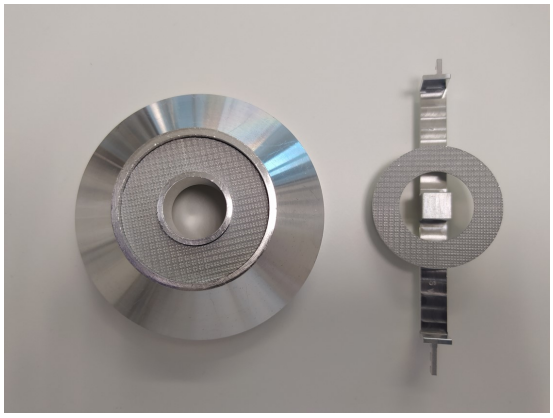

(b) Cell XS-SV3.

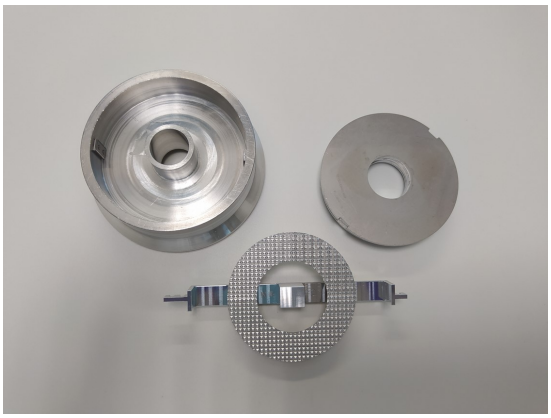

(c) Cell XS-WM.

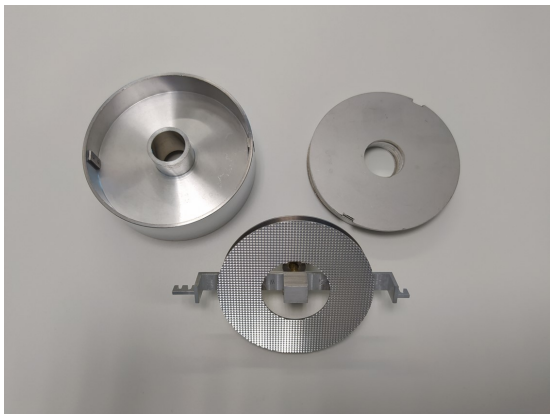

(d) Cell XS-WL0.

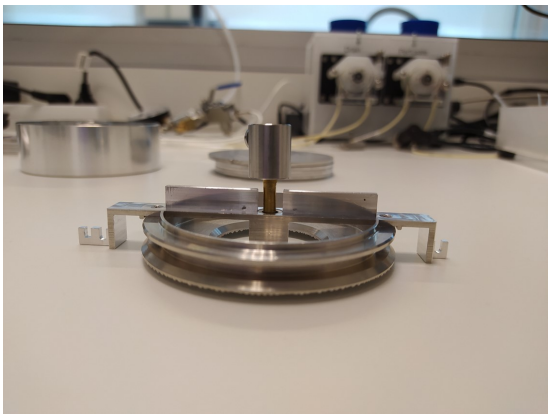

(e) Cell XS-WL0 lid.

Figure 2.2: Cells used throughout this study in the RST-XS.s ring shear tester.

Table 2.1: Vertical tensions applied during the three Yield Locus tests performed with each cell to each powder sample.

Test	σ_{pre} (Pa)	σ_{sh} (Pa)			
Test 1	1000	300	500	800	300
Test 2	2000	400	1000	1600	400
Test 3	3000	600	1500	2400	600
Test 4*	500	200	300	400	200

** When necessary. Not possible with cell XS-SV3.*

For some of the powders tested, a lower point on the Yield Locus curve was necessary. In these cases test 4 in table 2.1 was performed.

Table 2.2: Vertical tensions applied during the three Wall Yield Locus tests performed with each cell to each powder sample.

Cell	Test	σ_w (kPa)					
XS-WM	Test 1	10.0	8.2	6.4	4.6	2.8	1
	Test 2	7.5	6.1	4.7	3.3	1.9	0.5
	Test 3	5.0	4.1	3.1	2.2	1.2	0.3
XS-WL0	Test 1	1.00	0.82	0.64	0.46	0.28	0.10
	Test 2	0.75	0.62	0.48	0.35	0.21	0.08
	Test 3	0.50	0.41	0.32	0.23	0.14	0.05

These tests were performed with an n=1, except for API 1, for which an n=3 was used, to assess the repeatability of the tests performed.

2.1.2 Mathematical treatment and validation

Vertical stresses:

A rough estimation of the vertical stresses present at the outlet of a hopper can be done for conical hoppers with the help of Equation 2.1, where d is the hopper outlet diameter [8] [9] [67] [68].

$$\sigma_v = 0.2 \cdot g \cdot \rho_b \cdot d \tag{2.1}$$

Knowing the vertical stress, an estimation of the major principal stress, σ_1, may be done by making an approximation assuming that the vertical stress value is equal to the minor principal stress, σ_2. Equation 2.2 is used for this purpose. [8] [9] [67] [68]

$$\sigma_1 = \frac{1 + \sin \varphi_E}{1 - \sin \varphi_E} \cdot \sigma_v \tag{2.2}$$

These formulas are a mere approximation and should not be used for hopper design purposes, since they take into account neither the wall friction nor the hopper vertical angle.

This calculation was made for the outlet of funnels with outlet diameters of 4 cm such as the ones represented in Figures 2.5 and 2.6 and for model industrial scale silos, which have hopper outlet diameters of 9.67 cm and 20 cm.

For the purpose of this approximation, a medium value of the φ_E and ρ_b obtained in each test was used. [6]

Minimum outlet diameter required for mass flow:

To understand which cells give more accurate results, the data obtained from the ring shear tester were treated mathematically according to Mehos [69] and the mathematical results were validated by discharging the powders through funnels with an opening diameter of 4 cm and different wall angles (45°, 30°, 25° and 15°). The mathematical treatment applied allowed to determine theoretically if there would be mass flow on these hoppers.

First, the data obtained for each pre-consolidation tension is fitted according to equations 2.3 to 2.6 [1] [69]:

- Flow function, (σ_1,σ_c): it can be regressed either quadratically or linearly.

$$\sigma_c = a\sigma_1^2 + b\sigma_1 + c \tag{2.3}$$

  Parameter a is given the value of 0 if a linear regression is desired.

- Effective angle of friction, φ_E:

$$\varphi_E = a \ln \sigma_1 + b \tag{2.4}$$

- Bulk density, ρ_b:

$$\rho_b = \rho_{bmin} + \alpha\sigma_1^{\beta} \tag{2.5}$$

- Wall Yield Locus:

$$\tau_w = a(\sigma')^2 + b\sigma_w + c \tag{2.6}$$

Once again, parameter a is given the value of 0 if a linear regression is desired.

Once these regressions are obtained, it is possible to begin the computation of the minimum outlet diameter required for mass flow, B_{min}, for a certain wall angle. This calculation is an iterative process and will be described next.

On a first approach, the wall angle is stipulated and an estimation of the Flow Factor (ff) is made. A value of 1.4 is a good suit for this first guess. [1] With these values and with the regressions for the flow function and bulk density a first calculation of σ_{crit} and B_{min} is made.

With these values φ_E and φ_X are computed and ff is updated.

With the new Flow Factor a new cycle of calculations begins which will be repeated until the results converge.

This algorithm is represented in figure 2.3.

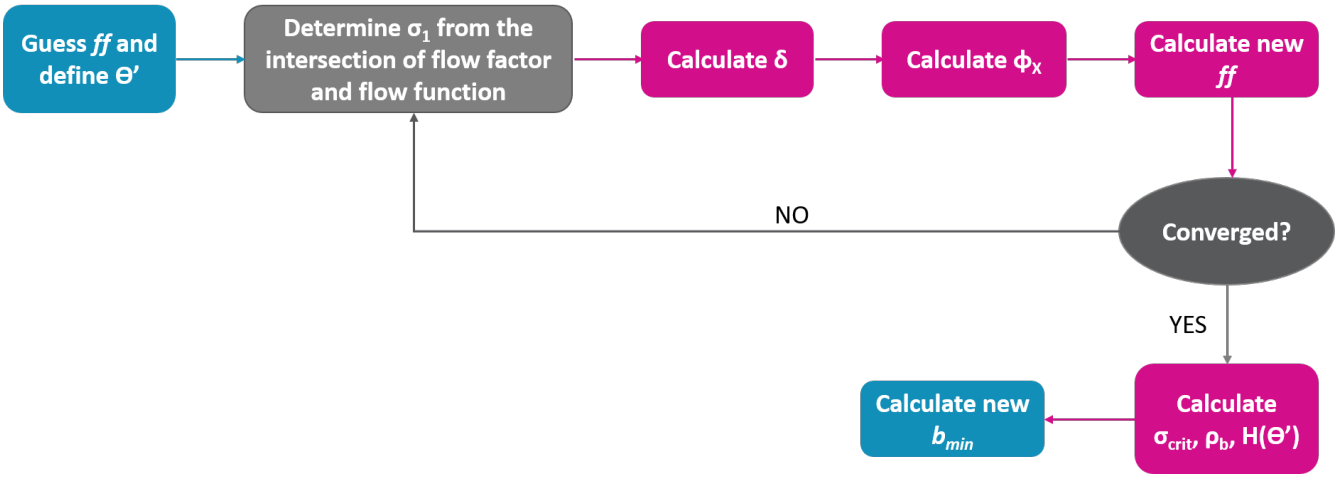

Figure 2.3: Algorithm used for the calculation of B_{min}.

For the powders that have predictions of funnel flow, the critical rathole diameter required to collapse the rathole, D_F, was calculated using equations 2.7 to 2.8 [1] [8].

First, the major principal stress is estimated at the outlet of the silo, using the Janssen equation (Equation 2.7) [16]:

$$\sigma_1 = \frac{\rho_b g R_H}{k \tan(\varphi_X)} \left[1 - \exp\left(\frac{-k(\tan\varphi_X)h}{R_H}\right)\right] \tag{2.7}$$

Where h is the height of the powder in the cylindrical zone of the silo, R_H is the hydraulic radius of the cylinder (in this case where the silo is cylindrical, an approximation can be made where R_H is equal to 1/4 of the diameter), and k is the Janssen coefficient (typically 0.4 [1] [69]).

Next, the rathole diameter, D_F, is calculated, using Equation 2.8 [9] [18]:

$$D_F = \frac{G(\varphi_X) f_C}{\rho_b g} \tag{2.8}$$

Where $G(\varphi_X)$ is plotted in Jenike's bulletins 108 and 123 [9] [18], and represented in Figure 2.4 [1].

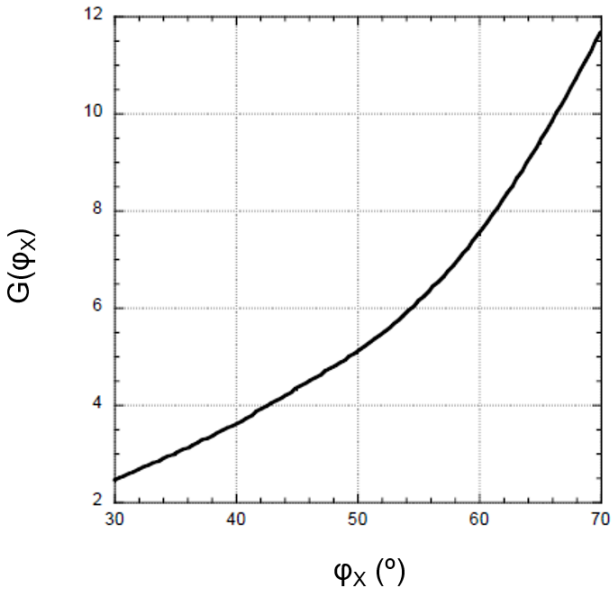

Figure 2.4: Plot of G(φ_X).

This procedure was followed for hoppers with wall angles of 45°, 30°, 25° and 15° and if the resulting B_{min} was larger than 4 cm then one would assume that there would be obstruction of flow by arching.

To validate the results obtained with this method, 800 g of each powder were ran through the funnels schematized in figure 2.5 and represented in figure 2.6, which have an opening diameter of 4 cm and wall angles of 45°, 30°, 25° and 15° as those used in the mathematical treatment.

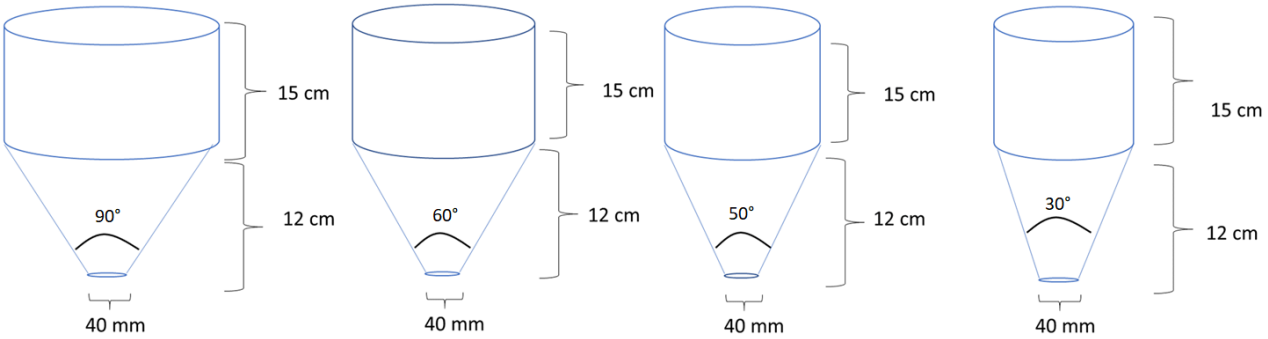

Figure 2.5: Schematic representation of the hoppers used.

Figure 2.6: Hoppers used for validation purposes.

Warren-Spring equation validation

Additional calculations were made to adjust the Warren-Spring equation (given by Equation 2.9) to the experimental data obtained and to adjust the unconfined and steady state Mohr circles to the experimental yield locus curve, following two different reasoning routes to calculate the steady state Mohr circle.

$$\tau = \tau_c \cdot \left(1 + \frac{\sigma}{T}\right)^{\frac{1}{n}} \tag{2.9}$$

In equation 2.9, τ is the shear stress, τ_c stands for cohesion, σ is the normal tension applied, T represents the tensile strength and n is an exponent which typically has values between 1 and 2 and is stated to characterize flowability. [8] [70]

First, Equation 2.9 was fitted to the experimental data using the tool *Solver* from *Microsoft Excel*, excluding the pre-shear point.

Then, to calculate the unconfined state Mohr circle, it was assumed that the yield locus curve is tangent to this circle and that this circle passes through the point (0,0). Logically, it was also assumed that the tangency point lies in the left hemisphere of the circle. Hence, $0 < \sigma_B < \sigma_c/2$, where σ_B represents the normal tension at the tangency point between the Warren-Spring curve and the unconfined state Mohr circle.

From these premises and taking into account that the first derivative of the warren-spring equation and the first derivative of the Mohr circle (i.e. the slopes of these curves) have to be the same in

the tangency point, the Warren-Spring equation can be made to obey equations 2.10 and 2.11, which describe the intersection of the Warren-Spring curve and the unconfined state Mohr circle and the fact that their slopes have to be the same at the tangency point.

Once again, *Microsoft Excel's Solver* tool was used to minimize the difference between each branch of equations 2.10 and 2.11 by altering the value of σ_B and σ_c. [71]

$$\tau_c \cdot \left(1 + \frac{\sigma_B}{T}\right)^{\frac{1}{n}} = \sqrt{(\sigma_c - \sigma_B) \cdot \sigma_B} \tag{2.10}$$

$$\frac{\tau_c}{n \cdot T} \cdot \left(1 + \frac{\sigma_B}{T}\right)^{-1+\frac{1}{n}} = \frac{1}{2} \cdot \frac{(\sigma_c - 2 \cdot \sigma_B)}{\sqrt{(\sigma_C - \sigma_B) \cdot \sigma_B}} \tag{2.11}$$

Finally, to calculate the steady state Mohr circle, two different reasonings were used.

- Reasoning 1

On the one hand, this circle is not only tangent to the warren-spring equation, but also includes the pre-shear point (σ_0, τ_0), meaning that the distance from the center of this circle (M_A) to the tangency point (R_A) – Equation 2.12– is the same as the distance from the center to the pre-shear point (R_0) – Equation 2.13.

$$R_A^2 = \tau_c^2 \cdot \left(1 + \frac{\sigma_A}{T}\right)^{2/n} \left[1 + \left(\frac{\tau_c}{n \cdot T}\right)^2 \cdot \left(1 + \frac{\sigma_A}{T}\right)^{-2+2/n}\right] \tag{2.12}$$

$$R_0^2 = (\sigma_0 - M_A)^2 + \tau_0^2 \tag{2.13}$$

In this step, *Microsoft Excel's Solver* tool was used to minimize the distance between R_0 and R_A by altering the value of σ_A, since both radiuses are dependent on the value of σ_A.

- Reasoning 2

On the other hand, an approach similar to that made for the unconfined state Mohr circle can be done, where the family of semi-circles that passes through the pre-shear point is written as Equation 2.14, where M is the abciss of the generic center of the circle – point (M,0). This way, the Warren-Spring equation can be made to obey equations similar to equations 2.10 and 2.11, but applied to the steady state Mohr circle: 2.15 and 2.16, where σ_A represents the normal stress at the tangency point between the Warren-Spring curve and the steady-state Mohr circle. [71]

$$\tau = \sqrt{(\tau_0^2 + \sigma_0^2) + 2M_A\,(\sigma - \sigma_0) - \sigma^2} \tag{2.14}$$

$$\tau_A^2 = \tau_c^2 \cdot \left(1 + \frac{\sigma_A}{T}\right)^{\frac{2}{n}} = \left(\tau_0^2 + \sigma_0^2\right) + 2M\,(\sigma_A - \sigma_0) - \sigma_A^2 \tag{2.15}$$

$$\frac{(M_A - \sigma_A)^2}{(\tau_0^2 + \sigma_0^2) + 2M_A(\sigma_A - \sigma_0) - \sigma_A^2} = \left(\frac{\tau_c}{n \cdot T}\right)^2 \cdot \left(1 + \frac{\sigma_A}{T}\right)^{-2+\frac{2}{n}} \tag{2.16}$$

Once again, the difference between the branches of equations 2.15 and 2.16 is minimized by altering the values of σ_A and M_A, using the *Solver* tool, from *Microsoft Excel*. In order to ease this method and avoid the results falling in a relative minimum, a visual approximation can be made by drawing a straight line perpendicular to the Warren-Spring curve close to the last measured incipient flow point. This eases considerable the estimate of the tangency point and allows to have an adequate first estimate to run *Solver*.

2.2 Part II - Powder characterization

Similar to the work described in the previous section of chapter (Section 2.1), the fundamental properties of a variety of powders were assessed through Yield Locus and Wall Yield Locus tests using Schulze's Ring Shear tester RST-XS.s.

2.2.1 Materials

Aside from the five powders analysed in part I, ten more powders were analysed using cells XS-Mr and XS-WL0:

- Filler 1B (FMC Biopolymer);
- Filler 1C (FMC Biopolymer);
- Filler 2B (Meggle);
- Filler 2C (KERRY);
- Filler 4 (JRS PHARMA);
- Binder 1B (Hovione);
- Binder 2 (Hovione);
- API 2 (Fagron GmbH & Co.);
- Lubricant 1 (PETER GREVEN);
- Disintegrant 1(DUPONT IE);

Different grades of the same material are signalized with letters after the number that refers to the material itself. Additional data for each powder used can be found in Appendix A.

Following the selection of the adequate cells to use in the first part, in this part, only cells XS-Mr and XS-WL0 were used.

The Yield Locus tests performed in this part of the study were the same tests as the ones described in Table 2.1 in Section 2.1 (n=1). Vertical tensions applied during the wall yield locus tests performed are sumarized in Table 2.3:

Table 2.3: Vertical tensions applied during the Wall Yield Locus test performed to each powder sample.

Cell	σ_w (kPa)							
XS-WL0	2.00	1.50	1.00	0.50	0.25	0.18	0.10	0.05

Each Wall Yield Locus test was performed with five repetitions in one go, so although only one test was performed for each powder, the number of repetitions is equivalent to n=5.

The analyzed powders were divided according to their main function in pharmaceutical tablet formulation in order to ease comparison between powders.

An investigation to understand the influence of sieving in the results obtained with the RST-XS.s was also conducted, where sieved API 1 was analysed and the results were compared with those of non-sieved API 1.

2.2.2 Mathematical treatment

The experimental data obtained was treated mathematically as described in subsection 2.1.2, but only for a hopper with a vertical hopper angle of 30°, in order to obtain a value which could summarize all the different parameters obtained – the minimum outlet diameter required for mass flow B_{min} – to ease interpretation.

2.3 Part III - Blend characterization

In the third part of this monograph, a set of five blends were analysed with Schulze's RST-XS.s and then were used to produce a number of tablets which were weighed in order to find the relationship between weight oscillation and the results obtained with RSE-XS.s.

Finally, a PCA was ran in order to better understand the existing relationships between the many parameters yielded on a yield locus or a wall yield locus test.

2.3.1 Blend manufacturing

Four 500 g blends were prepared with the compositions described in Table 2.4. Blend 1 is a control blend, where there is no quantity of API. Blends 2, 3 and 4 gradually increase the quantity of API by increments of 20%.

Table 2.4: Composition for Blends 1 to 4 in % (w/w).

Powder	Blend 1	Blend 2	Blend 3	Blend 4	Blend 5
Filler 2A	44	34	24	14	23
Filler 3	50	40	30	20	0
Disintegrant 1	5	5	5	5	5
Lubricant 1	1	1	1	1	1
API 1	0	20	40	60	40
Filler 1B	0	0	0	0	30
Glidant 1	0	0	0	0	1

Additionally a fifth blend, also weighing a total of 500 g, was prepared, with the composition described in Table 2.4 with the purpose of understanding whether a blend with poor flowability could be created while using API 1.

During the manufacturing of the blends, all powders were weighed in an analytical balance and poured in a 500 mL HPDE jar, except for lubricant 1. The jar was then inserted in a TURBULA® model T2F Shaker-Mixer and blended at 32 rpm for 10 minutes. Lubricant 1 was only added to the blend after this first blending step and the mixture was once again blended in the TURBULA® for 5 more minutes at 32 rpm.

The TURBULA® utilized is illustrated in Figure 2.7.

2.3.2 Blend characterization

After blending, the blends were tested in the RST-XS.s. The parameters of the tests performed are described in tables 2.1 (Test 1, 2 and 3) and 2.3. This data was then related to the corresponding data values about each components of the blend in order to obtain a ”blending law”.

2.3.3 Mathematical treatment - shear and wall friction data

The rheological data obtained for the five blends was treated mathematically as described in Subsection 2.2.2.

In order to make a comparison with the pure components of the blend, the value of FFC was predicted using the FFC values of the pure materials and Equation 2.17, where FFC_b corresponds to the FFC

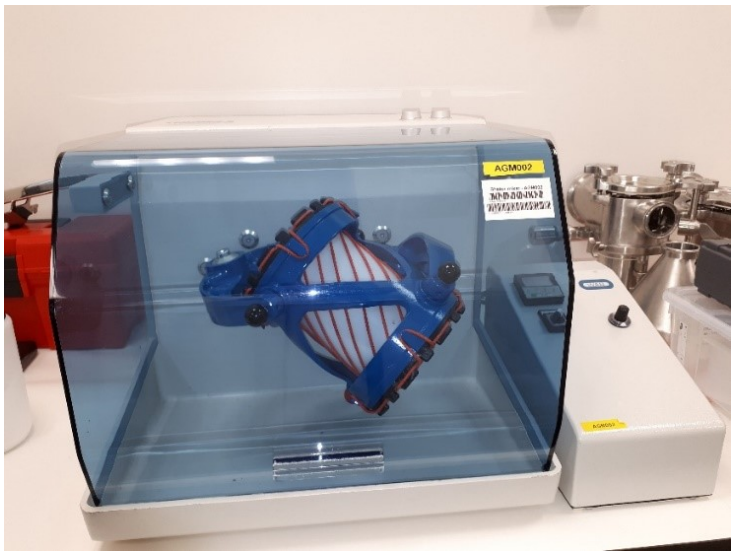

Figure 2.7: TURBULA T2F Shaker-Mixer.

value of the blend, FFC_m corresponds to the FFC value of the each material used to make the blend and y_m is the %(v/v) of each material m.

$$FFC_b = \sum(y_m \cdot FFC_m) \tag{2.17}$$

2.3.4 Principal Component Analysis

The data obtained experimentally and by mathematical treatment were processed using the software *SIMCA* ® (*Sartorius*). This software allows the user to perform statistical analysis such as PCA, Partial Least Squares (PLS) regressions and others. The data obtained was input into the software and a PCA was ran, in order to understand how the variables measured relate to each other and what relation do the blends tested have with the powders that they contain.

A first model was created with 21 observations (the sixteen powders tested including sieved API1 and the five blends) and 30 variables, where for each pre-consilidation tension a σ_1, σ_C, ρ_b, φ_E, φ_{Lin}, φ_{SF}, FFC ratio, FFρ ratio and τ_C were inserted, together with the un-tapped bulk density, the B_{min} calculated and the particles' x_{50} when it was available.

The built-in function *Autofit* was used to define the initial number of Principal Components (PC) necessary for the model. The quantity of Principal Component (PC) was then adjusted with the criteria of having the least possible number of PC possible (to simplify the analysis made) that would still maintain an explained variance (R2X) value above 0.7 to have a model with highly predictive accuracy. [72] [73] [74]

Afterwards, an analysis was made to understand which of the variables used could be removed from

the model in order to simplify it, but still keeping its core. This was done by studying the correlations between the variables used. After defining the new set of variables, the model was refined and then analysed.

2.3.5 Tabletting

Each blend was poured into a Riva Piccola classica with module, equiped with a forced feeder, to make tablets under five different conditions (for blends 1 and 2 only four different conditions were used, excluding condition 5). The equipment is illustrated in Figure 2.8 [60] and the conditions used are described in Table 2.5. The rotating speed of the feeder and the turret were changed from batch-to-batch, as well as the tablet production time.

Before starting the tablets batches, the parameters that the equipment requires had to be adjusted. This way, the fill depth was adjusted in order to obtain tablets that had a weight of about 250 mg.

Table 2.5: Conditions used in tableting.

	Condition 1	Condition 2	Condition 3	Condition 4	Condition 5
Turret speed (rpm)	30	30	30	50	75
Feeder speed (rpm)	20	30	40	40	40
Time (s)	60	60	45	45	30

2.3.6 Mathematical treatment - discharge rate and feeding time

In order to verify whether the filling time that each condition used was enough, the filling time and the discharge rates were calculated and compared.

The filling time for each turret condition was calculated using Equation 2.18 [75], in which T_{fill} is the filling time, L_f is the length of the feeder exposed to the turret, R_4 is the pitch circle radius and r is the turret speed mentioned in Table 2.5.

$$T_{fill} = \frac{60000 L_f}{2\pi R_4 r} \tag{2.18}$$

For the Riva Piccola, the dimensions used are L_f= 150 mm and R_4= 75 mm.

After calculating the filling times, the mass discharge rate ($\dot{m}_s$) into a die was calculated using Equation 2.19 [1], where ρ_{B0} is the bulk density at the outlet of the punch, A_0 is the cross-sectional area of the die, B is the diameter of the punch outlet, g is the gravitational acceleration and θ' is the vertical wall angle of the punch. An approximation was made where the value of ρ_{B0} was assumed to be that of the bulk density obtained at a pre-consolidation of 1 kPa. Also, another approximation was made where the vertical wall angle of the punch considered was of 1° since the wall is vertical.

Figure 2.8: Riva Piccola classica with module.

$$\dot{m}_s = \rho_{b0} A_0 \sqrt{\frac{Bg}{4 \tan \theta'}} \tag{2.19}$$

Knowing the discharge rates and that tablets with a weigh of 250 mg were to be obtained, the time necessary to fill 250 mg for each blend was calculated in order to verify that this time is inferior to the filling time calculated with Equation 2.18.

The results obtained were then validated with the actual production of the tablets.

2.3.7 Mathematical treatment - weight variation

The mean weight value and the Relative Standard Deviation (RSD) were calculated for each batch produced to understand whether there was an influence of the API quantity in each blend on the weight variation of the tablets produced.

Approximately a hundred tablets were produced in each batch, from which 20 tablets were randomly selected and weighed in an analytical balance.

The RSD was calculated using Equation 2.20 [76], where S is the standard deviation and $\bar{x}$ is the mean weight value.

$$RSD = 100 \cdot \frac{S}{\bar{x}} \tag{2.20}$$

The standard deviation was computed using *Microsoft Excel 2016* function STDEV.P, but it may also be calculated using Equation 2.21 [77], where n stands for the number of samples used, 20 in this case.

$$S = \sqrt{\frac{\sum(x_i - \bar{x})^2}{n-1}} \tag{2.21}$$

2.4 Complementary analysis

In order to better understand the morphology of the powders tested, Scanning Electron Microscopy (SEM) techniques were employed, using a *HITACHI S-2400* analytical Scanning Electron Microscope from *HITACHI* [78] with the image acquisition software *Bruker Esprit 1.9* (see Figure 2.9). This analysis was made for all of the powders tested except for the Blends.

An analysis of Particle Size Distribution (PSD) was also made using a *Sympatec* HELOS-BR-RODOS-L-ASPIROS [79] (see Figure 2.10). This equipment was used to analyse some of the dry fine grained products studied in this work at a pressure of 0.2 bar and with the R5 lens. The x_{10}, x_{50} and x_{90} were measured and three repetitions were used. The missing data for the rest of the powders analyzed was retrieved from the literature. The results are presented in Appendix A.

(a) Image collection stage. **(b)** Image review stage.

Figure 2.9: HITACHI S-2400 analytical SEM.

Figure 2.10: HELOS-BR-RODOS-L-ASPIROS.

3

Results - Part I: Cell characterization

Contents

In chapter 1, the general outline of the *Schulze Ring Shear Cell* tester RST-XS.s was described, where different types of cells that carry the samples for testing were mentioned. The appropriate cell to use for a certain test depends on the type of test, on particle size and on the range of normal tensions applied throughout the test.

The individual results for each test performed can be found in Appendix B.

3.1 Powder characterization

Yield Locus tests

In this section, the general shear data that can be obtained with RST-XS.s (flow functions, density curves, friction angles and FFC value) was acquired for five powders of different cohesion with two different shear cells (XS-Mr and XS-SV3) in order to compare the results yielded by these two cells and conclude which would be more adequate for further studies in the pharmaceutical industry.

- Flow functions:

The following figures show the flow functions obtained for the five powders tested with cell XS-Mr (3.1(a)) and with cell XS-SV3 (3.1(b)).

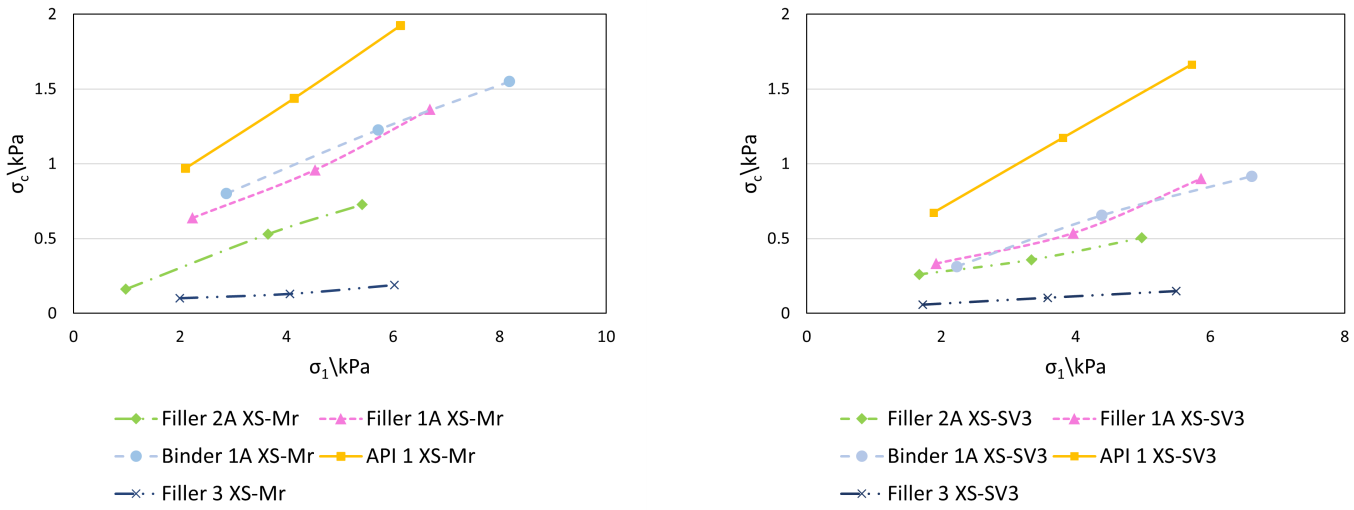

(a) Cell XS-Mr

(b) Cell XS-SV3

Figure 3.1: Flow functions obtained with shear cells XS-Mr and XS-SV3.

The results obtained with cells XS-Mr (Figure 2.2(a)) and XS-SV3 (Figure 2.2(b)) show that the shear cells do not yield the same results. In fact, cell XS-SV3 yields smaller shear stresses. The reason for this difference lies in the geometry of both cells and in the different surface characteristics. Due to the different surface of the lid of the XS-SV3 cell, the shear zone develops in a different way and becomes more narrow within a shorter time. This results in a decrease of the shear stress compared to cell XS-Mr which has vanes at the lid. [80] In fact, Wang, et al. (2021) [81] state that cell geometry has a bigger impact on the results yielded for finer powders than for coarse powders. As a consequence, shear cell XS-SV3 yields results that correspond to a best-case scenario.

Furthermore, the amount of sample used impacts the results obtained: tests made with cell XS-Mr tend to be more repeatable than those performed with cell XS-SV3, since cell XS-Mr holds a larger sample volume. [80] Care should be taken when selecting the methodologies to predict downstream processability.

A flow function at lower unconfined yield strengths and major principal stresses has lower FFC (considering $FFC = \sigma_c/\sigma_1$), thus corresponding to a better flowability [82]. According to cell XS-SV3, filler 1A and binder 1A's flow functions are close to filler 2A's. Cell XS-Mr, on the other hand, yields higher flow functions for these two powders, being now in the middle of API 1 and filler 2A. This suggests once more that Cell XS-SV3 yields a best-case scenario.

It's worth mentioning that the order in flowability is maintained in both cells: API 1 having the worst flowability, followed by binder 1A and filler 1A, which are very similar, filler 2A and the one with the best flowability, filler 3. Thus, comparative studies can be performed with both cells as long as the same cell is used throughout the whole study [8] [34] [80]. This can also be verified when looking at the values of FFC obtained in each test, i.e. for each of the three normal tensions applied. These values are illustrated in figures 3.2 to 3.4.

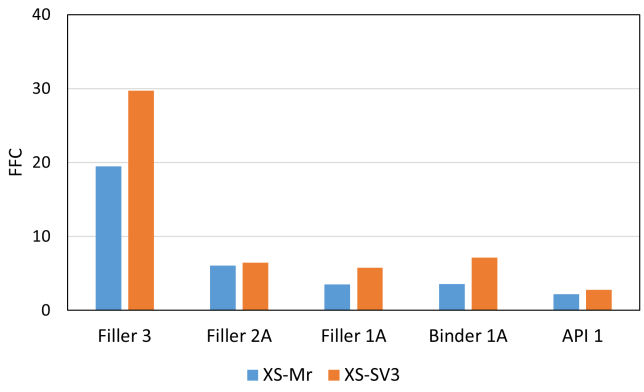

Figure 3.2: FFC at $\sigma_{pre} = 1kPa$

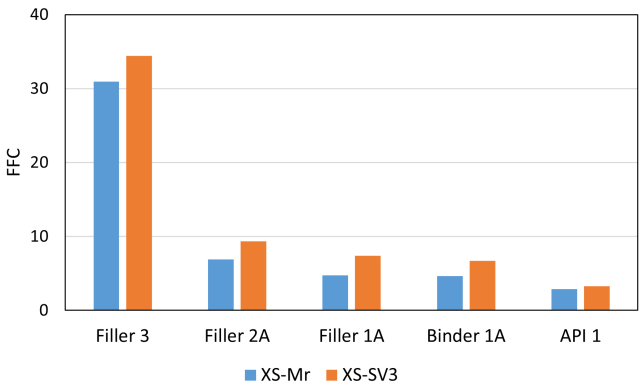

Figure 3.3: FFC at $\sigma_{pre} = 2kPa$

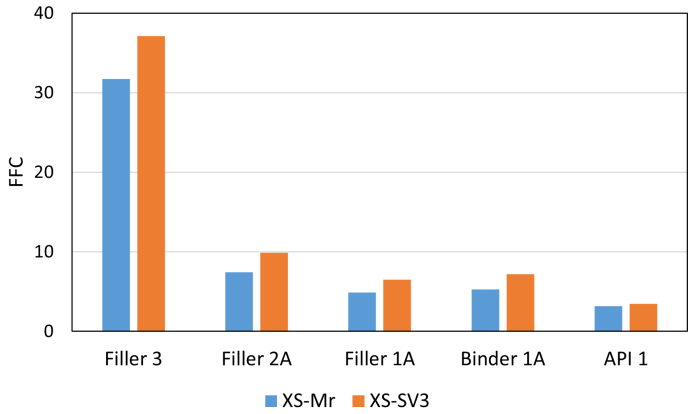

Figure 3.4: FFC at $\sigma_{pre} = 3kPa$

These figures demonstrate that FFC values are always higher when using the smaller cell - XS-SV3.

- Complementary data:

Regarding other data provided by the Yield Locus tests, the same trend is visible, where there is a clear difference between the results obtained with cells XS-Mr and XS -SV3.

Looking at Figure 3.5 where the density is plotted over σ_1, the bulk density obtained with XS-SV3 much lower than that with XS-Mr, just like what happens with φ_E in Figure 3.6.

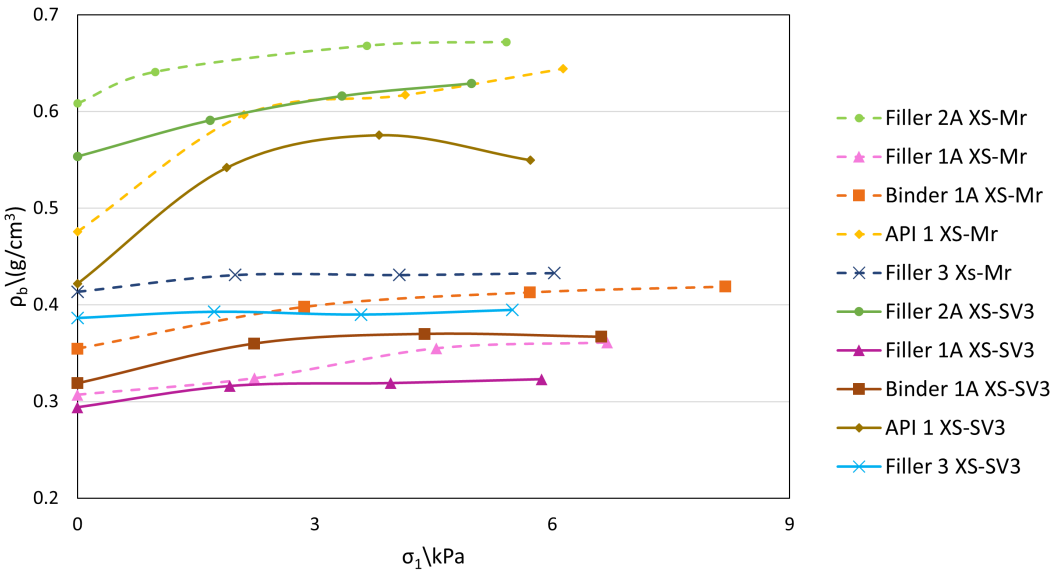

Figure 3.5: Bulk density obtained for each test performed.

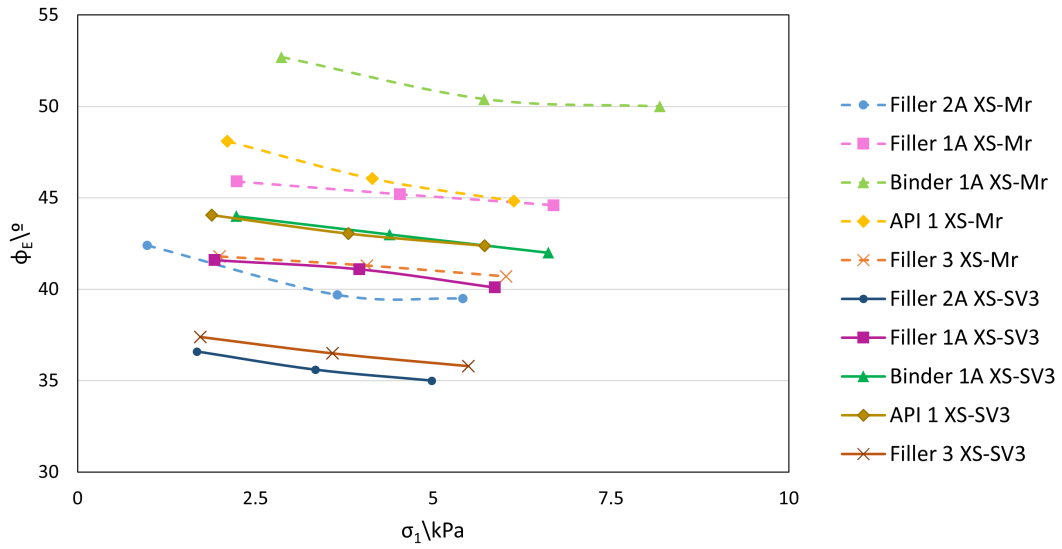

Figure 3.6: Angle of internal friction, φ_E, obtained for each test performed.

Wall friction tests

After comparing the two shear cells, the wall shear cells XS-WM and XS-WL0 were also compared. For that, these cells were used to obtain the wall yield locus for the five powders mentioned above.

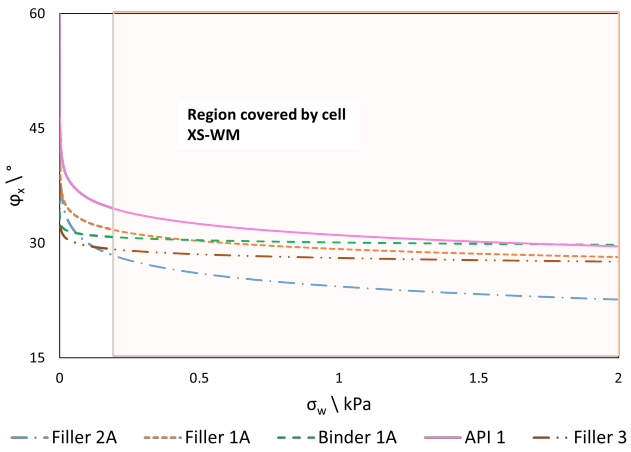

(a) Linear scale on the σ_W axis.

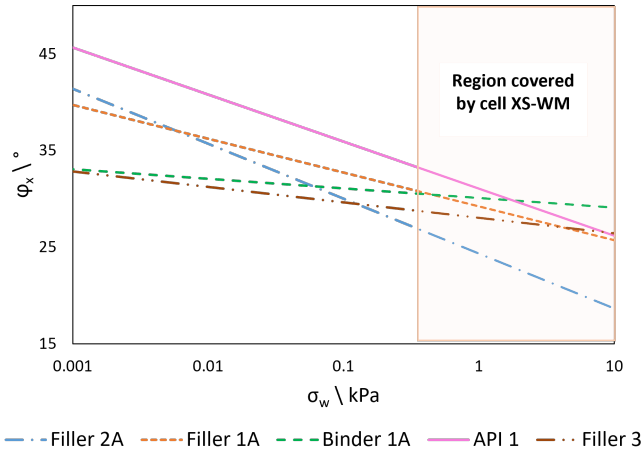

(b) Logarithmic scale on the σ_W axis.

Figure 3.7: Curve $\varphi_X(\sigma_W)$ obtained for each powder with the data of cells XS-WM and XS-WL0 combined.

Regarding the results obtained with the Wall Friction cells, it became clear that the decision of which cell to use must take into consideration not only the powder to be analyzed, but also the adequate normal tension range to be applied.

The data obtained with both cells was combined to build the plots of $\varphi_X(\sigma_W)$ for each powder. Figure

3.7 shows these different plots of φ_X over σ_W for each of the analyzed powders generated by both cells combined with a linear scale on the XX axis – Figure 3.7(a) – or with a logarithmic scale – Figure 3.7(b).

The shaded area shows the lower limit of XS-WM's σ_w range (194 Pa to 23 kPa), which does not comprise the initial part of the logarithmic plots, only covered by XS-WL0 cell (σ_w range: 0 Pa to 13 kPa). It's important to mention that some pharmaceutical operations performed at a smaller scale than other industries have very small stresses associated [6], for example during the discharge of hoppers where values of σ_1 of less than 1 kPa may be reached at times. This causes a need to extrapolate the plot for lower σ_W values when XS-WM wall friction cell is used.

In fact, generally the normal stress existing at the wall is considerably smaller than the major stress in the bulk [8] and looking at Table 3.1, the range of σ_W at the lab-scale and industrial scale will not be higher than 1.513 kPa, which is still in the range of tensions that cell XS-WL0 can apply, but it will be lower than 120 Pa, which is no longer in the range of cell XS-WM.

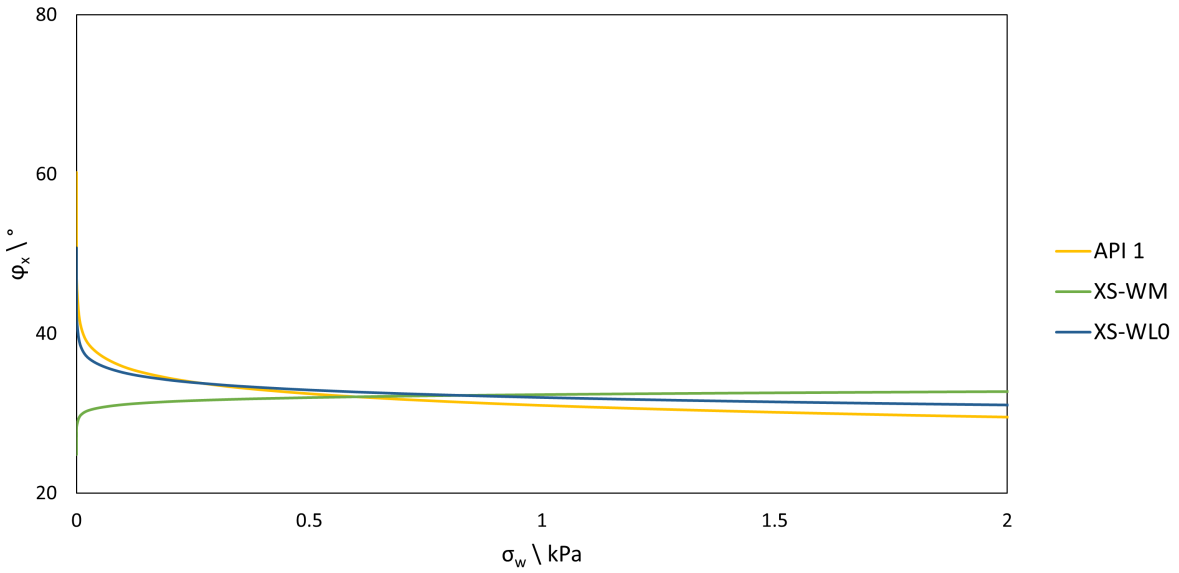

Figure 3.8: Curve $\varphi_X(\sigma_W)$ obtained for API 1 with the data of cells XS-WM and XS-WL0 combined and the extrapolation of this plot obtained with each cell separately.

Figure 3.8 shows a simulation of the extrapolations of the φ_X plot for the most cohesive powder – API 1– for ranges that aren't covered by each cell individually, comparing them with the plot resulting from both cells simultaneously. Results show that for lower tensions, XS-WM generates less accurate data, which might propagate the error associated if used in further design calculations.

3.2 Mathematical treatment

3.2.1 Vertical Stresses

The vertical stresses at the outlet of the funnels described in figures 2.6 and 2.5 and at the end of model industrial hoppers were calculated using equations 2.1 and 2.2. These results are present in Table 3.1.

The vertical stresses obtained vary from 25 Pa to 259 Pa while the major principal stresses vary from 120 Pa to 1513 Pa. With this information, the range of vertical tensions applied should be adapted, including lower vertical tensions. However, that would have to be done using a low shear cell like cell XS-Lr0 [32], which is not available.

Table 3.1: Calculation of the major principal stresses in the outlet of industrial and lab-scale silos.

Powder	Cell	lab-scale silos (d=4 cm)		Industrial silos (d=9.76 cm)		Industrial silos (d=20 cm)	
		σ_v (kPa)	σ_1 (kPa)	σ_v (kPa)	σ_1 (kPa)	σ_v (kPa)	σ_1 (kPa)
Filler 3	XS-Mr	0.034	0.165	0.082	0.403	0.169	0.826
	XS-SV3	0.031	0.122	0.075	0.297	0.154	0.608
Filler 2A	XS-Mr	0.052	0.244	0.126	0.596	0.259	1.221
	XS-SV3	0.048	0.183	0.117	0.446	0.240	0.914
Filler 1A	XS-Mr	0.027	0.160	0.066	0.391	0.136	0.802
	XS-SV3	0.025	0.120	0.061	0.294	0.125	0.601
Binder 1A	XS-Mr	0.032	0.257	0.079	0.627	0.169	0.826
	XS-SV3	0.029	0.152	0.070	0.370	0.154	0.608
API 1	XS-Mr	0.049	0.303	0.119	0.738	0.243	1.513
	XS-SV3	0.044	0.232	0.106	0.567	0.218	1.162

3.2.2 Minimum outlet diameter required for mass flow

The mathematical treatment described in section 2.1.2 was applied to all five powders studied, simulating flow conditions in hoppers with the dimensions of the funnels existent in the lab, illustrated in figures 2.6 and 2.5.

This way, the minimum outlet diameter required for mass flow in each of the funnels was calculated for these five powders, to predict whether or not there would be mass flow when discharging the powders through the funnels.

The results obtained for filler 2A and filler 3 are especially worthy of attention and will be described in detail in the following subsections. The other three powders will be discussed more briefly.

Filler 1A, binder 1A and API 1

The predicted behaviour for filler 1A, binder 1A and API 1 was mass flow with both cells, as can be seen in Table 3.4.

The same trend can be seen here where the minimum outlet opening calculated with the data from cell XS-SV3 is always smaller than that calculated with cell XS-Mr, which comes as a result of the different flow functions. This corroborates once again the idea of cell XS-SV3's data corresponding to a best-case scenario.

Filler 2A

- Cell XS-Mr

At first, the values obtained with the data from cell XS-Mr predicted that there would be arching in every hopper. After validation, these predictions did not agree with experimental findings, so another point with a lower pre-consolidation tension was measured (test 4 on Table 2.1). After obtaining the lower point it became obvious that the measurement made for test 1 shall be considered as an outlier, as shown in Figure 3.9.

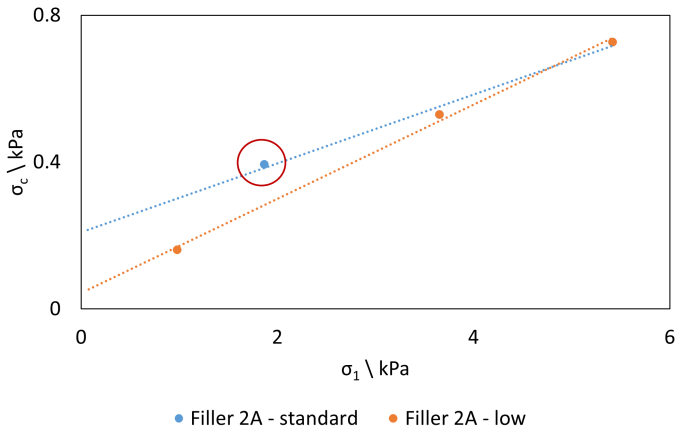

Figure 3.9: Flow functions for filler 2A obtained without test 4 (Standard) or with test 4 (Low).

Based on the data obtained with cell XS-Mr with test 4, the mathematical model predicted that there would be funnel flow in all four hoppers. Thus, one should take extra care when choosing the applied pressures during a yield locus test.

The critical rathole diameter, D_F, was calculated for this powder from the data obtained with this cell. This parameter does not depend on the vertical wall angle, θ', or on the outlet opening diameter. Instead it depends on the diameter of the cylindric part of the silo and on the height of the powder in the silo. A D_F of 4.1 cm was obtained for this powder.

- Cell XS-SV3

Based on the data obtained with cell XS-SV3 the model predicted that there would be arching in all hoppers, since the predicted minimum outlet opening for all hoppers is higher than 4 cm (the real outlet diameter), as can be seen on Table 3.2. Since cell XS-SV3 has a lower limit of applicable normal tensions of 275 Pa, it wasn't possible to perform test 4 with this cell.

Table 3.2: Mathematical treatment of filler 2A.

Cell	Hopper wall vertical angle (º)	Critical σ (kPa)	Critical σ_1 (kPa)	B_{min}(cm)
XS-Mr	All	Funnel flow - $D_F = 4.1$ cm		
XS-SV3	45	0.39	0.16	7.6
	30	0.28	0.15	6.6
	25	0.26	0.15	6.3
	15	0.22	0.14	5.8

Filler 3

- Cell XS-Mr

With the data obtained from cell XS-Mr the mathematical model predicted that there would be mass flow for filler 3 for all hoppers, since the predicted minimum hopper outlet diameter opening was smaller than 4 cm for all hoppers, as shown in Table 3.4.

- Cell XS-SV3

The prediction made with the data obtained with cell XS-SV3 for filler 3 was that there would be funnel flow in all hoppers.

The reason for the difference in prediction for filler 3 lies in the difference between the flow functions yielded by both cells. Since the flow function obtained with cell XS-SV3 was lower than the one obtained with cell XS-Mr, the σ_1 and σ_W values used to compute the angles of internal and wall friction are lower as well. This results in the normal tension values for cell XS-SV3 falling in the zone where the angle of wall friction is higher than the angle of internal friction, as is possible to see in Figures 3.10(b). In practice, this would mean that the friction at the wall would be higher than that at the bulk, resulting in the formation of a rat hole (funnel flow).

Similarly to what was done for filler 2A, the D_F was also calculated for filler 3 with the data from this cell, obtaining a critical rathole diameter of 1.4 cm.

Table 3.3 summarizes the mathematical treatment for filler 3.

Table 3.3: Mathematical treatment of filler 3.

Cell	Hopper wall vertical angle (º)	Critical σ (kPa)	Critical σ_1 (kPa)	B_{min} (cm)
XS-Mr	45	0.13	0.06	3.6 (Mass flow)
	30	0.10	0.06	3.3 (Mass flow)
	25	0.09	0.06	3.2 (Mass flow)
	15	0.08	0.06	2.9 (Mass flow)
XS-SV3	All	Funnel flow - D_F = 1.4 cm		

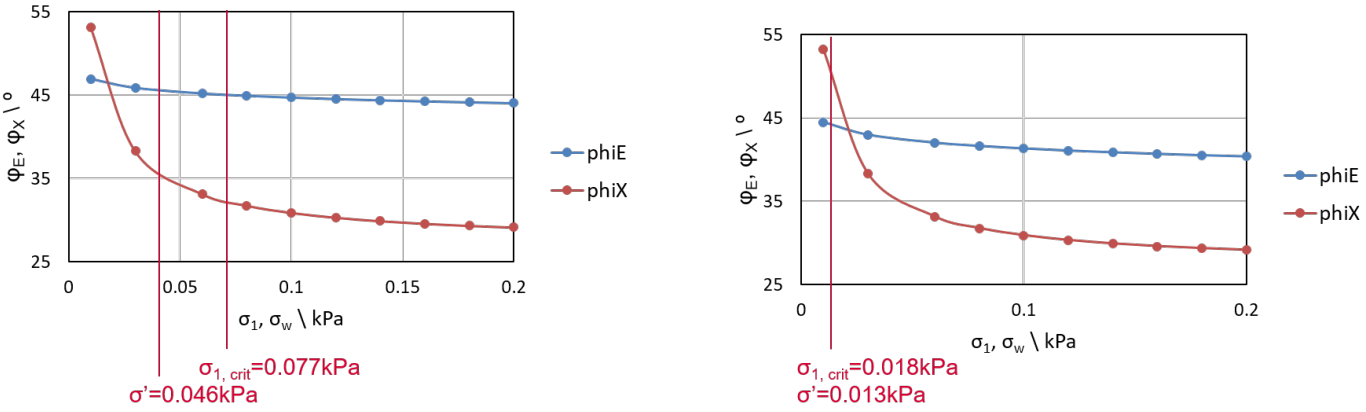

(a) Cell XS-Mr.

(b) Cell XS-SV3.

Figure 3.10: Curve $\varphi_X(\sigma_W)$ obtained for filler 3 with the data of cells XS-WM and XS-WL0 combined and curves $\varphi_E(\sigma_1)$ obtained with each cell. The red lines represent the vertical stresses rigorously calculated at the outlet of the lab-scale silos.

3.2.3 Validation

To validate the predictions made by the model built to mathematically treat the experimental data, 800 g of each of the five powders were discharged through the funnels, in order to visually verify whether there was mass flow, funnel flow or arching.

Table 3.4 synthesises the results obtained by mathematically treating the data obtained from RST-XS.s, comparing them with the results obtained when flowing 800 g of the studied powders on the lab-scale hoppers represented in figures 2.5 and 2.6.

The results showed that the model predicted reality accurately for filler 1A, binder 1A and API 1, while for the more free-flowing powders like filler 2A and filler 3 the prediction was only partially accurate.

In the case of filler 2A, Cell 1 yielded data with which a D_F of 4.1 cm was obtained. This diameter is very close to the actual outlet diameter of the validation funnels, which means that the prediction is very close to experimental results.

In the case of filler 3, however, the critical rathole diameter predicted was of 1.4 cm and although the validation funnels have an outlet opening diameter of 4 cm, funnel flow still happened.

Table 3.4: Prediction of flow resultant of mathematical treatment of yield locus and wall yield locus data obtained with cells XS-Mr, XS-SV3 and XS-WM and comparison with real scenario.

Powder	Hopper vertical slope (°)	Mathematical treatment according to Mehos [69]			Result (real)
		B min (cm)		Result (predicted)	
		XS-Mr	XS-SV3		
Filler 2A	45	—-	7.56	XS-Mr:Funnel flow	Funnel flow
	30	—-	6.59		Funnel flow
	25	—-	6.32	XS-SV3:Arching	Mix flow
	15	—-	5.81		Mass flow
Filler 3	45	3.62	—-	XS-Mr:Mass flow	Funnel flow
	30	3.27	—-		Mix flow
	25	3.15	—-	XS-SV3:Funnel flow	Mix flow
	15	2.94	—-		Mass flow
Filler 1A	45	33.80	26.72	Arching	Arching
	30	27.92	24.63		
	25	26.49	23.92		
	15	24.05	22.48		
Binder 1A	45	28.33	12.95	Arching	Arching
	30	23.18	11.40		
	25	21.97	10.96		
	15	19.99	10.13		
API 1	45	42.07	27.70	Arching	Arching
	30	32.91	21.85		
	25	31.10	20.67		
	15	28.29	18.79		

It is worth noticing that with any shear tester, yield loci can be determined more accurately for more cohesive powders than for free-flowing ones, as would be the case of filler 3 and filler 2A (see Table 3.4), since the shear stresses are higher and thus the yield locus lies at higher shear stresses, so that small differences occurring from test to test have less (relative) influence on the size of the unconfined yield strength stress circle and, thus, on unconfined yield strength. Furthermore, for free- or good-flowing materials often more extrapolation is required to determine the unconfined yield strength which increases the influence of fluctuation of the individual shear points further. The result is the tendency the less cohesive a material is the more the unconfined yield strength fluctuates from test to test. [80]

Even though the prediction for filler 3 and filler 2A wasn't as accurate as it has been for other powders, the model still predicted that the rathole generated by filler 3 would be smaller than the one by filler 2A, which coincides with experimental observations, as one can see here in Figure 3.11.

These results show that the mathematical model applied can be used in future studies knowing

(a) Filler 2A.

(b) Filler 3.

Figure 3.11: Ratholes formed by filler 2A and filler 3 in funnels with a wall vertical angle of 45°.

however that it yields more accurate predictions for more cohesive powders.

3.2.4 Warren-Spring equation validation

The Warren-Spring equation was fitted to the experimental data obtained with both cells for the five powders tested in this first stage of the work developed. After fitting the Warren-Spring equation, the unconfined state and the steady state Mohr circles were calculated as well. The results obtained can be found in Appendix D. The results obtained with the two different reasonings for the steady state Mohr circle were coherent having a deviation in the range of 10^{-6} to 10^{-2}.

The deviation between the results obtained in this mathematical treatment and the results included in the output of the equipment *RST-XS.s* was also calculated and is presented in Table 3.5.

Table 3.5: Deviation scale range between some data obtained through the mathematical treatment and the data obtained in the output of *RST-XS.s*.

Step	Deviation scale range
τ_c	$10^{-2} - 10^{-1}$
σ_c	$10^{-2} - 10^{-1}$
σ_1 (R1)	$10^{-5} - 10^{-3}$
σ_1 (R2)	$10^{-4} - 10^{-2}$

It is possible to see that the values of τ_c and σ_c are the ones that most deviate from those obtained by the equipment. This can be explained due to the fact that the Warren-Spring curve is being fitted to three points only and that these three points are not in a low shear zone. This way, there is a big extrapolation of the data in the lower normal tensions zone, inducing a higher error in these calculations. Knowing that the unconfined state Mohr circle highly depends on the values of cohesion (τ_c) and tensile strength (T), it was to be expected that this value also presented a higher error compared to the major

principal stresses. These last ones however, take into consideration two extra points – the center of the circle and the pre-shear point – reducing the error associated with these.

It is important to refer that between each yield locus test, the sample is sheared back to the steady state, in order to ensure test reproductibility. This way, the fact that the steady state Mohr circle includes the pre-shear point is what lowers the error associated with the calculation, since the pre-shear point is the reference point for the yield locus tests made.

It was possible to notice a logarithmic correlation between the values of n and flowability. In fact, the lower the FFC, the higher the value of n (see Figure 3.12, which is coherent with the literature). [70]

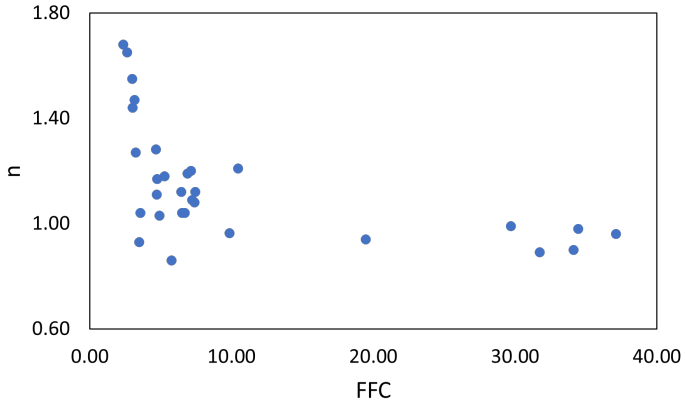

Figure 3.12: Logarithmic correlation between n and FFC.

Since n is supposed to be a value between 1 and 2, the values of n that at first were lower than 1 were forced to be equal or higher than 1. [8] [70] It is worth mentioning that the more cohesive a powder is, the more pronounced is the curvature of the Warren-Spring equation and thus, the more difficult is the fitting of the equation to the three non-low shear data points. This way, it is suggested that these tests should be repeated with lower consolidating stresses and a higher number of data points.

Ideally, the tangency point between the steady state Mohr circle and the yield locus curve would be the end of the yield locus curve. However, it was verified that, experimentally, this point always fell between the second and third consolidation stresses instead of after the third consolidation stress and the pre-shear point. This might be explained by the fact that the consolidation stresses are quite high and that the last consolidation stress is very close to the pre-shear consolidation stress.

In this work there was no way to measure tensile strength in order to compare it with the results obtained from the Warren-Spring equation. Nonetheless, other authors have found that this calculation is coherent with experimental measurements, such as Triñanes et al. [83]

Nevertheless, the equation presents a good fit to the experimental data and may be used in the future to predict the Mohr circles' placement and the values that may be calculated from them.

4

Results - Part II: Powder characterization

Contents

Following the selection of the most adequate cells to perform rheology tests in the area of pharmaceuticals, various pharmaceutical powders were tested with cells XS-Mr and XS-WL0 and were compared considering their function.

4.1 Fillers

Filler 3 and filler 4 are both excipients engineered to ensure good powder flow. [84] [85] [86]

Filler 2A, 2B and 2C are all powders that were optimized for direct compression and are characterized by large spheroidal agglomerates formed because of the water present. [87] [88] Finally, filler 1 is used as a compression aid, as a flow enhancer, and a filler for direct compression of tablets. It may also be used as a binder for wet granulation. Each grade of filler 1 corresponds to a specific particle size distribution and moisture content. [89] Additional data for these powders is present in Appendix A, including SEM imaging and Particle Size Distribution.

- **Flow functions**

Many of the powders tested fall into the same region of the plot (central region) illustrated in Figure 4.1 except for filler 1A which seems to have the worst flowability and filler 3, which has the best flowability.

It is also possible to verify that filler 1A reached considerably higher σ_1 values for each pre-consolidation tension than the other powders. In fact, in Figure A.2(a) it's possible to see that filler 1A particles include a significant fraction of elongated particles, which tend to re-orientate when subjected to normal tensions, affecting force transmission and frictional behaviour. These particles tend to orient themselves in flow-direction, perpendicular to the major principal stress' direction, which allows for a higher compaction and, consequently, higher values of σ_1. [90] [91] [92] [93] [94]

The ratios FFC calculated for each test performed are presented on figures 4.2 to 4.4 and it follows the same order as the flow functions presented in Figure 4.1.

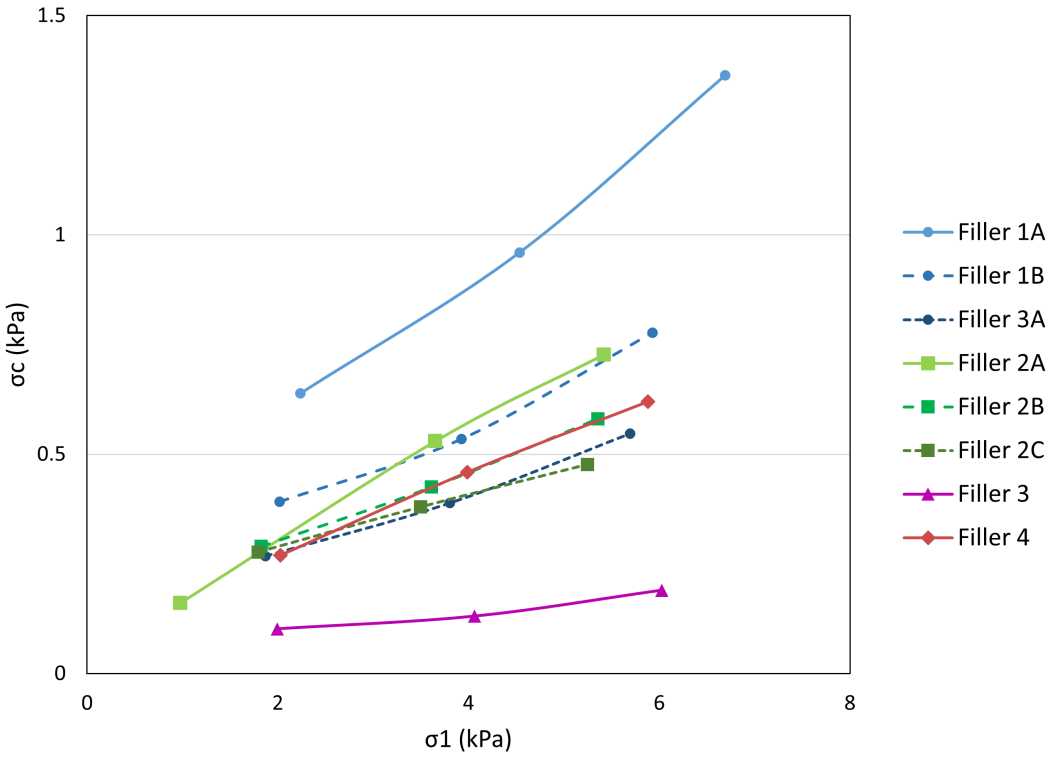

Figure 4.1: Flow functions obtained with cell XS-Mr for all the filler powders tested.

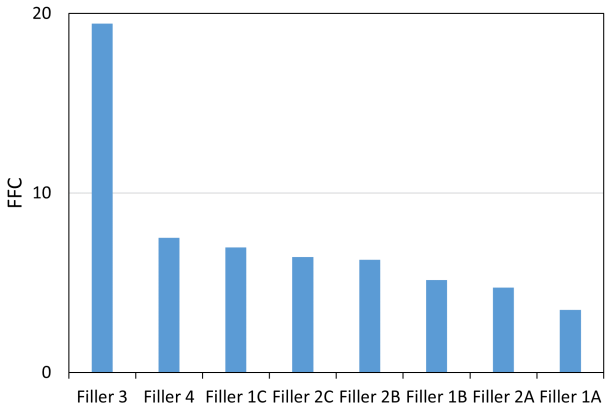

Figure 4.2: FFC at $\sigma_{pre} = 1kPa$

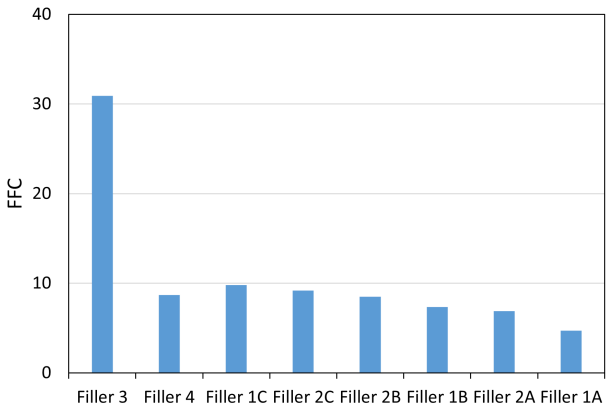

Figure 4.3: FFC at $\sigma_{pre} = 2kPa$

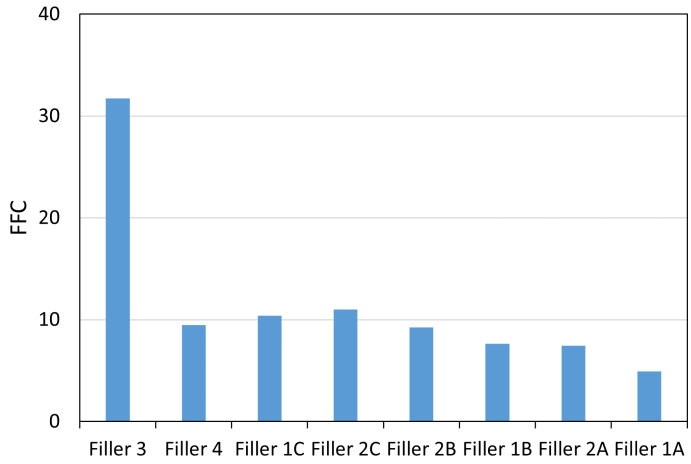

Figure 4.4: FFC at $\sigma_{pre} = 3kPa$

- **Bulk density**

The results for bulk density are aligned with the expectations: three distinct groups of bulk densities can be observed (fillere 1, filler 2 and filler 3 and 4) and an increase in density between the filler 1 and the filler 3 and 4 powders was verified.

Filler 2B and filler 2C had very similar bulk density curves with very close values of apparent bulk density (0.57 g/cm^3), which is coherent with the literature, which states that the bulk density for both of these products is of 0.58 g/cm^3. [87] [95]

Filler 1B and filler 1C also have very close apparent bulk densities (0.34 g/cm^3 and 0.35 g/cm^3, respectively), which also coincides with the values in literature. [96]

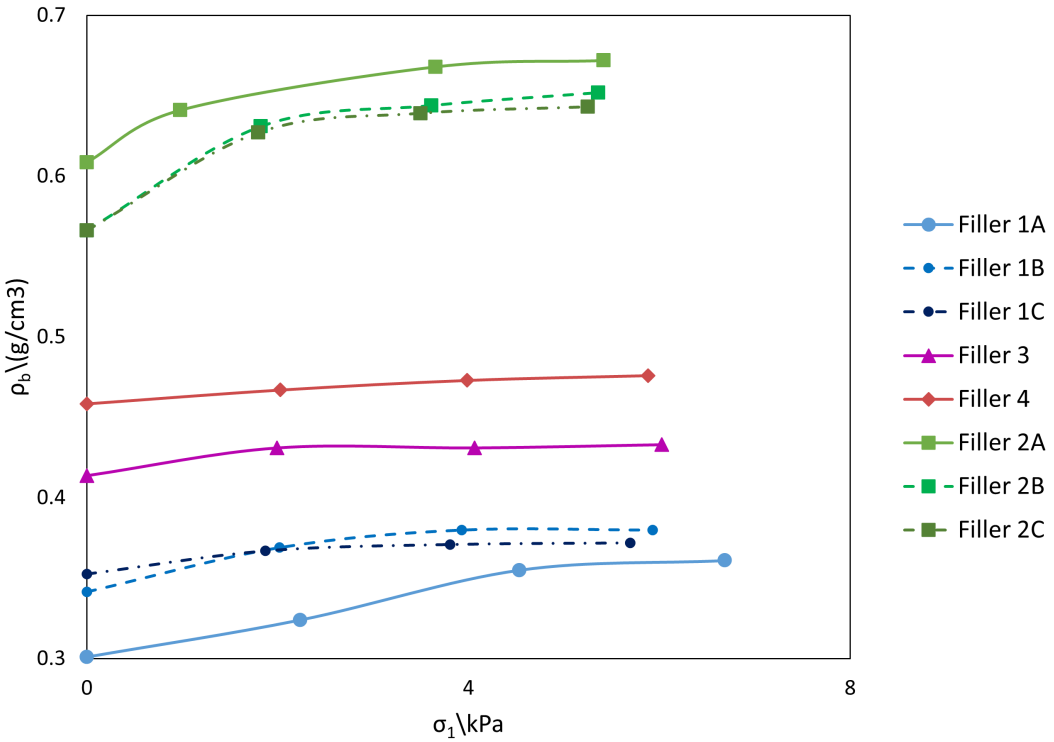

Figure 4.5: Bulk densities obtained for each filler powder in each Yield Locus test.

- **Effective angle of internal friction**

Figure 4.6 shows the effective internal frictions of the filler powders obtained experimentally by shear testing.

Azéma et al. [91] [92] found that φ_E varies nearly linearly with the elongation parameter, which is related to the aspect ratio, since there is an increase in friction forces and contact orientations with the increase of this parameter. Thus, filler 1A has the highest φ_E of all filler powders, which makes sense since it is the filler powder with the most elongated particles. In fact, the three powders that exhibit higher φ_E are the ones that have elongated particles (filler 1A, filler 1B and filler 3).

For the non-elongated particle powders, Figure 4.6 shows that the internal friction angles for filler 2B, filler 4 and filler 1C are very similar (maximum deviation from average of 1.6%), which suggests that particle size does not have a strong influence in the effective internal friction angle or at least not in this size range. This conclusion is in agreeance with what was investigated by Liu, et al. (2015) [97].

Aside from this, a trend is seen among the filler 2 powders, where an increase in finer particles content leads to an increase in φ_E. The particle size distributions for the filler 2 powders can be found in reference [95], while the particle size for filler 2C can be found in Appendix A. This trend is in agreement with the literature, which states that for powders with particle sizes of smaller order (Pharmaceutical

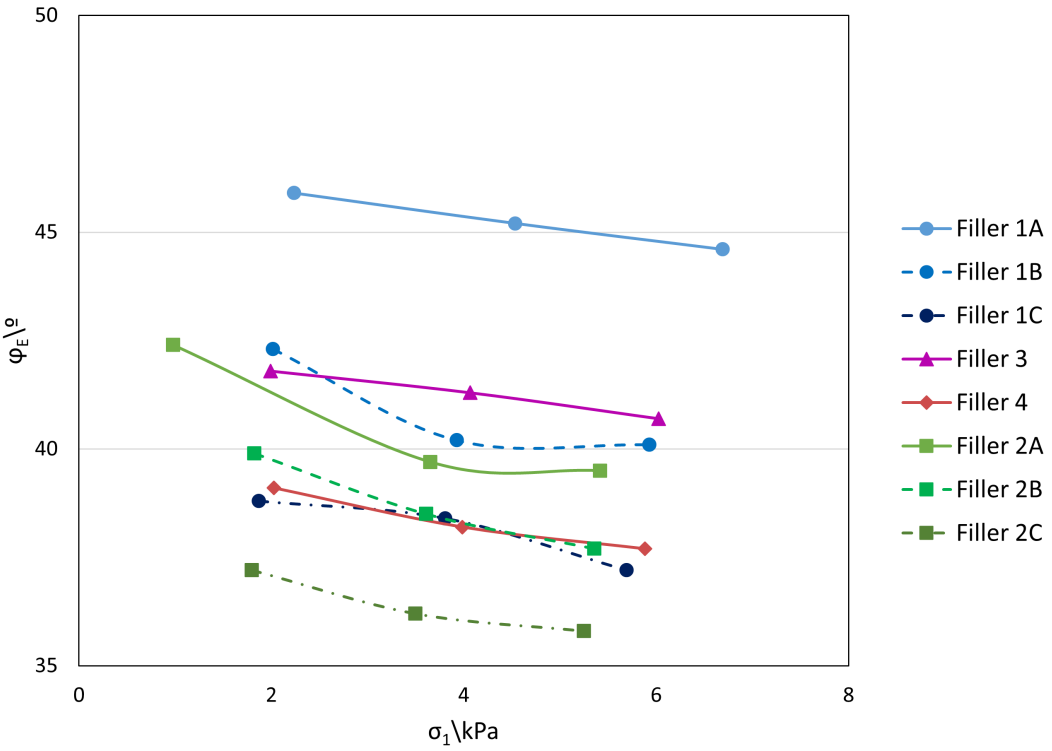

Figure 4.6: Effective internal friction angles obtained for each filler powder in each Yield Locus test.

powders, for example), generally, the increase in fines content is unfavorable to flowability properties [8], while for powders of larger particle sizes (sand, for example), an increase in fines content leads to a decrease in the internal friction angle. [98] [99]

- **Wall friction**

Figure 4.7 shows the wall friction angle curves obtained for each filler powder. Once again the elongated particles show higher φ_X values, with filler 1A having the highest values.

It's possible to notice with the filler 1 powders the trend where larger particles lead to lower friction angles. However, the inverse trend is observed for the filler 2 powders.

It is worth noticing that while for higher normal wall tensions filler 2A presents the lowest wall friction angles, for lower normal wall tensions it shows high friction at the wall.

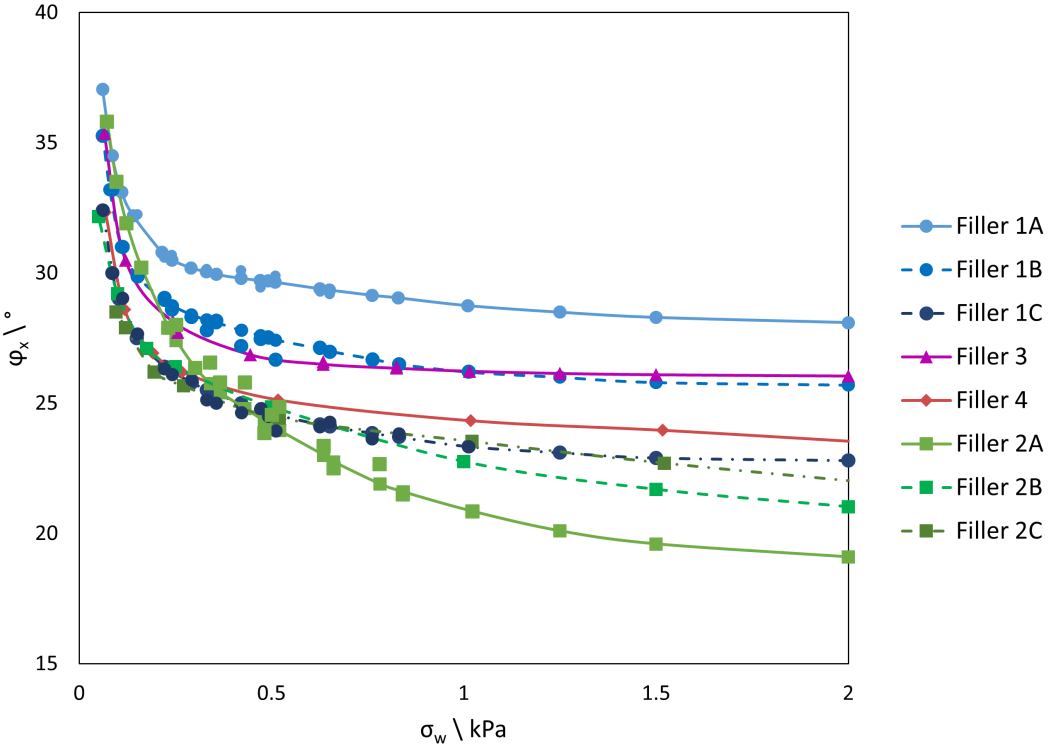

Figure 4.7: Wall friction angle curves obtained for each filler powder.

- **Mathematical treatment**

Table 4.1: B_{min} calculated with the experimental data obtained for the filler powders studied for a hopper with a vertical wall angle of 30°.

Powder	B_{min} (cm)
Filler 1A	27.9
Filler 1B	14.7
Filler 1C	9.9
Filler 3	3.3
Filler 4	3.4
Filler 2A	funnel flow*
Filler 2B	6.5
Filler 1C	7.2

*Critical rathole diameter of 4.1 cm

Table 4.1 shows that flowability can't be predicted from only one of the properties considered (flow functions, FFC, bulk density, internal angle of friction, wall friction angle). Instead, one must take into account all these parameters, since they all are part of the context of a bulk solid.

This way, if mass-flow is desired, then filler 3 is the material that requires the smallest hopper outlet, while filler 1A is the one that requires the largest outlet, as expected.

In the previous chapter it was discussed that filler 2A only generates funnel flow for the hoppers modeled (vertical wall angles of 45°, 30°, 25° and 15°). If funnel flow is acceptable, then the critical rathole diameter will be of 1.8 cm.

4.2 Binders, API, disintegrant and lubricant

Aside from the 8 Filler powders tested, three binders, two API, one disintegrant and one lubricant were tested as well. These few powders were analysed together.

Binder 1A and binder 2 are two polymers widely used in the formulation of Amorphous Solid Dispersions (ASD) to increase the solubility of Biopharmaceutical Classification System (BCS)' class II and IV powders, having a major role in the pharmaceutical industry. [100] [101] [102]

API 1 is used as an antibiotic to treat bacterial infections. It can also be used as medication to treat severe acne. [103] [104] API 2, on the other hand, is used to stop the growth of fungi and treat a variety of fungal infections. [105] [106] Here in this chapter, an additional test set is performed with sieved API 1 in order to study the effect of sieving in the results obtained with the RST-XS.s.

The disintegrant included in this study is disintegrant 1, which is used in low concentration in tablet formulations (typically 0.5% to 5% in %(m/m) [57] [58]) to facilitate the rapid disintegration of tablets and granules and enhance drug dissolution rates. [107] [108]

Finally, the lubricant used in this study is lubricant 1. It is also used in low concentrations (typically 0.2% to 1% in %(m/m) [57] [58]) and it is used to decrease friction between particles and in the interface between the particles and the wall, ensuring a consistent physical performance of tablets. [109] [110] [111]

Additional data for these powders is present in Appendix A, including SEM immaging and Particle Size Distribution.

- **Flow functions**

Figure 4.8 displays the flow functions obtained for the seven powders discussed in this subsection and the sieved API 1 powder.

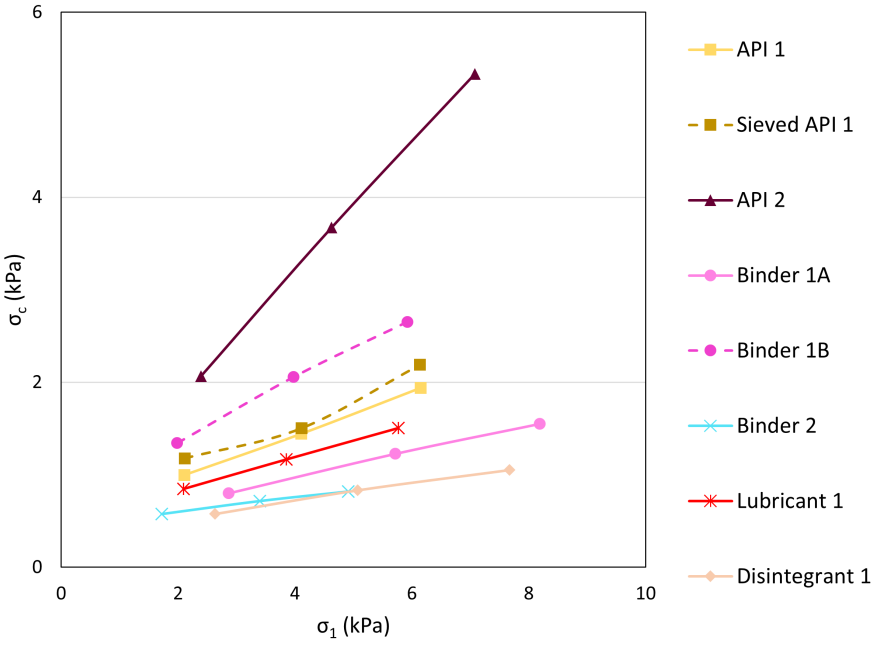

Figure 4.8: Flow functions obtained with cell XS-Mr for the binder, API, disintegrant and lubricant powders tested.

In Figure 4.8, both binder 1B and API 2 stand out for having higher unconfined yield strengths, followed by API 1 and lubricant 1. API 2 has the smallest particle size of all the powders studied and its particles are cristalline and angular (see Figure A.9(a) in Appendix A). Binder 1B is composed also of small-sized particles and its particles have a shriveled surface, which can be seen in Figure A.8. Having these irregular surface shapes, adjacent particles can establish a high number of interparticle contacts, which results in an increase in unconfined yield strength according to Johanson et al. [112], for small stresses.

On the other hand binder 1A, disintegrant 1 and API 2 as well stand out for having high major principal stresses. Looking at figures A.7, A.1(a) and A.9(a), binder 1A has the most elongated particles, followed by disintegrant 1. API 2 is composed of a fraction of particles that display a little elongation. Once again, this is an effect of prolate anisotropy, just like the case of filler 1A, filler 1B and filler 3 in section 4.1. [90] [91] [92] [93] [94]

Regarding the flow function of sieved API 1, it is very similar to that of non-sieved API 1, but obtaining slightly higher unconfined yield strengths with tests 1 and 3 of Table 2.1. Thus, sieving did not have a pronounced effect on the flow function of the material.

Figures 4.9 to 4.11 display the values of FFC obtained for each binder, API, disintegrant and lubricant powder studied, where we notice that the FFC ratio values calulated for each test follow the same order as the flow functions in Figure 4.8, as expected.

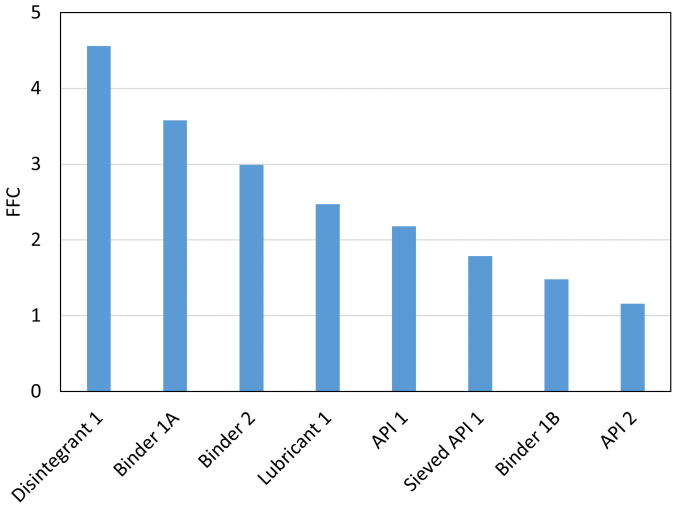

Figure 4.9: FFC at $\sigma_{pre} = 1kPa$.

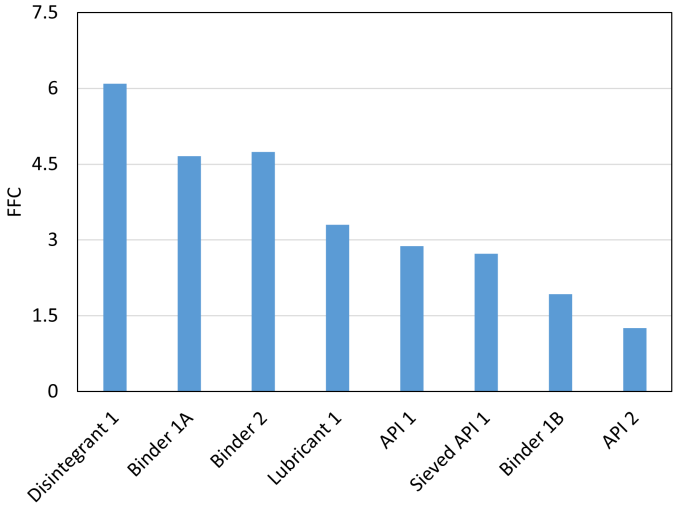

Figure 4.10: FFC at $\sigma_{pre} = 2kPa$.

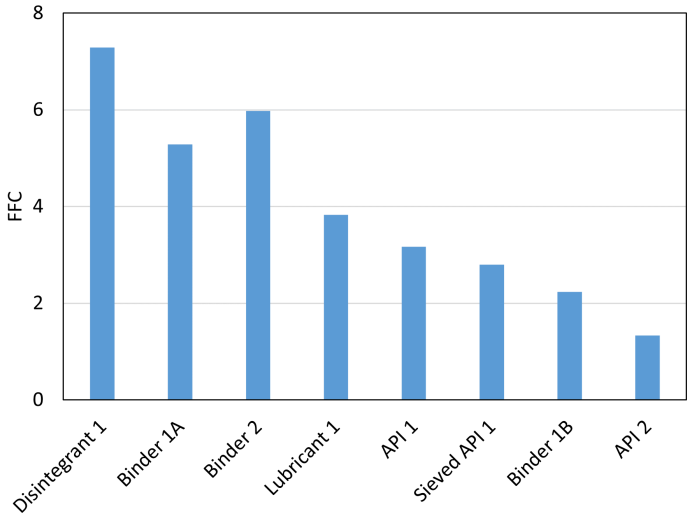

Figure 4.11: FFC at $\sigma_{pre} = 3kPa$.

Similarly to the observations made for the flow functions, sieved API 1's FFC value at a pre-consolidation tension of 2kPa (corresponding to test 2 from Table 2.1) is very close to that of non-sieved API 1, which suggests that the test 2 from Table 2.1 with sieved API 1 might have been an poorly executed and should be repeated (since the tests with the sieved material were only performed with an n=1).

On the other hand, there is a drastic difference between the FFC values obtained for binder 1A and

binder 1B, which was to be expected due to the reasons explained before.

- **Bulk density**

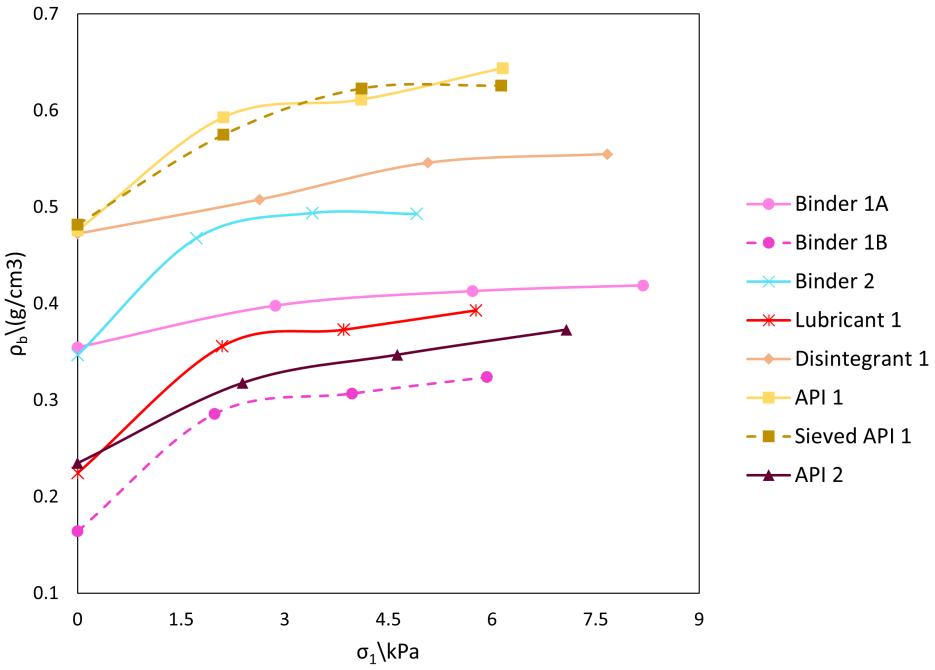

Figure 4.12: Bulk densities obtained with cell XS-Mr for the binder, API, disintegrant and lubricant powders tested.

In Figure 4.12 the bulk densities for the binder, API, disintegrant and lubricant powders studied in this section are represented.

Binder 1A shows a considerable decrease in bulk density when spray dried, being binder 1B the powder with the lowest bulk density out of the fifteen powders studied. This is in agreement with the literature and happens due to the high void fraction on the binder 1B bulk, since its particles' surface is covered in wrinkles and since its particles are typically hollow, which can be seen in Figure A.7(a) in appendix A. [100] [113]

Binder 1A and binder 2 have very similar un-tapped bulk densities (0.35 g/cm^3), but binder 2 is more compactable than binder 1A. The same happens with disintegrant 1 and API 1, being API 1 the most compactable of the two.

While API 1 and API 2 are both APIs, they belong to different classes of drugs. API 2 belongs to azole antifungals and API 1 belongs to tetracycline antibiotics. [103] [105] Therefore the difference between their bulk density curves was to be expected, being API 1 considerably denser than API 2.

The bulk density curves for both the sieved and non-sieved API 1 powders are very similar. Therefore, we can conclude that sieving has had no impact on the bulk density and compactability of API 1.

- **Effective angle of internal friction**

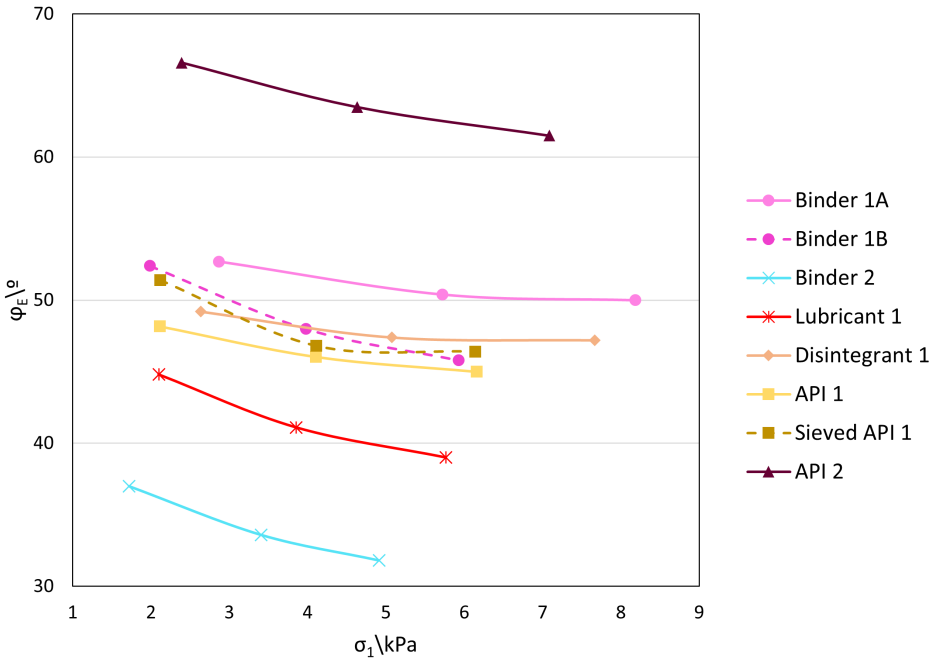

Figure 4.13: Effective internal friction angles obtained for each binder, API, disintegrant and lubricant powder in each Yield Locus test.

API 2 is the powder that exhibits the highest angles of internal friction of all the fifteen powders tested, being the powder with stronger friction in the bulk. As explained before, API 2 is made of a fraction of elongated angular particles and, as discussed before, the higher the elongation factor, the higher the φ_E, as well as the higher the level of angularity of a particle, the higher the φ_E. [8] [114] [115] Therefore, the shape of API 2's particles could explain the high values of φ_E that this powder demonstrates.

Binder 1A is second powder with higher effective internal friction angles and the binder powder that exhibits the highest φ_E, since it is the only binder powder tested that has elongated particles. [91] [92]

Binder 1B also presents an elevated friction in between particles, which has to do with the particle shape. [112] It's worth noticing that binder 1B no longer has elongated particles, which means that the values of σ_1 attained are no longer exceptionally high compared to those of binder 1A.

Binder 2 has the lowest angles of internal friction of all the powders tested, since its particles are mostly spheroidal. In fact, spheroidal particles tend to flow easier than non-spheroidal particles and spheroidal particles with a larger particle size tend to flow easier than those with a smaller particle size. [8] [91] [92] [112]

The difference between the sieved and non-sieved API 1 curves is more pronounced for the φ_E measurements, especially for the lower normal tensions.

- **Wall friction**

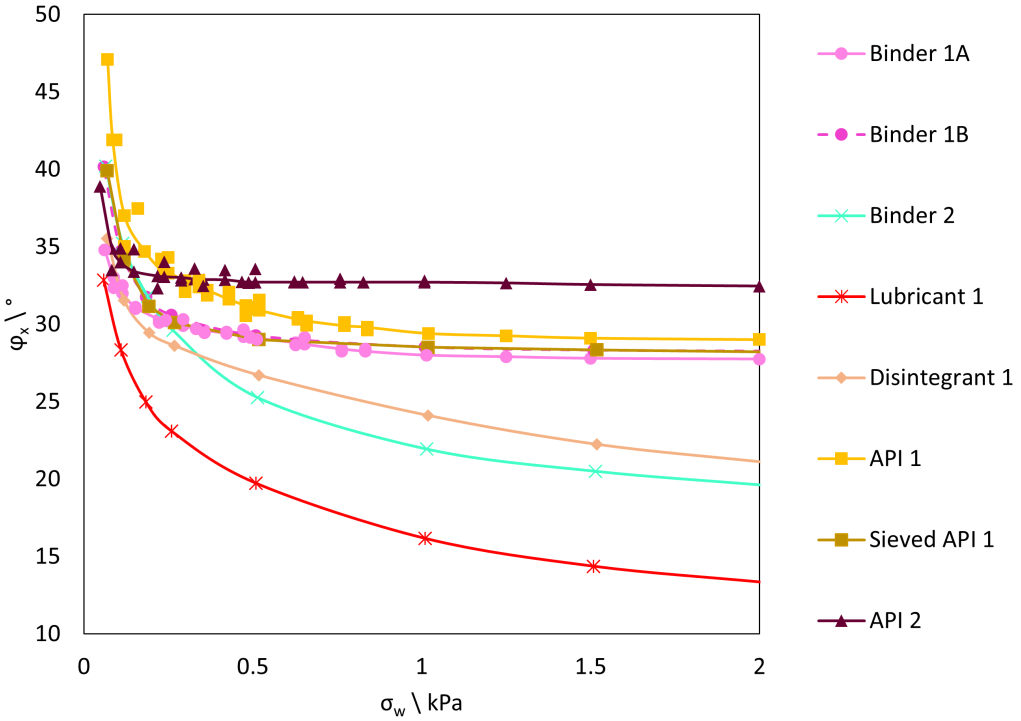

Figure 4.14: Wall friction angle curves obtained for each binder, API, disintegrant and lubricant powder.

Figure 4.14 displays the $\varphi_x(\sigma_w)$ curves obtained for the powders studied in this section.

On a first glance, lubricant 1 stands out for having the lowest wall friction angles. Being a lubricant, lubricant 1's main feature is having low wall friction. [49] In Figure 4.14 it's possible to see that lubricant 1 has indeed low wall friction angles in comparison with the φ_X curves obtained for the other powders. This low wall friction is a result of lubricant 1's particle shape, which can be seen in A.11(a). This powder has plate-like particles that have both a polar and a lipophilic part. These particles delaminate and the lipophilic part is oriented so that waxy hydrophobic layers are formed. The low-friction characteristic of this powder is due to the weak links between the layers formed, allowing them to slide relatively to each other. This also allows the particles to coat adjacent particles when making blends, which lowers the bulk and wall friction of the blend as a whole. [116] [117] [118] [119] [120]

API 2, on the other hand, stands out for stabilizing in the highest wall friction angle. It was reported that smaller particle sizes yield larger wall friction angles [8] [121] [122], which would make sense here, since, aside from lubricant 1, the particles with the smallest particle sizes show the highest wall friction angles (API 2, API 1 and binder 1B).

Regarding the effect of sieving, the difference between the φ_X curves for sieved and non-sieved API 1 is more pronounced at lower normal wall tensions than at higher σ_W, where the curves stabilize in

close values (28.2° and 29° for sieved and non-sieved, respectively).

Binder 1A and binder 1B display very similar φ_X curves for higher normal wall tensions, but for lower normal wall tensions, binder 1B presents higher wall friction angles. This would suggest that Spray Drying these particles had little to no effect on their wall friction.

- **Mathematical treatment**

Table 4.2: B_{min} calculated for the binder powders for a hopper with a vertical wall angle of 30°.

Powder	B_{min} (cm)
Binder 1A	23.2
Binder 2	26.7
Binder 1B	105.6
Lubricant 1	46.2
Disintegrant 1	15.7
API 1	32.9
Sieved API 1	39.8
API 2	258.9

The powder that requires the smallest outlet diameter to be able to have mass flow is disintegrant 1, while API 2 is the one that requires the largest outlet opening, followed by binder 1B.

There is a drastic difference between binder 1A and binder 1B. This difference is in agreement with the FFC values obtained in figures 4.9 to 4.11. These results are also coherent with the fact that bulk density impacts flowability deeply, since during the spray drying process there is a considerable decrease in bulk density. This decrease is confirmed by Figure 4.12.

These results show once again that many parameters, such as bulk density, must be taken into consideration in order to assess the flowability of a powder.

The B_{min} calculated for lubricant 1 and disintegrant 1 show that these powders do not have a very good flowability. Disintegrant 1 has a B_{min} value in line with that of filler 1B, while lubricant 1 has a B_{min} larger than the ones obtained for all filler powders. The typical concentration (%(m/m)) of these powders in tablet formulations is very low (0.5% to 1% for lubricant 1 and 0.5% to 5% for disintegrant 1 [57] [58]), therefore it would be expected that including these powders in blends would not have a substantial influence in their flowability. However, due to lubricant 1's characteristics as a lubricant, adding this component in small proportions enhances flowability considerably. It is important to mention that, although disintegrant 1 and filler 1B do not seem to have great flowability, they are often considered a good standard for some processes, such as direct compression. In fact, Calvin Sun (2011) [123] refers in his study that filler 1B can be considered the reference for minimum acceptable flowability for direct compression.

Regarding the effect of sieving on the final result for B_{min}, there is a slight difference between the yielded B_{min}, being that sieving increased the minimum outlet opening.

4.3 Comparison between all powders studied

In this section a plot of the flow functions of all powders tested except for API 2 is presented, summarizing the results obtained, which is displayed in Figure 4.15. API 2's flow function was removed due to its high values of σ_1 and σ_c, improving the resolution of the plot for the other flow functions.

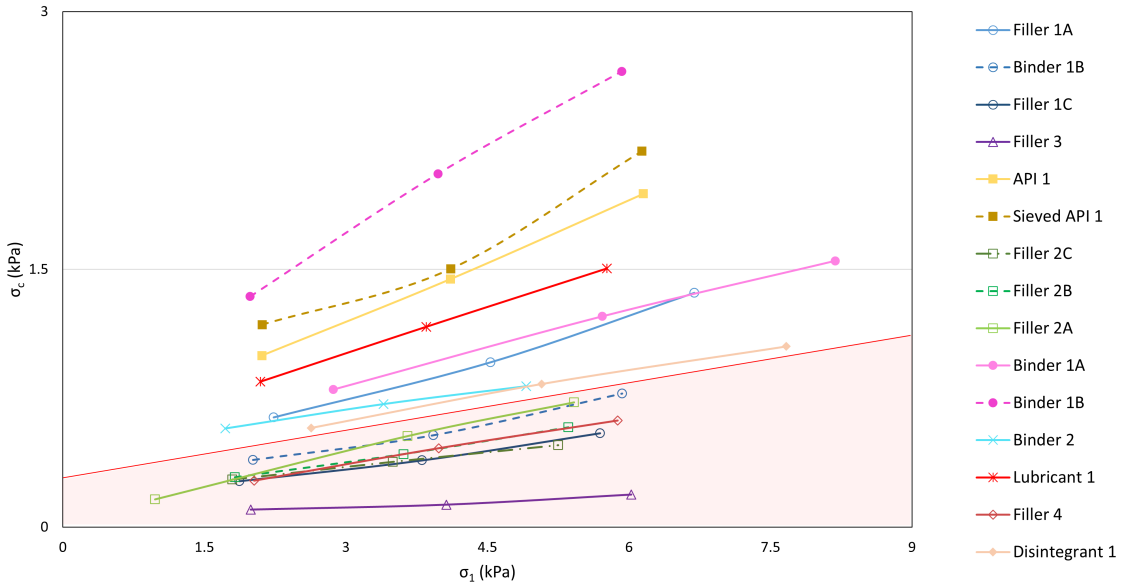

Figure 4.15: Flow functions obtained with cell XS-Mr for all powders tested except for API 2. The shaded region of the plot separates the fillers from the other powders tested.

In Figure 4.15 it is possible to notice that the filler powders have the lowest flow functions, being all present in the purple shaded region, except for filler 1A. This tells us that fillers have better flowability than the other excipients used in a formulation, which makes sense, since the fillers correspond to 20% to 90% of a formulation [57] [58] and must be selected also based on their flow properties. [124] Filler 1A not being in the shaded area was also to be expected, since this powder has a dual function as a filler-binder, having a flow function and FFC values very similar to those of binder 1A. [89] [125]

5

Results - Part III: Blend characterization

Contents

Five blends were prepared according to Table 2.4 for this stage of the work developed. These blends were characterized in order to predict what their behaviour during tableting would be like and to understand the influence of the blend in the flowability of the API used (API 1).

The blends were used to produce tablets and a mass uniformity test was performed, to further understand the influence of the formulations used in the attributes of the final tablets.

5.1 Blend characterization

- **Flow functions**

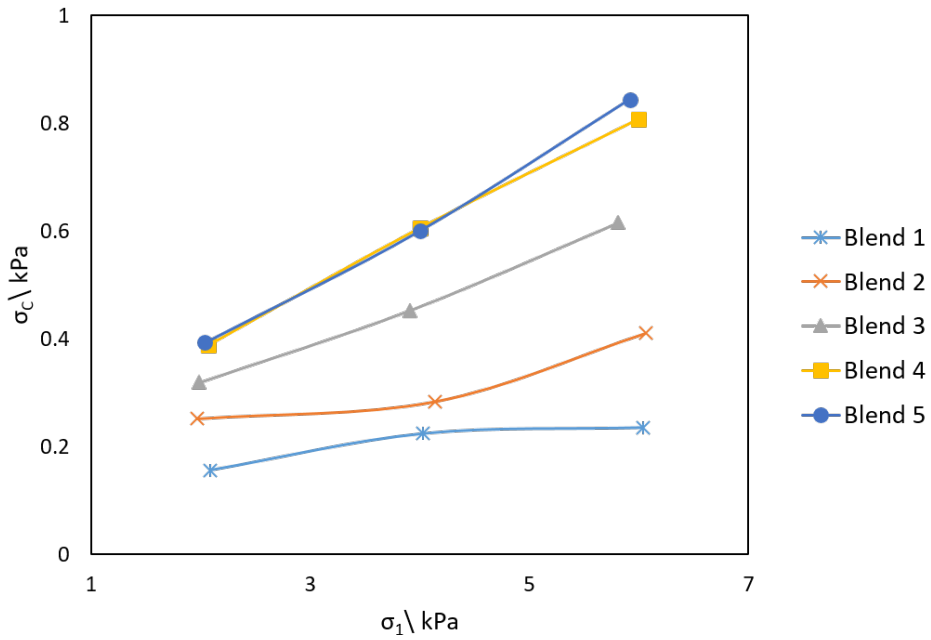

Figure 5.1: Flow functions obtained for the five blends.

From blends 1 through 4 there is a gradual increase in σ_c and in σ_1, which was to be expected, since the quantity of API used (API 1) with a small particle size and angular particles is increased and the materials with best flowability were reduced.

Even though Blend 5 has the same amount of API 1 as Blend 3, its flow function is very similar to that of Blend 4, which means that the replacement of filler 3 for filler 1B and glidant 1 had a considerably negative impact on flowability. In fact, filler 3 is the powder tested that showed the best flowability. In theory, filler 1B and glidant 1 should be a reasonable combination to substitute filler 3. However, filler 1B is the filler powder that requires the second largest outlet opening when calculating B_{min}, as explained in Subsection 4.1, so the results obtained (slight decrease in flowability) were to be expected.

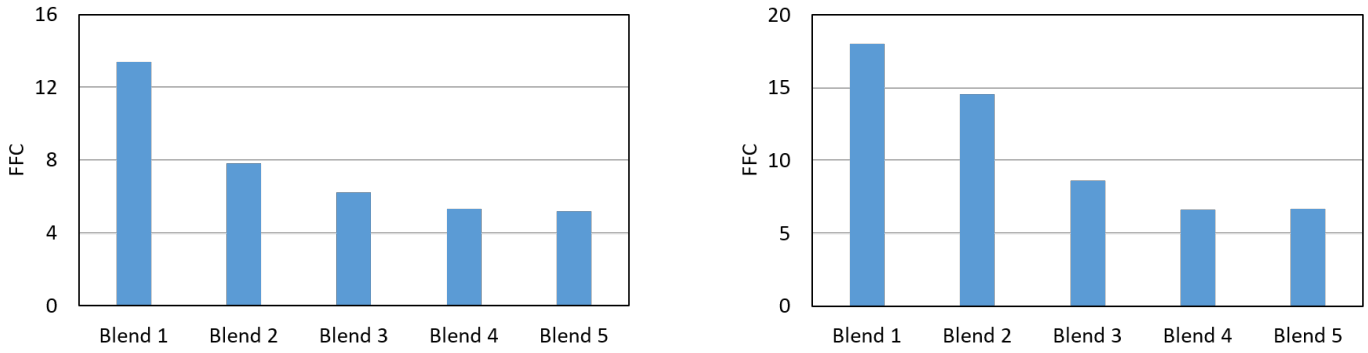

(a) $\sigma_1 = 1$ kPa

(b) $\sigma_1 = 2$ kPa

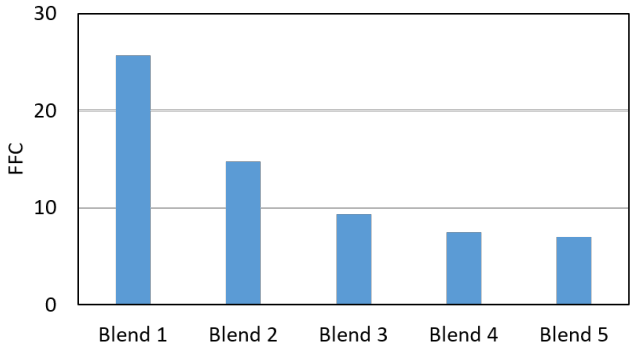

(c) $\sigma_1 = 3$ kPa

Figure 5.2: Ratios FFC calculated for each test performed for each blend.

The FFC ratio values follow have the same behaviour as the flow functions represented in Figure 5.1, showing that there is a decrease in flowability from Blends 1 to 4 and that Blend 5 has a flow behaviour similar to Blend 4.

- **Bulk density**

It is possible to observe an increase in bulk density from blends 1 to 4, which was to be expected, since API 1 (ρ_{b0}=0.48 g/cm^3) is one of the powders tested with higher bulk density and higher compressibility.

Blend 5 however shows a great reduction in bulk density compared to Blend 3, which comes from the substitution of filler 3 (ρ_{b0}=0.41 g/cm^3) by filler 1B (ρ_{b0}=0.34 g/cm^3) and glidant 1 (ρ_{b0}=0.048 g/cm^3 [126]).

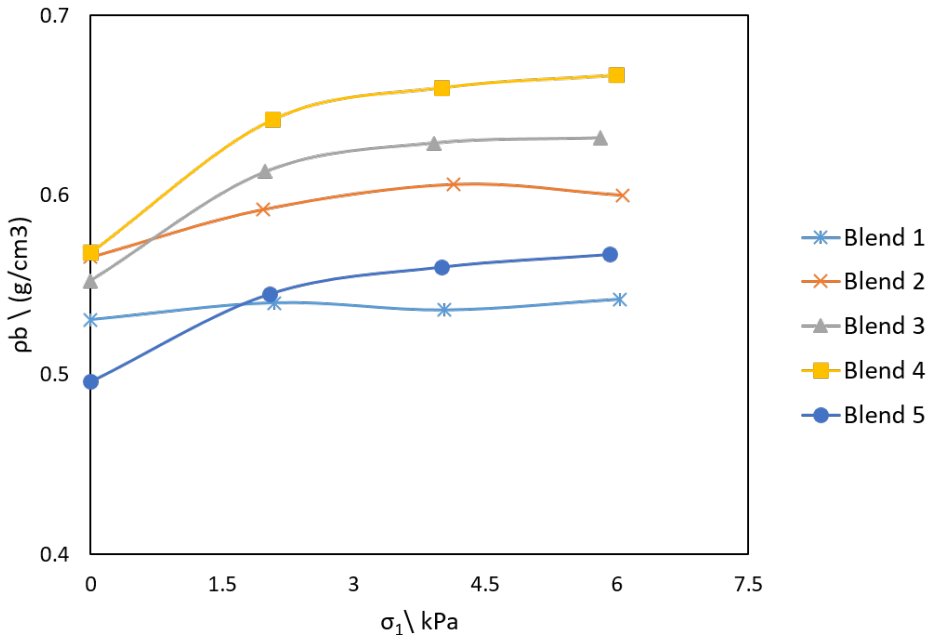

Figure 5.3: Bulk densities obtained for each blend in each Yield Locus test.

- **Angle of internal friction**

At a first glance over Figure 5.4, the curve for Blend 2 does not follow the normal trend for a $\varphi_E(\sigma_1)$ plot. This might indicate that the measurement made for test 2 of Table 2.1 might be wrong.

The internal friction angle obtained for test 1 of Table 2.1 also appears to be very high, which might also indicate a possible mistake while performing this test.

These anomalies prevent the extraction of solid conclusions on the evolution of φ_E with the increase of API 1. Theoretically it would make sense to see an increase in this angle from blend to blend, since API 1 has high values of φ_E itself. In fact, this increase in φ_E is verified from Blend 3 to Blend 4.

Finally, from Blend 3 to Blend 5 a slight decrease in φ_E is observed. Filler 1B's internal friction angle curve is also slightly below that of filler 3. Zegzulka et al. [127] state that glidant 1 has an angle of internal friction of 30.6° $\pm$ 0.9° (measured in FT4 rheometer), so this powder might also contribute to the decrease in φ_E.

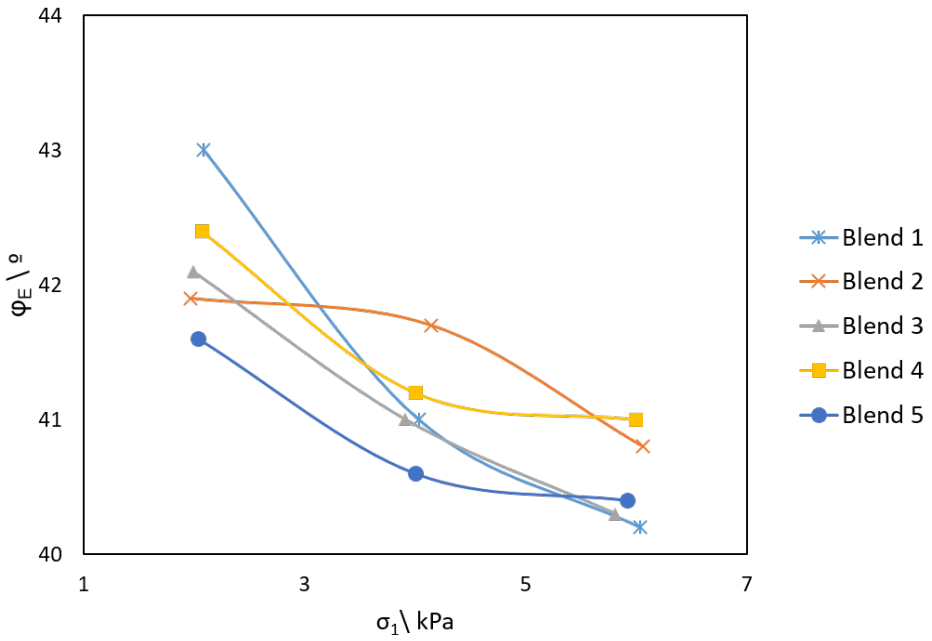

Figure 5.4: Internal friction angles obtained for each blend in each Yield Locus test.

- **Angle of wall friction**

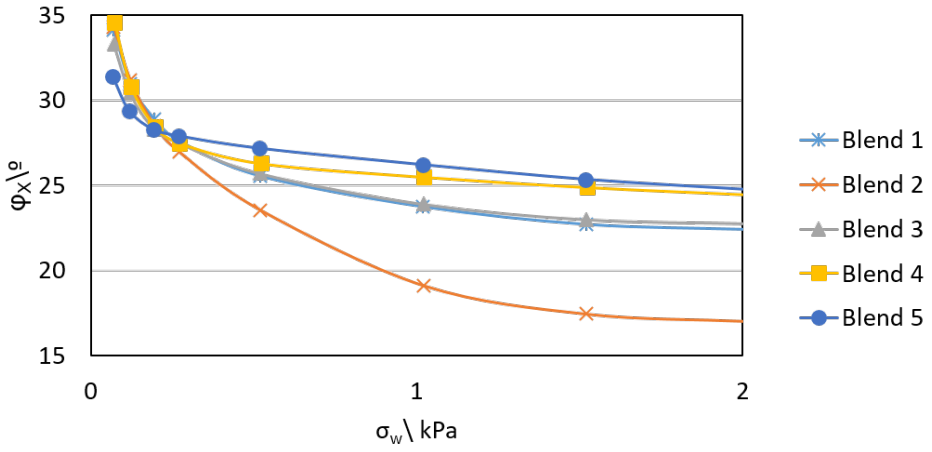

Figure 5.5: Wall friction angles obtained for each blend in each Yield Locus test.

Looking at Figure 5.5 the φ_X curves overlap for lower normal wall tensions and deviate for higher wall tensions.

Blend 2 shows a considerable decrease in φ_X for higher tensions. In further studies this test should be repeated to investigate this difference.

Blends 1 and 3 have very similar curves, just like blends 4 and 5 and between the two sets of

curves there is a variation of about 2°. This variation is negligible, so the wall friction angle was mostly unaffected by the addition of API or the substitution of filler 3. It was expected for the substitution of filler 3 not to have a great influence on φ_X, since filler 3's and filler 1B's φ_X curves are very similar (see Subsection 4.1).

5.1.1 Mathematical Treatment

The data obtained were treated to calculate B_{min} for a lab-scale silo with a wall vertical angle of 30°.

The values for B_{min} obtained for each blend are presented in Table 5.1

Table 5.1: B_{min} calculated for the blends for a hopper with a vertical wall angle of 30°.

Blend	1	2	3	4	5
B_{min} (cm)	6.0	7.4	7.7	8.4	8.8

A trend can be seen from blend 1 to blend 4 where the B_{min} increases, which was to be expected, since a component with poor flowability was added consecutively.

From the data obtained with Blend 5 a B_{min} very similar to that of Blend 4 was calculated, so there was an increase in the minimum necessary outlet opening for mass flow from Blend 3 to Blend 5.

From the rheological information obtained, one could conclude that in further processing (i.e. during tableting) the blends would have flow problems during dye filling in the nest step of this work. However, knowing that the *Riva Piccola* feeder has an external flow aid (i.e. rotating blades), it is to be expected that there will be little to no weight variation in the tablets produced.

A prediction of the FFC ratios for each blend for each pre-consolidation tension was made in the "law of mixtures" framework: the FFC values obtained for each individual component were multiplied by the component's %(v/v). The results obtained are compared in Table 5.2 with the real FFC ratios obtained for each blend.

In general, predictions show a considerable error in comparison with the real FFC ratios obtained, especially those calculated for Blend 3, which presents the highest errors.

It is possible to conclude that the law of mixtures does not hold for blend FFC prediction, being fallible and not accurate. This could be justified by the blending process and what it involves. In this process, some phenomena exist such as the breaking of agglomerates due to high shear forces [128] or the coating of the particles by the lubricant [117] or the overall interaction between powder particles [129]. However, this estimation can be used for comparison purposes, since it predicts accurately that FFC increases with an increasing pre-consolidation normal tension and that it decreases from blend to blend.

Table 5.2: Predicted FFC values of blends based on single excipients' FFC values.

Blend	Pre-consolidation tension	predicted FFC	real FFC	error (%)
Blend 1	1 kPa	12.1	13.4	9.8
	2 kPa	18.8	18.0	4.4
	3 kPa	19.5	25.7	23.9
Blend 2	1 kPa	10.1	7.8	29.2
	2 kPa	15.6	14.6	7.1
	3 kPa	16.3	14.75	10.2
Blend 3	1 kPa	8.1	6.2	30.0
	2 kPa	12.4	8.6	43.8
	3 kPa	13.0	9.44	37.4
Blend 4	1 kPa	6.1	5.3	14.7
	2 kPa	9.2	6.6	39.5
	3 kPa	9.7	7.4	30.4

5.1.2 Principal Component Analysis

The first PCA performed took into account every measurement made for each Yield Locus test (see Table 2.1 and Figure C.2).

Using the tool *Autofit*, a total of 4 PC was suggested by the software. However, with only two PC an explained variance (R2X) of 78% is already attained (with a predicted variance, Q2, of 62%). The scores and loadings plot generated with this model can be found in Appendix C.

Using this model, it was apparent that the measurements made for each variable ended up grouping close together (e.g. the measurements of φ_E at a σ_{pre} of 1, 2 and 3 kPa were very close together in the loadings plot) and opening the *Correlation Matrix* from the *Statistics* tab these variables had correlation factors above 90%. Therefore, the average of these measurements was taken into account instead, reducing the number of variables used as input to 12. A correlation matrix for these 12 variables was created from the tab *Statistics*, displayed in Table 5.3.

Looking at Table 5.3, we can observe that there is a strong correlation between the tapped and untapped bulk densities. The major principal stress also strongly correlates to the angle of internal friction at steady-state flow, φ_{SF}. This is the angle obtained between a line that intersects the origin and the pre-shear point and the XX axis. This correlation was to be expected, knowing that the pre-shear point is one of the major factors needed to be able to draw a Mohr's circle and that this circle is what allows the calculation of the major principal stress. [8] [1] [130]

The unconfined yield strength (σ_c) and the cohesion (τ_c) strongly correlate as well, with a linear correlation. This has been remarked by Sun et al. (2019) [131] and Wand et al. (2016) [132] before. It's worth to notice as well that these two variables vary non-linearly with FFC and FF$_\rho$, describing a

Table 5.3: Correlation table obtained for the final PCA model with 21 observations and 12 variables.

	σ_1	σ_c	ρ_{b0}	ρ_b	φ_E	φ_{Lin}	φ_{SF}	FFC	FFρ	τ_c	B_{min}	x_{50}
σ_1	**1.00**	0.39	-0.25	-0.31	0.72	0.74	**0.93**	-0.17	-0.24	0.30	0.19	-0.52
σ_c		**1.00**	-0.60	-0.41	0.88	-0.24	0.65	-0.60	-0.65	**1.00**	0.83	-0.80
ρ_{b0}			**1.00**	**0.93**	-0.44	0.30	-0.36	0.34	0.55	-0.61	-0.50	0.64
ρ_b				**1.00**	-0.36	0.10	-0.35	0.11	0.34	-0.42	-0.37	0.47
φ_E					**1.00**	0.24	**0.91**	-0.37	-0.43	0.84	0.66	-0.77
φ_{Lin}						**1.00**	0.56	0.34	0.33	-0.32	-0.36	-0.01
φ_{SF}							**1.00**	-0.28	-0.34	0.59	0.40	-0.69
FFC								**1.00**	**0.96**	-0.60	-0.39	0.88
FFρ									**1.00**	-0.65	-0.43	0.74
τ_c										**1.00**	0.84	-0.76
B_{min}											**1.00**	-0.84
x_{50}												**1.00**

logarithmic variation, as illustrated in figures C.3 to C.6. These findings are also coherent with what is described by Wang et al. (2016) [132].

FFC and FFρ also exhibit a strong correlation, which was to be expected, since FFρ is calculated based on FFC, using Equation 5.1, with ρ_w = 1000 kg/m^3 (liquid water at 0 ℃, 1 bar). [8] [133]

$$FF_\rho = FFC \cdot \frac{\rho_b}{\rho_w} \tag{5.1}$$

This way, variables τ_C, FFρ, ρ_{b0} and φ_{SF} were removed from the model for further simplification, leaving 8 variables.

In the new model, *Autofit* only suggested two PC, attaining an R2X of 76%. However, three PC were used, with an explained variance of 88%.

Looking at figures 5.6 and 5.7 and at the contribution of each variable to each PC we can conclude that PC[1] describes mostly σ_c (written as SigC in the model), φ_E, x_{50} (written as d50 in the model), B_{min} and FFC, describing variables related to internal friction, cohesion, particle size and flowability, in a way that powders with higher cohesion and internal friction will have poorer flowability, while powders with higher particle size will tend to flow easier. It's worth noticing that these remarks do not take into account particle shape, which also has a great influence on flowability. These conclusions are coherent with the discussion made in Chapter 4.

PC[2] describes σ_1 (written as sig1 in the model) and φ_{Lin} datapoints, where a powder with higher σ_1 will also have higher values of φ_{Lin} and φ_{SF}.

PC[3] was added, since it is the principal component that best describes bulk density.

Figures 5.8 and 5.9 display the biplots obtained for this model.

API 2 was considered an outlier by the model both in the Hoteling's T2 plot and in the Scores scatter-

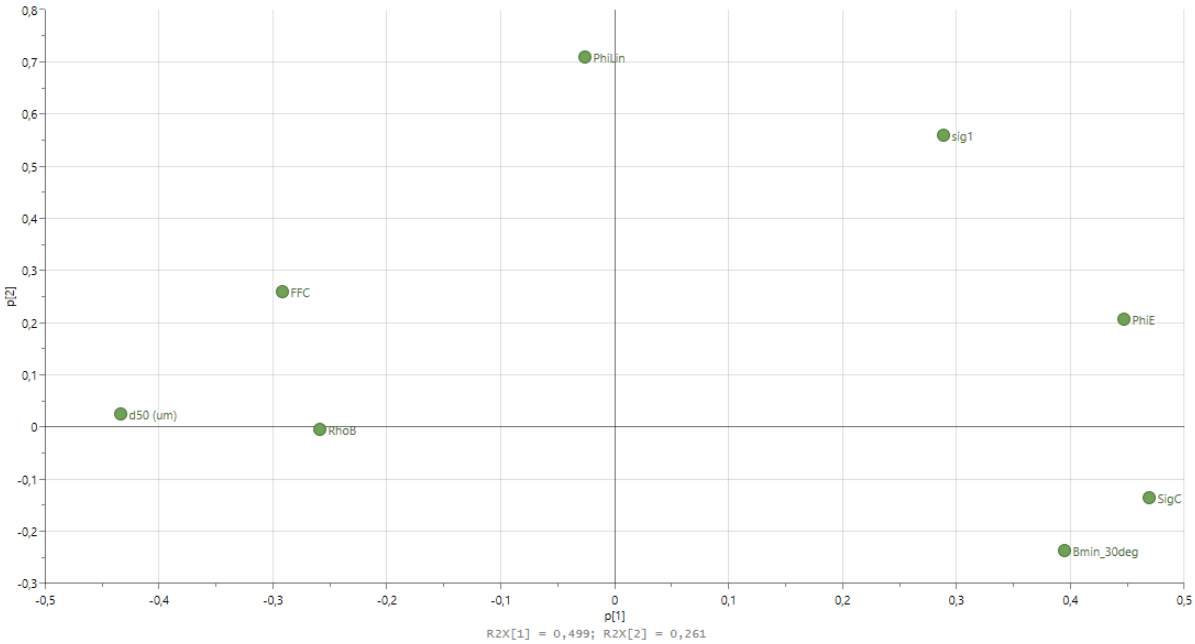

Figure 5.6: Loadings plot obtained with the original PCA model generated with 21 observations and 8 variables for components PC[1] and PC[2].

plot. In the practical scenario, this only means that API 2 is the most different powder out of all powders tested, since the samples being evaluated are different, which is in agreeance with the experimental results obtained.

It is interesting to observe the proximity of Blend 1 to filler 3, since this component constitutes the largest fraction of the blend (50%, see Table 2.4). It is also worth noticing that the blends made are successively dislocating to the right side of the plot with the increase in API 1 content. This happens since the unconfined yield strength of the blends increases with their API content, while the FFC decreases. Blend 5 (see Table 2.4) is closer to filler 1B in comparison to Blend 3, which makes sense, since in this blend filler 3 was replaced by filler 1B and glidant 1. Besides this, we highlight that the blends are located in the plot toward the region that is described by better flowability in general, which suggests that these blends could be used in the manufacture of tablets with API 1, since they increase this API's flowability considerably.

PC[1] separates the filler powders and the blends from the rest of the powders due to the fact that these powders flow easier, clustering in the left section of the plot, while the rest of the powders are in the right side of the plot, tending to have higher σ_c and φ_E values, leading to higher B_{min} values as well.

In Figure 5.9 the powders are clearly organized by their bulk density, being the powders with higher bulk density closer to the superior left corner, while those with lower bulk density are closer to the inferior right corner. Once again, the filler powders and the blends are clustered in the left region of the plot, having typically higher bulk densities than the other powders tested.

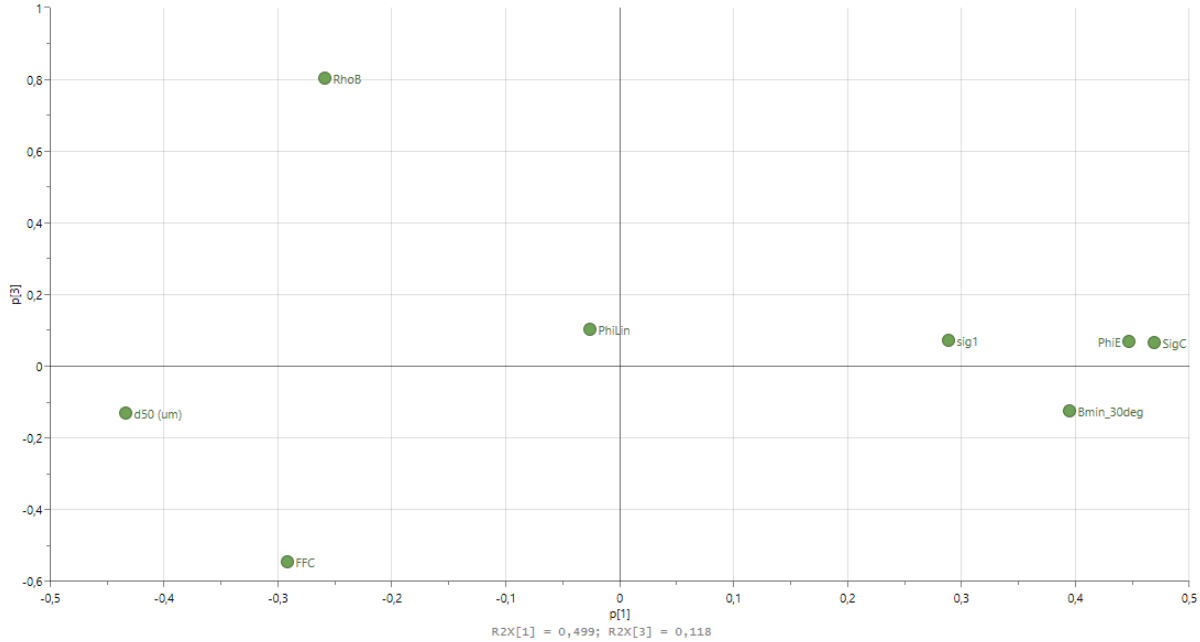

Figure 5.7: Loadings plot obtained with the original PCA model generated with 21 observations and 8 variables for components PC[1] and PC[3].

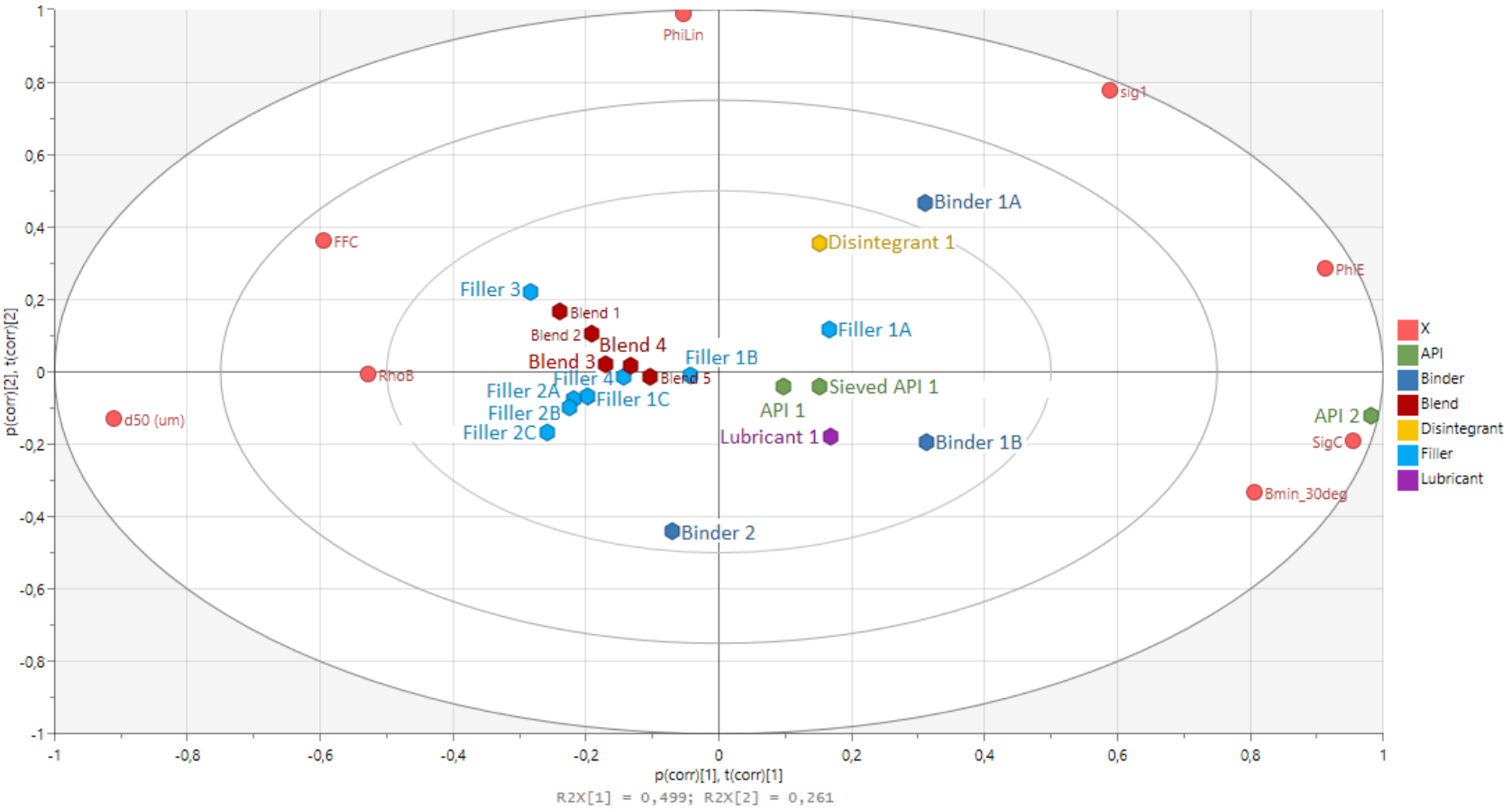

Figure 5.8: Biplot plot obtained with the original PCA model generated with 21 observations and 8 variables for components PC[1] and PC[2].

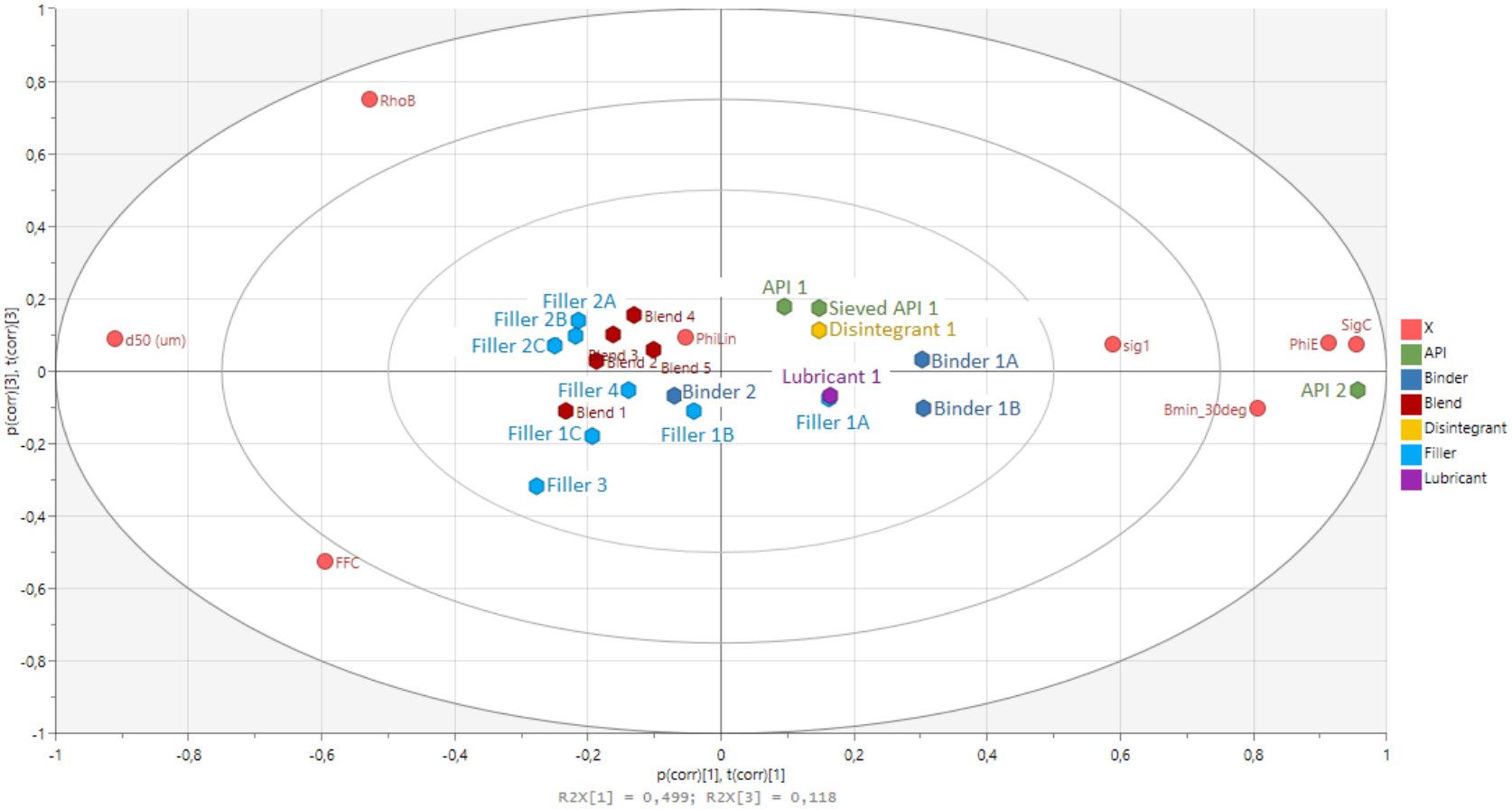

Figure 5.9: Biplot plot obtained with the original PCA model generated with 21 observations and 8 variables for components PC[1] and PC[3].

5.2 Tableting

After characterization, the blends were used to produce tablets using five (in some cases four) different conditions. Before the production of a batch with a new blend, the process parameters needed to be adjusted. Table 5.4 shows the filling depth adjusted for each blend and the minimum and maximum normal force exerted by the punches. For blends 1 and 2 only four tableting conditions were used, while for the rest of the blends a fifth condition with a faster turret speed (75 rpm) was used. It's possible to verify that the variation between the forces exerted by each punch is not very large.

Table 5.4: Parameters adjusted for tableting.

Blend	Filling depth (mm)	Condition	Minimum punch force (kN)	Maximum punch force (kN)
1	6.72	1	6.02	6.34
		2	5.48	5.87
		3	5.57	6.09
		4	6.10	6.42
2	6.72	1	8.70	9.21
		2	8.95	9.55
		3	9.11	9.62
		4	8.78	9.71
3	6.19	1	8.71	9.70
		2	9.93	10.32
		3	10.01	10.61
		4	8.04	8.71
		5	6.71	7.88
4	6.00	1	10.61	11.06
		2	10.23	11.12
		3	11.21	11.67
		4	7.88	8.78
		5	7.30	7.96
5	6.60	1	7.46	7.80
		2	6.59	7.64
		3	7.55	7.89
		4	5.26	5.71
		5	4.33	4.65

5.2.1 Dicharge rate and feeding time

The filling time (the time available for the discharge of powder from the punch to the die), T_{fill}, was calculated for each of the turret's speeds, being the results obtained present in Table 5.5.

Table 5.5: Filling time calculated for turret speeds of 30, 50 and 75 rpm.

Turret speed (rpm)	T_{fill} (ms)
30	636.6
50	382.0
75	254.6

Then, the mass discharge rate for each blend at the punch outlet was calculated as well as the time necessary to discharge 250 mg of the blend powder into the die, t_{250}, being the results displayed in Table 5.6.

Table 5.6: Mass discharge rate and time necessary to discharge 250 mg of powder into a dye calculated for each blend.

Blend	$\dot{m}_s$ (kg/s)	t_{250} (ms)
1	0.043	5.8
2	0.047	5.3
3	0.049	5.1
4	0.051	4.9
5	0.043	5.8

These calculations are highly influenced by the bulk density, so we can observe that the results are higher or lower times according to the bulk densities of the blends.

This way, theoretically it is possible to produce tablets with weights of 250 mg with these blends and conditions, since the t_{250} is lower than T_{fill} for all conditions. This was validated experimentally via the production of tablets using the Riva Piccola classica with module (see Figure 2.8) and it was indeed possible to produce these tablets without problems.

5.2.2 Mass variation

Looking at Table 5.4 one can already know to some extent to expect in respect to the mass of the tablets: small mass variations. Figures 5.10 and 5.11 represent the standard deviations associated with each batch produced. Both figures represent the same set of data, but in different displays, to ease interpretation. In Figure 5.10, the RSD is represented for each blend, varying in terms of turret/feeder speed. In Figure 5.11, the RSD is represented for each condition, varying with the blends.

No patterns were detected in Figure 5.10, suggesting that turret and feeder speed may have no influence on tablet mass variation. However, in Figure 5.11, there is a consistent increase in RSD from blends 2 to 4, suggesting that the increase in the content of the poorly flowing API and, therefore, the increase in bulk density and cohesion, does influence the mass variation, increasing it. These findings are coherent with the literature. [134]

In fact the relative standard deviations obtained for the tablets weighed are very low (considering that the European Pharmacopoeia states that when performing a mass uniformity test, "the tablets comply with the requirements if not more than 1 individual mass is outside the limits of 85–115% of the average mass. The tablets fail to comply with the test if more than 1 individual mass is outside these limits, or if 1 individual mass is outside the limits of 75–125% of the average mass." [135] [136]) In this case, the highest absolute deviation of an individual tablet's mass to the average mass is of 2.6%.

The low deviations suggest once again that the blend used might be a good blend to produce tablets with API 1. However, we must not discard the possibility of having had a better-than-average batch of API 1. Therefore further studies should be made on these formulations and API.

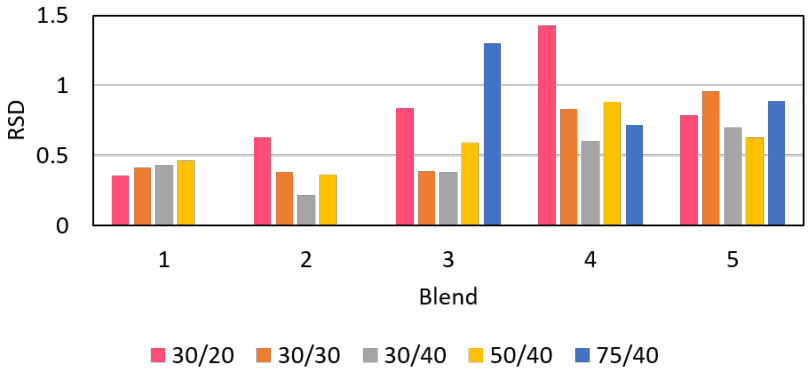

Figure 5.10: Relative standard deviation to the average tablet weight obtained for each tableting condition and each blend, varying the turret and feeder speed for each blend.

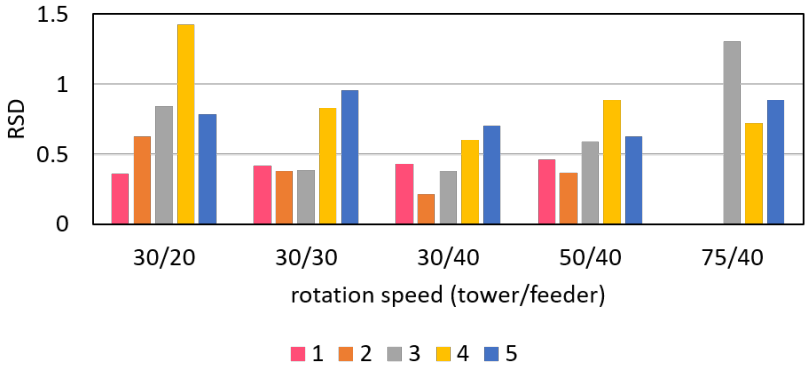

Figure 5.11: Relative standard deviation to the average tablet weight obtained for each tableting condition and each blend, varying the blend for each condition.

6

Conclusion

Results from Part I, where five powders of different cohesions (FFC between 2.2 and 19.5 at pre-consolidation stress of 1kPa) were tested, performing a total of 58 shear tests and 44 wall friction tests, showed that XS-Mr generates higher cohesion values for powders than XS-SV3, and the latter represents, in general, a best-case scenario in terms of minimum orifice for powders to flow. XS-WL0 wall friction shows to be more adequate at smaller stresses, and therefore more representative of smaller scale processes. Also, this cell covers a wide range of compression tensions and can be used also for large scale processes, being more versatile than XS-WM. Therefore, the most adequate cells to analyse pharmaceutical powders from the four cells studied are cell XS-Mr and cell XS-WL0. It is important to mention that for comparative purposes of flowability characterization, the same cells must be used throughout the whole study, since the geometry of the cells impacts the flow profile of the powder inside the cell. This difference particularly crucial when comparing cells XS-Mr and XS-SV3, since their volumes are considerably different, as well as the geometries in the base and lid. Besides this, further studies should be made with cell XS-Lr0 as well, to understand the advantages of this cell over the two shear cells used.

The fit of the equation of Warren-Spring to the experimental data was assessed and successful and the prediction of the values of σ_1 and σ_c had a very reasonable accuracy. This equation is essential in the analysis and prediction of important parameters for the design of silos (σ_1, σ_c), which allow the good design of silos, avoiding the risk of negatively impacting the final product due to arching or funnel flow problems. An accurate prediction of the values of σ_c and σ_1 was to be expected, since some research has already been done on this topic and had good results. However, in this work, it was seen that the equation has a good fit to the data of not only cohesive powders, but also free-flowing ones. This equation can also be used to predict the values of cohesion (τ_c) and tensile strength (T). For these predictions to be accurate, more than three compression points must be used to trace the yield locus curve and approximate the curvature coefficient of the Warren-Spring equation. However, it must be noticed that in practice, the way the tests are designed using the *RST-XS.s* does not allow the user to perform a great number of tests and obtain many points, since the same sample is used throughout the whole set of tests and slight physical degradation may occur in each test due to the compression forces applied. In the case where a normal tester is used, where one point is obtained per sample, the problem lies with the quantity of material used and a small quantity of tests will be performed to not waste too much of it. Therefore, there is an equilibrium between the accuracy of the Warren-Spring prediction of the cohesion and tensile strength parameters and the amount of powder used or its physical degradation.

In the second part of this work, 74 shear tests and 26 wall friction tests were performed. It is proved that flowability should not be evaluated only by the FFC ratio, but should consider also other shear properties, wall shear parameters and particle shape and size. It is also observed that the equipment

yields results that are coherent with the characteristics of the powders tested and meet the expectations. In further studies, the results obtained by mathematically treating the data in this section should be validated by flowing the powders through hoppers, as it was done in part I. However, this would imply having a large quantity of all powders tested.

The adapted mathematical model was successfuly adapted and can be used to compare the flowability of powders in silos by comparison of Bmin, the mininum outlet diameter of a hopper that allows mass flow. This parameter is more adequate than FFC to compare the flowability of powders in the same hypothetical bin, since it takes into account many factors that FFC does not, such as the internal friction angle or the wall friction. Nonetheless, care should be taken when analysing the output of the model, since it can also mean that there will be arching or funnel flow. It is also necessary to give an adequate input to the model, with at least three data points. This chapter made it possible to build a uniform database of flowability data for pharmaceutical powders. This mathematical model together with the Warren-Spring equation are useful tools that were proved to be very useful in the design of silos and hoppers.

Finally, in Part III, 18 shear tests and 5 wall friction tests were performed. Here, we see that utilizing blends designed for having excellent flowability characteristics, such as the ones formulated for this work, has a great impact on the flowability of the API used (API 1), decreasing the B_{min} value for a hypothetical hopper with a vertical wall angle of 30° from 32.91 cm (B_{min} estimated for API 1) to 8.4 cm (B_{min} estimated for Blend 4, which contains the highest quantity of API). This part of the work suggests that the formulations used might be indicated for direct compression with this API, since the blends showed great results in terms of rheological tests (Blend 4, with the highest quantity of API had results similar to those of Filler 2B) and and mass variability tests (RSD values below 2.6%) . However, it must be noticed that there might be a chance that the batch of API 1 used was better-than-average in terms of flowability. The quantification of these characteristics is deserving of a more thorough study, hence the author leaves as a suggestion for further studies the investigation on API 1 and the use of the blends mentioned for formulations with this API.

Bibliography

[1] G. Mehos, Ed., *STORAGE AND HANDLING OF BULK SOLIDS*, 1st ed. Westford, MA: www.mehos.net. [Online]. Available: www.mehos.net

[2] S. Fathollahi, E. Faulhammer, B. J. Glasser, and J. G. Khinast, "Impact of powder composition on processing-relevant properties of pharmaceutical materials: An experimental study," *Advanced Powder Technology*, vol. 31, no. 7, pp. 2991–3003, 2020. [Online]. Available: https://www.sciencedirect.com/science/article/pii/S0921883120302351

[3] H. Feise, *CHEMICAL ENGINEERING AND CHEMICAL PROCESS TECHNOLOGY – Vol. II - Handling of Solids – Transport and Storage*. Process Engineering, BASF AG, Ludwigshafen, Germany.

[4] JENIKE and JOHANSON, "The Physical Properties of Bulk Solids; or How to Get Through Airport Security," [Accessed November 2021]. [Online]. Available: https://jenike.com/physical-properties-bulk-solids-get-airport-security/

[5] M. Bradley, R. Berry, and R. Farnish, "Methods for design of hoppers. silos, bins and bunkers for reliable gravity flow, for pharmaceutical, food, mineral and other applications," 2012.

[6] S. V. Søgaard, T. Pedersen, M. Allesø, J. Garnæs, and J. Rantanen, "Application of Ring Shear Testing to Optimize Pharmaceutical Formulation and Process Development of Solid Dosage Forms," *Annual Transaction of the Nordic Rheology Society*, vol. 21, pp. 91–97, 2013. [Online]. Available: http://nordicrheologysociety.org/Content/Transactions/2013/15_SoegaardApplicationofRingShearTestingtoOptimizePharmaceuticalFormulationand.pdf

[7] D. Zurovec, J. Hlosta, J. Nečas, and J. Zegzulka, "Monitoring bulk material pressure on bottom of storage using dem," *Open Engineering*, vol. 9, no. 1, pp. 623–630, 2019. [Online]. Available: https://doi.org/10.1515/eng-2019-0080

[8] D. Schulze, Ed., *Powders and Bulk Solids: Behavior, Characterization, Storage and Flow*, 1st ed. Berlin: Springer, 2010.

[9] A. W. Jenike, “Storage and flow of solids,” *Bulletin No 123*, 1970.

[10] J. Marion, “Preventing flow problems with reliable bulk solids handling equipment design,” [Accessed October 2021]. [Online]. Available: https://www.processingmagazine.com/material-handling-dry-wet/powder-bulk-solids/article/15587856/preventing-flow-problems-with-reliable-bulk-solids-handling-equipment-design

[11] B. Van Snick, W. Grymonpré, J. Dhondt, K. Pandelaere, G. Di Pretoro, J. Remon, T. De Beer, C. Vervaet, and V. Vanhoorne, “Impact of blend properties on die filling during tableting,” *International Journal of Pharmaceutics*, vol. 549, no. 1, pp. 476–488, 2018. [Online]. Available: https://www.sciencedirect.com/science/article/pii/S0378517318305751

[12] H. M. Beakawi Al-Hashemi and O. S. Baghabra Al-Amoudi, “A review on the angle of repose of granular materials,” *Powder Technology*, vol. 330, pp. 397–417, 2018. [Online]. Available: https://www.sciencedirect.com/science/article/pii/S0032591018301153

[13] R. Carr, “Evaluating flow properties of solids,” *Chem. Eng.*, vol. 72, p. 163–168, 1965.

[14] R. L. Brown and J. C. Richards, *Principles of Powder Mechanics: Essays on the Packing and Flow of Powders and Bulk Solids*, 1st ed. Cambridge: Pergamon, 1970.

[15] CouncilOfEurope, *European Pharmacopoeia supplement 5.3*, 5th ed. European Directorate for the Quality of Medicine, 2005.

[16] H. A. Janssen, “Tests on grain pressure in silos.” *Bulletin No 39*, pp. 1045–1049, 1895.

[17] M. Sperl, “Experiments on corn pressure in silo cells – translation and comment of janssen’s paper from 1895,” *Granular Matter*, vol. 8, 12 2005.

[18] A. W. Jenike, “Gravity flow of bulk solids,” *Bulletin No 108*, 1961.

[19] J. Carson, “Andrew jenike: A true visionary in particle technology,” *Procedia Engineering*, vol. 102, pp. 657–660, 2015, new Paradigm of Particle Science and Technology Proceedings of The 7th World Congress on Particle Technology. [Online]. Available: https://www.sciencedirect.com/science/article/pii/S1877705815001605

[20] J. Schwedes and D. Schulze, “Measurement of flow properties of bulk solids,” *Powder Technology*, vol. 61, no. 1, pp. 59–68, 1990. [Online]. Available: https://www.sciencedirect.com/science/article/pii/0032591090800668

[21] J. Orband and D. Geldart, “Direct measurement of powder cohesion using a torsional device,” *Powder Technology*, vol. 92, no. 1, pp. 25–33, 1997. [Online]. Available: https://www.sciencedirect.com/science/article/pii/S0032591097032129

[22] A. M. Rosàs, *Characterization and parametric study of the flow properties of cohesive powders at temperatures up to 850 ºC*. Technical University of Denmark, 2012.

[23] D. McGlinchey, *Characterisation of Bulk Solids*, 1st ed. Oxford: Blackwell Publushing, 2005.

[24] J. Schwedes, "Review on testers for measuring flow properties of bulk solids," *Granular Matter*, vol. 5, pp. 1–43, 05 2003.

[25] PowdersAndBulkSolids, "What is a Shear Test and Why Do I Need One?" [Accessed November 2021]. [Online]. Available: https://www.powderbulksolids.com/instrumentation-control/what-shear-test-and-why-do-i-need-one

[26] C. Woodcock and J. Mason, *Bulk Solids Handling: An Introduction to the Practice and Technology*, 1st ed. Dordrecht: Springer, 1987.

[27] H. Wilms and J. Schwedes, "Interpretation of ring shear tests," *Bulk Solids Handling*, vol. 5, pp. 1017–1020, 1985.

[28] M. G, *Entwicklung eines Ringschergerätes zur Messung der Fließeigenschaften von Schüttgütern und Bestimmung des Einflusses der Teilchengrößenverteilung auf die Fließeigenschaften kohäsiver Kalksteinpulver.Ph.D. thesis.*, 1st ed. Germany: Univ. Karlsruhe, 1976.

[29] H. MJ, "Über die festigkeitseigenschaften gestörter bindiger böden," *Ingeniørvidenskabelige Skrifter A*, vol. 45, 1937.

[30] DietmarSchulze, "The automatic Ring Shear Tester RST-01.pc," [Accessed November 2021]. [Online]. Available: https://www.dietmar-schulze.de/flyer/rst01pc_e.pdf

[31] R. Schmitt and H. Feise, "Influence of tester geometry, speed and procedure on the results from a ring shear tester," *Part. Syst. Charact*, vol. 21, pp. 403–410, 2004.

[32] D. Schulze, "Ring Shear Tester RST-XS.s," 2021, [Accessed September 2021]. [Online]. Available: https://www.dietmar-schulze.de/rstxss_e.html

[33] ——, "Ring Shear Tester RST-XS.s- smaller and more capabilites," [Accessed November 2021]. [Online]. Available: https://www.dietmar-schulze.de/flyer/rstxss_e.pdf

[34] ——, "Ring Shear Tester RST-XS.s - Operating instructions v1.2 ," 2019, [Accessed October 2021].

[35] ASTMInternational, "Standard Shear Test method for bulk solids using the Schulze Ring Shear Tester," [Accessed November 2021]. [Online]. Available: http://www.prabhaproducts.com/certification/D6773qyvt5147.pdf

[36] M. Fayed and L. Otten, Eds., *Handbook of Powder Science and Technology.*, 2nd ed. Boston: Springer, 2002. [Online]. Available: https://link.springer.com/book/10.1007/978-1-4615-6373-0#about

[37] D. Macri, R. Chirone, H. Salehi, D. Sofia, M. Materazzi, D. Barletta, P. Lettieri, and M. Poletto, "Characterization of the bulk flow properties of industrial powders from shear tests," *Processes*, vol. 8, no. 5, 2020. [Online]. Available: https://www.mdpi.com/2227-9717/8/5/540

[38] J. Fitzpatrick, S. Barringer, and T. Iqbal, "Flow property measurement of food powders and sensitivity of jenike's hopper design methodology to the measured values," *Journal of Food Engineering*, vol. 61, pp. 399–405, 02 2004.

[39] L. Marchetti and C. Hulme-Smith, "Flowability of steel and tool steel powders: A comparison between testing methods," *Powder Technology*, vol. 384, pp. 402–413, 2021. [Online]. Available: https://www.sciencedirect.com/science/article/pii/S0032591021001005

[40] M. C. Stöppler, "Medical Definition of Filler," 2021, [Accessed November 2021]. [Online]. Available: https://www.medicinenet.com/filler/definition.htm

[41] TheWithdrawlProject, "Pharmaceutical-grade Powder Filler," [Accessed November 2021]. [Online]. Available: https://withdrawal.theinnercompass.org/taper/pharmaceutical-grade-powder-filler

[42] PharmaExcipients, "Filler," [Accessed November 2021]. [Online]. Available: https://www.pharmaexcipients.com/filler/

[43] LFATabletPresses, "Tablet Binders," [Accessed November 2021]. [Online]. Available: https://www.lfatabletpresses.com/articles/tablet-binders

[44] AmericanPharmaceuticalReview, "Binder Excipients," [Accessed November 2021]. [Online]. Available: https://www.americanpharmaceuticalreview.com/180870-Binder-Excipients/?ctid=1&cid=25260

[45] PharmaEducation, "Tablet Binder : Types and Examples with concentration," [Accessed November 2021]. [Online]. Available: https://pharmaeducation.net/tablet-binder/

[46] Roquette, "Roquette Disintegrants and Superdisintegrants," [Accessed November 2021]. [Online]. Available: https://www.roquette.com/pharma/oral-dosage/disintegrant

[47] R. K. Tekade, Ed., *Basic Fundamentals of Drug Delivery*, 1st ed. Elsevier, 2019.

[48] A. Adejare, Ed., *Remington - The Science and Practice of Pharmacy*, 1st ed. Elsevier, 2020.

[49] J. Li and Y. M. Wu, “Lubricants in pharmaceutical solid dosage forms,” *Lubricants*, vol. 2, pp. 21–43, 03 2014.

[50] AmericanPharmaceuticalReview, “Lubricant Excipients,” [Accessed November 2021]. [Online]. Available: https://www.americanpharmaceuticalreview.com/pfu/7964385/soids/1402531/Excipient_Search/Lubricant

[51] M. Piran, “Active Pharmaceutical Ingredient Powders,” [Accessed November 2021]. [Online]. Available: https://www.teva-api.com/knowledge-center/active-pharmaceutical-ingredient-powders-why-lumping-and-flowability-are-an-industry-pain-that-is-difficult-to-re

[52] GlobalPharmaTech, “What Is an Active Pharmaceutical Ingredient (API)?” [Accessed November 2021]. [Online]. Available: https://www.globalpharmatek.com/blog/what-is-an-active-pharmaceutical-ingredient-api

[53] HosokawaMicronPowderSystems, “ACTIVE PHARMACEUTICAL INGREDIENTS,” [Accessed November 2021]. [Online]. Available: https://www.hmicronpowder.com/industry/pharmaceutical/active-pharmaceutical-ingredients/

[54] D. Santos, A. Maurício, V. Sencadas, J. Santos, M. Fernandes, and P. Gomes, *Spray Drying: An Overview*, 05 2018.

[55] M. Jain, L. Ganesh, B. Manoj, C. Randhir, B. Shashikant, and S. Chirag, “Spray drying in pharmaceutical industry: A review,” vol. 4, pp. 74–79, 04 2012.

[56] J. Carson and D. Craig, “Silo design codes: Their limits and inconsistencies,” *Procedia Engineering*, vol. 102, pp. 647–656, 2015, new Paradigm of Particle Science and Technology Proceedings of The 7th World Congress on Particle Technology. [Online]. Available: https://www.sciencedirect.com/science/article/pii/S1877705815001587

[57] R. C. Rowe, P. J. Sheskey, and S. C. Owen, *Handbook of Pharmaceutical Excipients*, 5th ed. American Pharmacists Association, 2006.

[58] G. S. Divya, K. Geetha, A. Pratyusha, and V. U. M. Rao, “Development of suitable pharmaceutical dosage forms through herbal plant extract,” *ICJPIR*, vol. 2, pp. 49–58, 09 2015.

[59] ShreeBhagwati, “Tablet Press and Tablet Compression Machine: Working Principle, advantages and working principle of Tablet Press,” [Accessed November 2021]. [Online]. Available: https://www.chitramechtech.com/working-principle-of-tablet-press/

[60] RivaS.A., “Piccola classica with module,” [Accessed October 2021]. [Online]. Available: https://www.rivasa.com/piccola-classica-module-en.html

[61] I. T. Jolliffe, Ed., *Principal Component Analysis. Springer Series in Statistics.*, 1st ed. New York: Springer-Verlag, 2002.

[62] Z. Jaadi, "A Step-by-Step Explanation of Principal Component Analysis (PCA)," 2021, [Accessed November 2021]. [Online]. Available: https://builtin.com/data-science/step-step-explanation-principal-component-analysis

[63] I. T. Jolliffe and J. Cadima, "Principal component analysis: a review and recent developments," *Philosophical Transactions of The Royal Society A*, vol. 374, 2016. [Online]. Available: https://royalsocietypublishing.org/doi/10.1098/rsta.2015.0202

[64] A. Horváth, *APPLICATION OF POWDER RHEOLOGY IN ASSESSING THE EFFECTS OF PHARMACEUTICAL ADDITIVES ON THE PHYSICAL PROPERTIES OF EXCIPIENTS AND TABLETS*. Budapest University of Technology and Economics, 2019.

[65] B. Van Snick, J. Dhondt, K. Pandelaere, J. Bertels, R. Mertens, D. Klingeleers, G. Di Pretoro, J. P. Remon, C. Vervaet, T. De Beer, and V. Vanhoorne, "A multivariate raw material property database to facilitate drug product development and enable in-silico design of pharmaceutical dry powder processes," *International Journal of Pharmaceutics*, vol. 549, no. 1, pp. 415–435, 2018. [Online]. Available: https://www.sciencedirect.com/science/article/pii/S0378517318305763

[66] S. Paul, S.-Y. Chang, J. Dun, W.-J. Sun, K. Wang, P. Tajarobi, C. Boissier, and C. C. Sun, "Comparative analyses of flow and compaction properties of diverse mannitol and lactose grades," *International Journal of Pharmaceutics*, vol. 546, no. 1, pp. 39–49, 2018. [Online]. Available: https://www.sciencedirect.com/science/article/pii/S0378517318302862

[67] P. C. Arnold and A. G. McLean, "Improved analytical flow factors for mass-flow hoppers," *Powder Technology 15*, pp. 279–281, 1976.

[68] P. C. Arnold, A. G. McLean, and A. W. Roberts, *Bulk solids: Storage, flow and handling*. TUNRA Ltd. The University of Newcastle, 1979.

[69] G. Mehos, "Hopper Design Workbook," 2021, [Accessed June 2021]. [Online]. Available: https://mehos.net/downloads

[70] M. D. Ashton, D. C.-H. Cheng, R. J. Farley, and F. H. H. Valentin, "Some investigations into the strength and flow properties of powders," *Rheologica Acta*, vol. 4, pp. 206–218, 1965.

[71] M. Peleg, M. D. Normand, and M. G. Corradini, "Interactive software for calculating the principal stresses of compacted cohesive powders with the warren-spring equation," *Powder Technology*, vol. 197, no. 3, pp. 268–273, 2010. [Online]. Available: https://www.sciencedirect.com/science/article/pii/S0032591009005531

[72] W. Chin and G. Marcoulides, “The partial least squares approach to structural equation modeling,” *Modern Methods for Business Research*, vol. 8, 01 1998.

[73] J. Henseler, C. Ringle, and R. Sinkovics, *The Use of Partial Least Squares Path Modeling in International Marketing*, 01 2009, vol. 20, pp. 277–319.

[74] A. Meri, “What are the values of r2 and q2 for the model to be acceptable in pls regression?” 05 2018.

[75] RivaS.A., *Riva Piccola Classica with module - User Guide*.

[76] StatisticsHowTo, “Relative Standard Deviation,” [Accessed November 2021]. [Online]. Available: https://www.statisticshowto.com/relative-standard-deviation/

[77] Investopedia, “Standard Deviation,” [Accessed November 2021]. [Online]. Available: https://www.investopedia.com/terms/s/standarddeviation.asp

[78] IST, “IST Nanotecnologia e Materiais; MicroLab - Electron Microscopy Laboratory,” [Accessed November 2021]. [Online]. Available: https://fenix.tecnico.ulisboa.pt/investigacao/ist-nm/microscopy

[79] SYMPATECGmbH, “HELOS/BR RODOS/L ASPIROS,” [Accessed November 2021]. [Online]. Available: https://www.sympatec.com/en/particle-measurement/sensors/laser-diffraction/helos/helos-br-rodos-l-aspiros/

[80] D. Schulze, “Private information.”

[81] C. Wang, S. Song, C. A. Gunawardana, D. J. Sun, and C. C. Sun, “Effects of shear cell size on flowability of powders measured using a ring shear tester,” *Powder Technology*, vol. 396, pp. 555–564, 2022. [Online]. Available: https://www.sciencedirect.com/science/article/pii/S0032591021009591

[82] J. Ashish, G. Swaroop, and K. Balasubramanian, “Effect of ammonium perchlorate particle size on flow, ballistic, and mechanical properties of composite propellant,” *Nanomaterials in Rocket Propulsion Systems*, pp. 299–362, 1 2019.

[83] P. García-Triñanes, S. Luding, and H. Shi, “Tensile strength of cohesive powders,” *Advanced Powder Technology*, vol. 30, no. 12, pp. 2868–2880, 2019. [Online]. Available: https://www.sciencedirect.com/science/article/pii/S0921883119302869

[84] J. Pharma, “Website for Filler 4,” [Accessed October 2021]. [Online]. Available: WebsiteforFiller4

[85] P. Excipients, “Website 1 for Filler 3,” [Accessed October 2021]. [Online]. Available: Website1forFiller3

[86] Knowde, “Website 2 for Filler 3,” [Accessed October 2021]. [Online]. Available: Website2forFiller3

[87] F. Farm, “Website for Filler 2C,” [Accessed October 2021]. [Online]. Available: WebsiteforFiller2C

[88] Meggle, “Website for Filler 2A,” [Accessed October 2021]. [Online]. Available: WebsiteforFiller2A

[89] IFF, “IFF Dupont Nutrition and biosciences - Filler 1,” [Accessed October 2021]. [Online]. Available: WebsiteforFiller1

[90] H. Ouadfel and L. Rothenburg, “‘Stress–force–fabric’ relationship for assemblies of ellipsoids,” *Mechanics of Materials*, vol. 33, no. 4, pp. 201–221, apr 2001.

[91] E. Azéma and F. Radjaï, “Stress-strain behavior and geometrical properties of packings of elongated particles,” *Phys. Rev. E*, vol. 81, p. 051304, May 2010, [Accessed October 2021]. [Online]. Available: https://link.aps.org/doi/10.1103/PhysRevE.81.051304

[92] T. Binaree, E. Azéma, N. Estrada, M. Renouf, and I. Preechawuttipong, “Combined effects of contact friction and particle shape on strength properties and microstructure of sheared granular media,” *Phys. Rev. E*, vol. 102, p. 022901, Aug 2020. [Online]. Available: https://link.aps.org/doi/10.1103/PhysRevE.102.022901

[93] I. Zuriguel, T. Mullin, and J. Rotter, “Effect of particle shape on the stress dip under a sandpile,” *Physical review letters*, vol. 98, p. 028001, 02 2007.

[94] R. C. Hidalgo, I. Zuriguel, D. Maza, and I. Pagonabarraga, “Role of Particle Shape on the Stress Propagation in Granular Packings,” *Physical Review Letters*, vol. 103, no. 11, p. 118001, sep 2009. [Online]. Available: https://link.aps.org/doi/10.1103/PhysRevLett.103.118001

[95] Meggle, “Product configurator - Filler 2B,” [Accessed October 2021]. [Online]. Available: WebsiteforFiller2B

[96] PharmaHub, “Poured and Tapped Bulk Density Measurements,” [Accessed October 2021]. [Online]. Available: https://pharmahub.org/dataviewer/view/excipients:db/excipients_measurements_tapped_poured/

[97] Y. Liu, X. Guo, H. Lu, and X. Gong, “An investigation of the effect of particle size on the flow behavior of pulverized coal,” *Procedia Engineering*, vol. 102, pp. 698–713, 11 2015.

[98] A. Rasti, H. Ranjkesh Adarmanabadi, M. Pineda, and J. Reinikainen, “Evaluating the effect of soil particle characterization on internal friction angle,” *American Journal of Engineering and Applied Sciences*, vol. 14, pp. 129–138, 02 2021.

[99] H. Mujtaba and K. Farooq, “Effect of void ratio and gradation on shear strength parameters of granular soils,” *Pakistan Journal of Science*, vol. 66, pp. 242–251, 2014.

[100] S. V. Bhujbal, B. Mitra, U. Jain, Y. Gong, A. Agrawal, S. Karki, L. S. Taylor, S. Kumar, and Q. T. Zhou, “Pharmaceutical amorphous solid dispersion: A review of manufacturing strategies,” *Acta Pharmaceutica Sinica B*, vol. 11, pp. 2505–2536, 8 2021.

[101] E. Browne, Z. Worku, and A. Healy, “Article on the influence of binder 2 on an amorphous solid dispersion.”

[102] R. B. Chavan, S. Rathi, V. G. Jyothi, and N. R. Shastri, “Cellulose based polymers in development of amorphous solid dispersions,” *Asian Journal of Pharmaceutical Sciences*, vol. 14, pp. 248–264, 5 2019.

[103] Webmd, “Website 1 for API 1,” [Accessed October 2021]. [Online]. Available: Website1forAPI1

[104] Drugs.com, “API 1 - Uses, Dosage, Side Effects,” [Accessed October 2021]. [Online]. Available: Website2forAPI1

[105] Webmd, “Website 1 for API 2,” [Accessed October 2021]. [Online]. Available: Website1forAPI2

[106] Drugs.com, “Website 2 for API 2,” [Accessed October 2021]. [Online]. Available: Website2forAPI2

[107] B. D. LTD., “Website 1 for Disintegrant 1,” [Accessed October 2021]. [Online]. Available: Website1forDisintegrant1

[108] IFF, “Website 2 for Disintegrant 1,” [Accessed October 2021]. [Online]. Available: Website2forDisintegrant1

[109] CPhIonline, “Website 1 for Lubricant 1,” [Accessed October 2021]. [Online]. Available: Website1forLubricant1

[110] healthline and D. R. Wilson, “Website 2 for Lubricant 1,” [Accessed October 2021]. [Online]. Available: Website2forLubricant1

[111] S.Zhaveri, “Website 3 for Lubricant 1,” [Accessed October 2021]. [Online]. Available: Website3forLubricant1

[112] K. Johanson, “Effect of particle shape on unconfined yield strength,” *Powder Technology*, vol. 194, no. 3, pp. 246–251, sep 2009.

[113] A. Ekdahl, D. Mudie, D. Malewski, G. Amidon, and A. Goodwin, “Effect of spray-dried particle morphology properties binder 2 amorphous solid dispersions.”

[114] K. Shinohara, M. Oida, and B. Golman, “Effect of particle shape on angle of internal friction by triaxial compression test,” *Powder Technology*, vol. 107, pp. 131–136, 01 2000.

[115] N. Stark, A. Hay, R. Cheel, and C. Lake, “The impact of particle shape on the angle of internal friction and the implications for sediment dynamics at a steep, mixed sand–gravel beach,” *Earth Surface Dynamics*, vol. 2, pp. 469–480, 08 2014.

[116] P. Hiremath, K. Nuguru, and V. Agrahari, “Material attributes and their impact on wet granulation process performance,” *Handbook of Pharmaceutical Wet Granulation: Theory and Practice in a Quality by Design Paradigm*, pp. 263–315, 1 2018.

[117] A. Choudhary, “PharmaGuideline - Lubricant Concentration in Pharmaceutical Products,” [Accessed October 2021]. [Online]. Available: https://www.pharmaguideline.com/2015/02/lubricants-and-their-concentration.html

[118] A. Uzunovic and E. Vranic, “Article on the impact of the concentration of lubricant 1.”

[119] S. Closs, Y. Roy, J. Boodram, S. Samudre, M. Adams, C. Minchom, and N. Mathis, “Article on the impact of the concentration of lubricant 1.”

[120] T. W. Scharf and S. V. Prasad, “Solid lubricants: a review,” *Journal of Materials Science*, vol. 48, pp. 511–531, 12 2013.

[121] C. Lanzerstorfer, C. Forsich, and D. Heim, “Reduction of wall friction of fine powders by use of wall surface coatings,” *Coatings*, vol. 11, no. 4, 2021. [Online]. Available: https://www.mdpi.com/2079-6412/11/4/427

[122] C. Lanzerstorfer, “Characterization of the flowability of fly ashes from grate-fired combustion of forest residues,” *Fuel Processing Technology*, vol. 150, pp. 10–15, 2016. [Online]. Available: https://www.sciencedirect.com/science/article/pii/S037838201630217X

[123] L. Shi, S. Chattoraj, and C. Sun, “Article on the flow properties of filler 1b.”

[124] M. Celik, *Pharmaceutical powder compaction technology*, 2nd ed. Informa Healthcare, 2011, drugs and the pharmaceutical sciences, v. 197.

[125] HoustonEnzimes, “Rice Bran vs. Cellulose: Do Fillers Really Make a Difference?” [Accessed October 2021]. [Online]. Available: https://www.houston-enzymes.com/learn/resources/article/rice-bran-vs-cellulose-do-fillers-really-make-a-difference

[126] CABOT, “Website for Glidant 1,” [Accessed October 2021]. [Online]. Available: WebsiteforGlidant1

[127] J. ZEGZULKA, L. JEZERSKÁ, F. ZÁDRAPA, M. ŽÍDEK, and G. Daniel, "Flow characterization methods of glidants," *NanoCon 2016*, oct 2016.

[128] LFATabletPress, "Importance of a good blend in the production of a pill," [Accessed November 2021]. [Online]. Available: https://www.lfatabletpresses.com/articles/importance-blend-uniformity

[129] T. Nguyen, *Particle – particle interactions in dry powder blending: Applying theoretical concepts to real-life particles*. University of Groningen, 2014.

[130] G. Mehos, M. Eggleston, T. Trautman, M. Freeman, and N. Stevens-Murphy, "Powder flow," *Tablets and Capsules*, 10 2017.

[131] D. J. Sun and C. C. Sun, "Proportionality between powder cohesion and unconfined yield strength from shear cell testing," *Heliyon*, vol. 5, no. 1, p. e01171, 2019. [Online]. Available: https://www.sciencedirect.com/science/article/pii/S2405844018366568

[132] Y. Wang, R. Snee, W. Meng, and F. Muzzio, "Predicting flow behavior of pharmaceutical blends using shear cell methodology: A quality by design approach," *Powder Technology*, vol. 294, 01 2016.

[133] A. Ryckaert, D. Van Hauwermeiren, J. Dhondt, A. De Man, A. Funke, D. Djuric, C. Vervaet, I. Nopens, and T. De Beer, "Tpls as predictive platform for twin-screw wet granulation process and formulation development," *International Journal of Pharmaceutics*, vol. 605, p. 120785, 2021. [Online]. Available: https://www.sciencedirect.com/science/article/pii/S0378517321005901

[134] S. M. Razavi, J. Scicolone, R. Snee, A. Kumar, J. Bertels, P. Cappuyns, I. Assche, A. Cuitiño, and F. Muzzio, "Prediction of tablet weight variability in continuous manufacturing," *International Journal of Pharmaceutics*, vol. 575, p. 118727, 10 2019.

[135] CouncilOfEurope, *European Pharmacopoeia supplement 6.4*, 6th ed. European Directorate for the Quality of Medicine, 208, tablets Monograph 0478.

[136] A. N. Zaid, R. J. Al-Ramahi, A. A. Ghoush, A. Qaddumi, and Y. A. Zaaror, "Weight and content uniformity of lorazepam half-tablets: A study of correlation of a low drug content product," *Saudi Pharmaceutical Journal*, vol. 21, no. 1, pp. 71–75, 2013. [Online]. Available: https://www.sciencedirect.com/science/article/pii/S1319016411001204

[137] Dupont, "Filler 1 Selection Guide," 2020.

A

Powder data

This appendix contains information regarding particle size distribution and SEM imaging.

A.1 SEM imaging

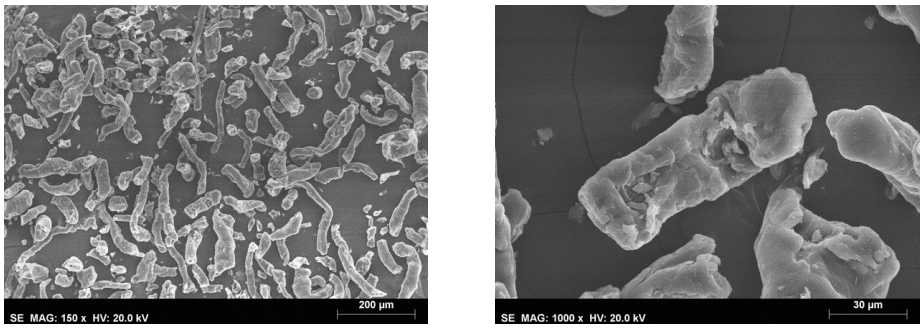

(a) Amplification: 150x. **(b)** Amplification: 1000x.

Figure A.1: SEM images for disintegrant 1 at amplifications of 150x and 1000x.

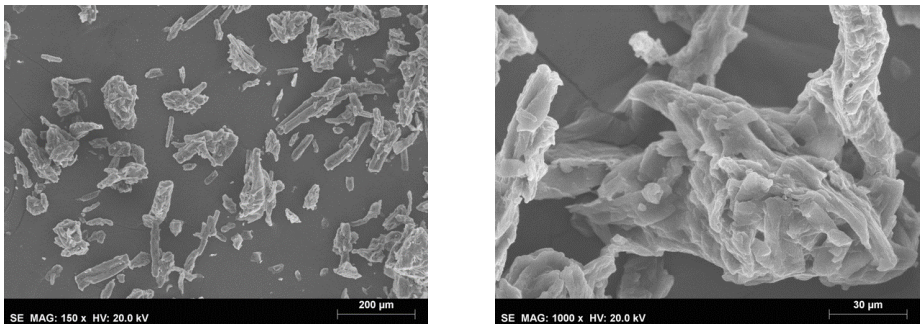

(a) Amplification: 150x. **(b)** Amplification: 1000x.

Figure A.2: SEM images for filler 1A at amplifications of 150x and 1000x.

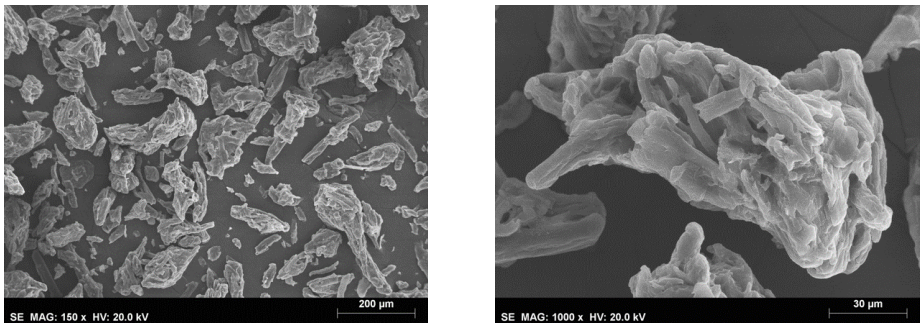

(a) Amplification: 150x. **(b)** Amplification: 1000x.

Figure A.3: SEM images for filler 1B at amplifications of 150x and 1000x.

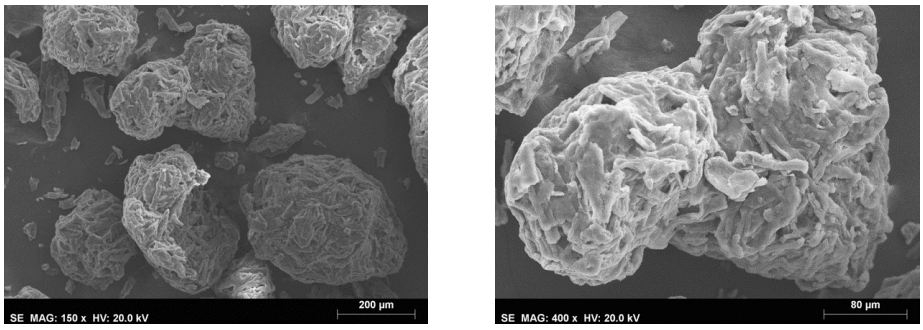

(a) Amplification: 150x. **(b)** Amplification: 400x.

Figure A.4: SEM images for filler 1C at amplifications of 150x and 400x.

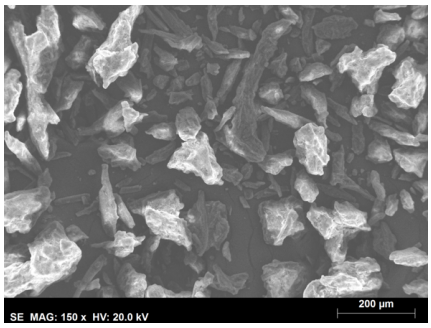

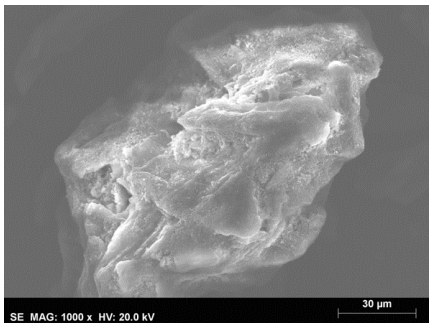

(a) Amplification: 150x. **(b)** Amplification: 1000x.

Figure A.5: SEM images for filler 3 at amplifications of 150x and 1000x.

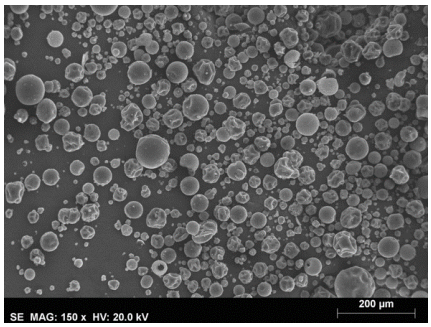

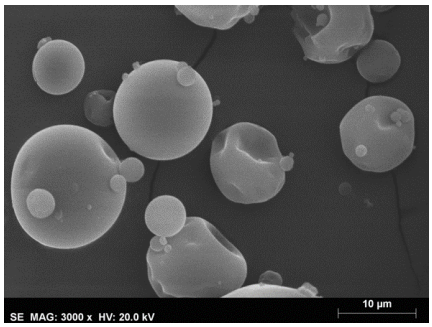

(a) Amplification: 150x. **(b)** Amplification: 3000x.

Figure A.6: SEM images for binder 2 at amplifications of 150x and 3000x.

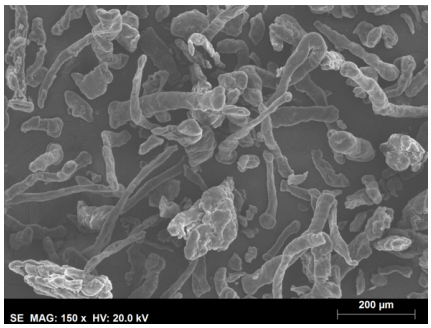

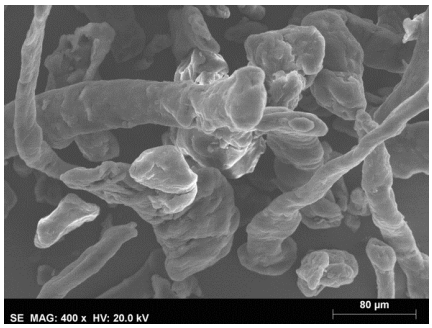

(a) Amplification: 150x. **(b)** Amplification: 400x.

Figure A.7: SEM images for binder 1A at amplifications of 150x and 400x.

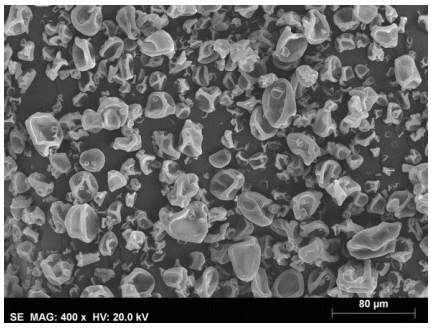

(a) Amplification: 400x.

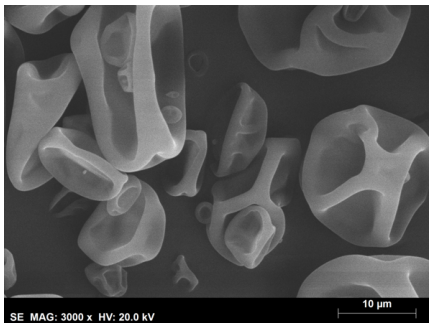

(b) Amplification: 3000x.

Figure A.8: SEM images for binder 1B at amplifications of 400x and 3000x.

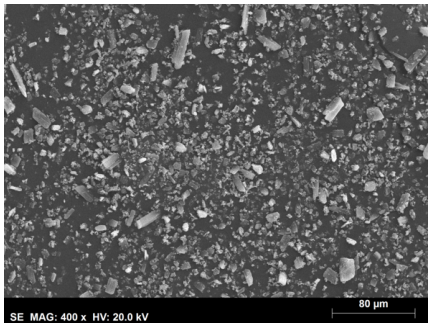

(a) Amplification: 400x.

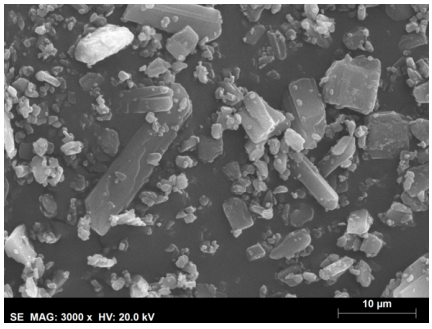

(b) Amplification: 3000x.

Figure A.9: SEM images for API 2 at amplifications of 400x and 3000x.

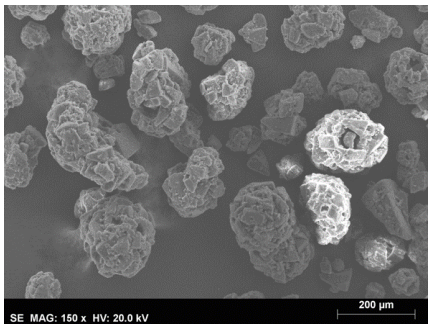

(a) Amplification: 150x.

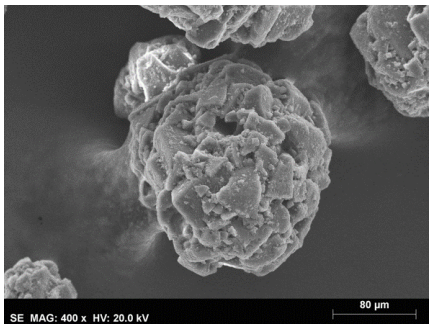

(b) Amplification: 400x.

Figure A.10: SEM images for filler 2C at amplifications of 150x and 400x.

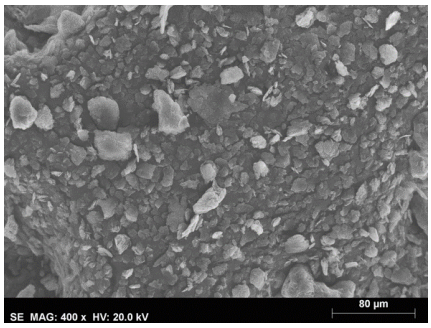

(a) Amplification: 400x.

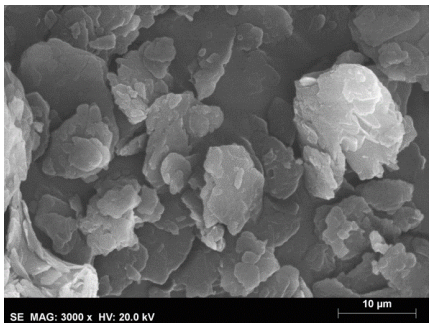

(b) Amplification: 3000x.

Figure A.11: SEM images for lubricant 1 at amplifications of 400x and 3000x.

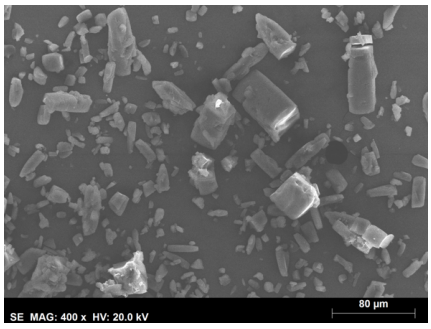

(a) Amplification: 400x.

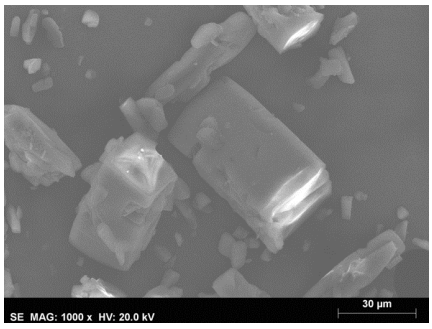

(b) Amplification: 1000x.

Figure A.12: SEM images for API 1 at amplifications of 400x and 1000x.

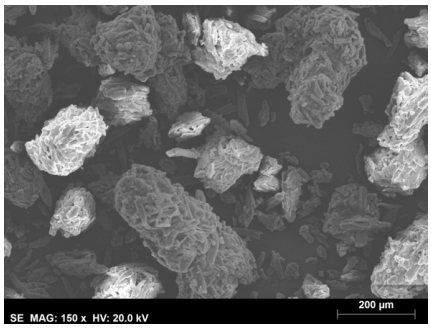

(a) Amplification: 150x.

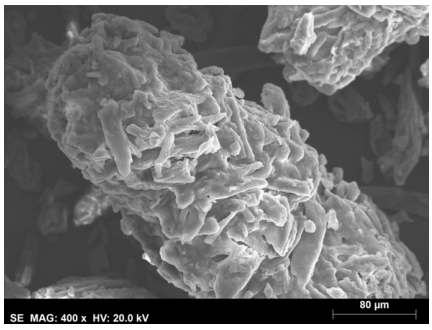

(b) Amplification: 400x.

Figure A.13: SEM images for filler 4 at amplifications of 150x and 400x.

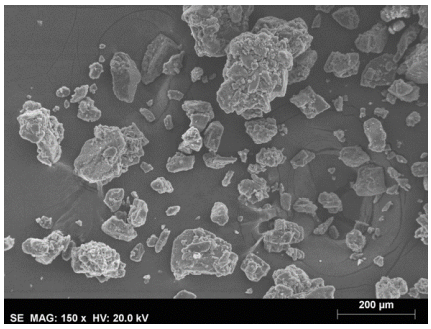

(a) Amplification: 150x.

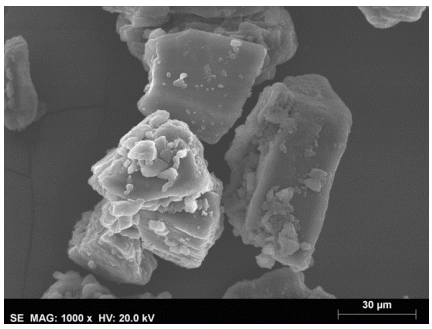

(b) Amplification: 1000x.

Figure A.14: SEM images for filler 2A at amplifications of 150x and 1000x.

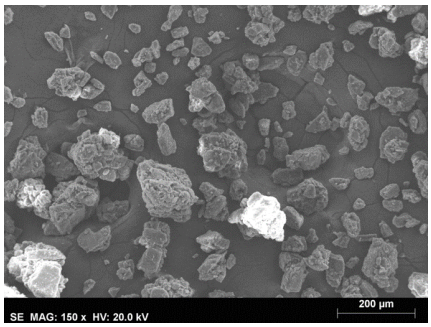

(a) Amplification: 150x.

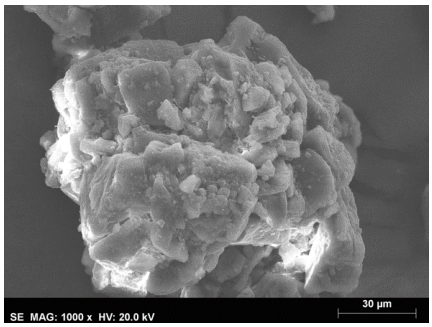

(b) Amplification: 1000x.

Figure A.15: SEM images for filler 2B at amplifications of 150x and 1000x.

A.2 Particle Size Distributions

No measurements were made for filler 1A in terms of paricle size distribution, but according to the literature, its typical x_{50} is of 50 μm. [137]

No measurements were made for filler 3 in terms of Particle Size Distribution. Since filler 3 is personalized and addapted to the buyer's needs, no information on x_{50} can be found in the literature.

No measurements were made in terms of particle size distribution for binder 1A.

No measurements were made in terms of particle size distribution for binder 1B and these values cannot be found on the literature since it is not a comercially available product.

No measurements were made in terms of particle size distribution for API 2.

No measurements were made in terms of particle size distribution for API 1 and these values cannot be found on the literature since it is not a commercially available product.

No measurements were made for filler 2A in terms of paricle size distribution, but according to the literature, its typical x_{50} is of 145 μm. [95]

No measurements were made for filler 2B in terms of particle size distribution, but according to the literature, its typical x_{50} is of 125 μm. [95]

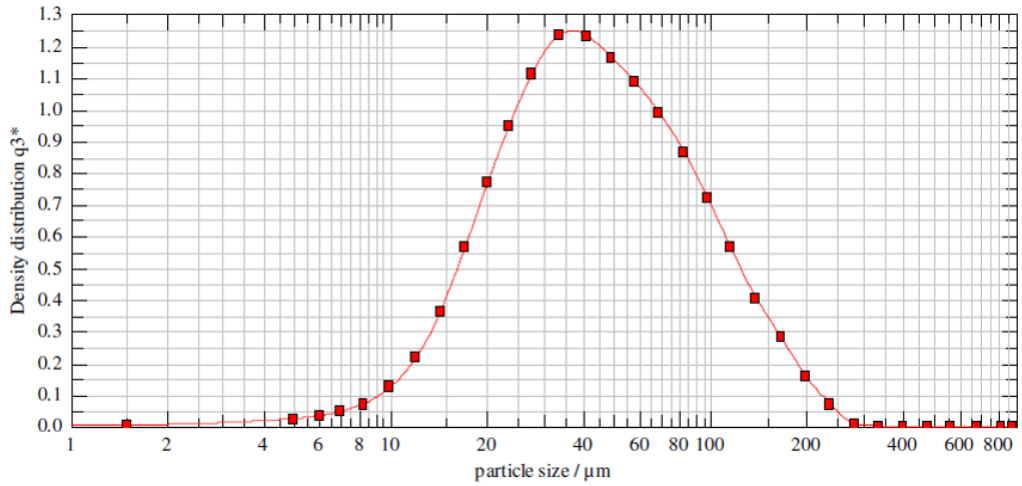

Figure A.16: Particle Size Distribution for disintegrant 1. $x_{50} = 42.67\mu m$

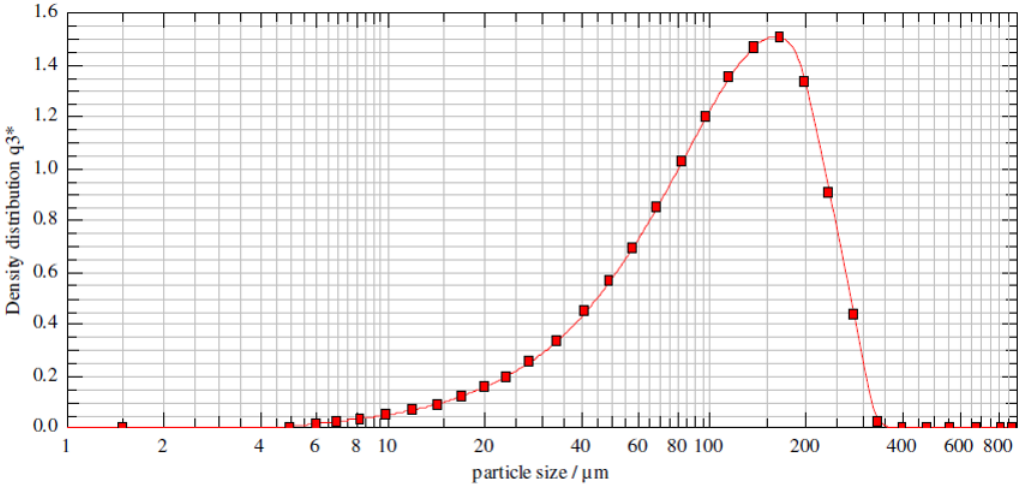

Figure A.17: Particle Size Distribution for filler 1B. $x_{50} = 113.4\mu m$

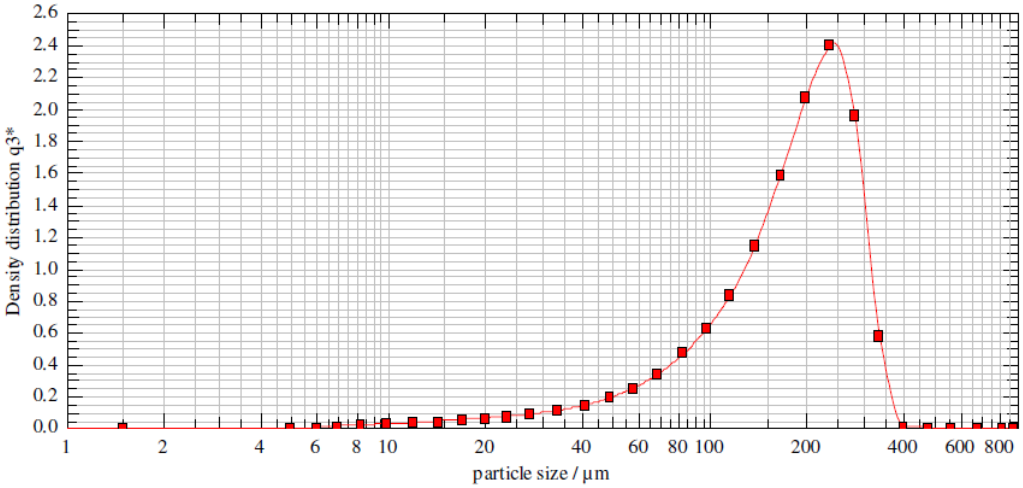

Figure A.18: Particle Size Distribution for filler 1C. $x_{50} = 187.5\mu m$

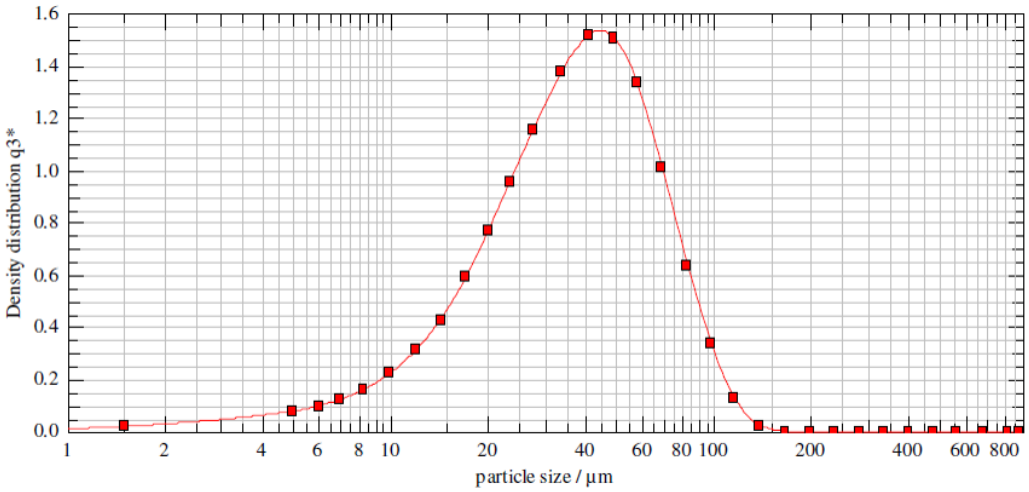

Figure A.19: Particle Size Distribution for binder 2. $x_{50} = 36.8\mu m$

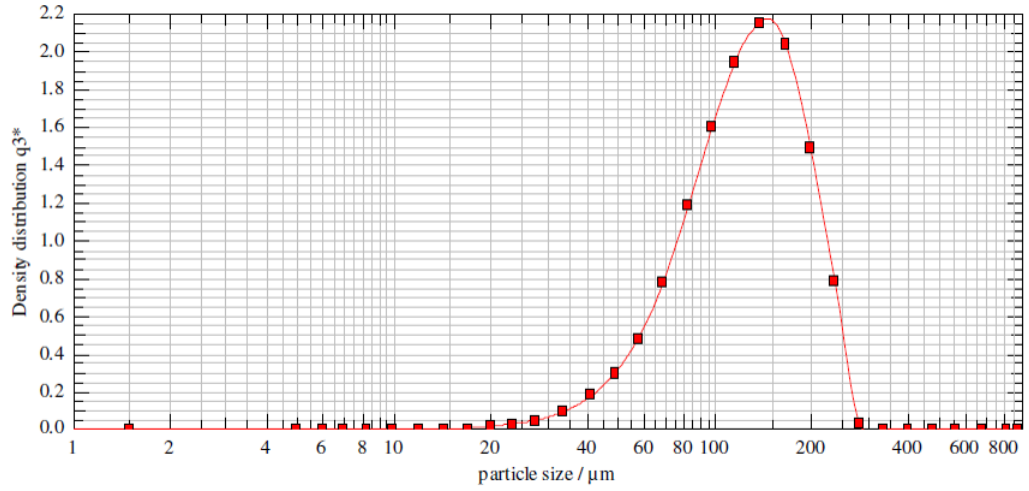

Figure A.20: Particle Size Distribution for SD filler 2C. $x_{50} = 125.9\mu m$

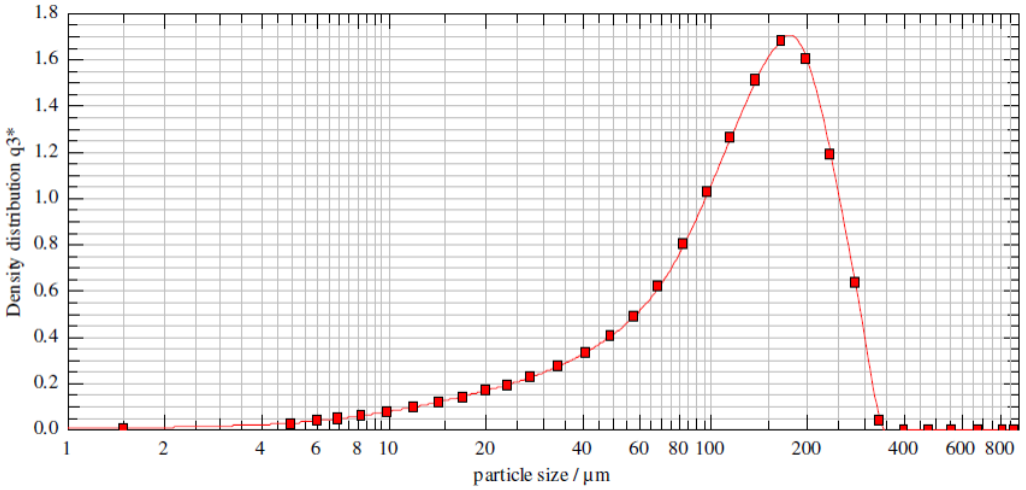

Figure A.21: Particle Size Distribution for filler 4. $x_{50} = 128.5\mu m$

B

Shear and wall friction tests performed

This appendix contains the results obtained in each test for each powder and blend.

B.1 Shear tests

Table B.1: Results obtained in the shear tests for filler 3.

		Pa	Pa	-	-	Pa	g/cm3	º	º	º	g/cm3
Cell	**Test**	**sigma1**	**Fc**	**FFc**	**Ffrho**	**tau,c**	**RhoB**	**phiE**	**phiLin**	**phiSf**	**rho, f**
XS-Mr	**1**	1993	102	19.46	8.38	24	0.431	41.8	40.6	37.5	0.418
	2	4065	131	30.95	13.34	30	0.431	41.3	40.5	37.7	0.407
	3	6025	190	31.72	13.74	45	0.433	40.7	40	37.2	0.416
XS-SV3	**1**	1726	58	29.71	11.67	15	0.393	37.4	36.7	33	0.388
	2	3584	104	34.44	13.31	27	0.386	36.5	35.8	33.3	0.383
	3	5495	148	37.12	14.65	39	0.395	35.8	35.2	33.3	0.388

Table B.2: Results obtained in the shear tests for filler 2A.

		Pa	**Pa**	**-**	**-**	**Pa**	**g/cm3**	**º**	**º**	**º**	**g/cm3**
cell	**test**	**sigma1**	**Fc**	**FFc**	**Ffrho**	**tau,c**	**RhoB**	**phiE**	**phiLin**	**phiSf**	**rho, f**
XS-Mr	**4**	978	161	6.08	3.9	39	0.641	42.4	38.5	36.8	0.615
	1	1866	394	4.74	3.08	99	0.65	41.6	36.3	35.9	0.607
	2	3653	530	6.89	4.6	132	0.668	39.7	36.2	34.9	0.604
	3	5418	727	7.45	5.01	182	0.672	39.5	36.3	34.7	0.597
XS-SV3	**1**	1675	260	6.45	3.81	71	0.591	36.6	32.6	31.9	0.541
	2	3341	358	9.32	5.75	95	0.616	35.6	32.9	31.4	0.549
	3	4981	505	9.86	6.21	139	0.629	35	32.5	31.1	0.571

Table B.3: Results obtained in the shear tests for filler 1A.

		Pa	Pa	-	-	Pa	g/cm3	º	º	º	g/cm3
cell	test	sigma1	Fc	FFc	Ffrho	tau,c	RhoB	phiE	phiLin	phiSf	rho, f
XS-Mr	1	2235	639	3.5	1.2	154	0.324	45.9	38.7	41.3	0.301
	2	4534	960	4.72	1.68	220	0.355	45.2	40.2	41.4	0.304
	3	6692	1364	4.91	1.77	318	0.361	44.6	39.8	40.9	0.316
XS-SV3	1	1923	333	5.78	1.83	83	0.316	41.6	38.4	36.9	0.298
	2	3960	537	7.38	2.35	130	0.319	41.1	37.9	37.3	0.292
	3	5864	901	6.51	2.1	227	0.323	40.1	36.3	36.6	0.292

Table B.4: Results obtained in the shear tests for binder 1A.

		Pa	Pa	-	-	Pa	g/cm3	º	º	º	g/cm3
cell	test	sigma1	Fc	FFc	Ffrho	tau,c	RhoB	phiE	phiLin	phiSf	rho, f
XS-Mr	1	2866	801	3.58	1.42	159	0.398	52.7	46.6	48.1	0.353
	2	5717	1227	4.66	1.92	241	0.413	50.4	45.8	47.2	0.36
	3	8186	1550	5.28	2.21	307	0.419	50	45.9	46.3	0.351
XS-SV3	1	2231	313	7.13	2.57	69	0.36	44	40.8	40.6	0.317
	2	4388	655	6.7	2.48	154	0.37	43	39.6	39.9	0.32
	3	6617	917	7.21	2.65	218	0.367	42	38.8	39.5	0.32

Table B.5: Results obtained in the shear tests for API 1.

		Pa	Pa	-	-	Pa	g/cm3	º	º	º	g/cm3
cell	test	sigma1	Fc	FFc	Ffrho	tau,c	RhoB	phiE	phiLin	phiSf	rho, f
XS-Mr	1	2104.50	970.25	2.18	1.30	244.00	0.60	48.10	34.90	40.80	0.48
	2	4143.50	1438.00	2.88	1.78	345.75	0.62	46.05	36.88	39.95	0.46
	3	6135.00	1923.50	3.17	2.06	464.00	0.64	44.83	36.68	39.28	0.49
XS-SV3	1	1885.50	672.75	2.81	1.52	171.25	0.54	44.05	34.28	37.43	0.47
	2	3809.40	1172.80	3.26	1.88	295.60	0.58	43.04	34.86	37.24	0.47
	3	5722.40	1662.80	3.45	1.90	418.80	0.55	42.38	34.72	37.04	0.45

Table B.6: Results obtained in the shear tests for filler 1B.

	Pa	Pa	-	-	Pa	g/cm3	º	º	º	g/cm3
Test	sigma1	Fc	FFc	Ffrho	tau,c	RhoB	phiE	phiLin	phiSf	rho, f
1	2017	392	5.15	1.9	96	0.369	42.3	37.5	37.9	0.34
2	3927	535	7.35	2.79	133	0.38	40.2	36.9	36.6	0.343
3	5929	777	7.63	2.9	192	0.38	40.1	37	36.7	0.341

Table B.7: Results obtained in the shear tests for filler 1C.

	Pa	Pa	-	-	Pa	g/cm3	º	º	º	g/cm3
Test	sigma1	Fc	FFc	Ffrho	tau,c	RhoB	phiE	phiLin	phiSf	rho, f
1	1871	268	6.98	2.56	70	0.367	38.8	35.3	35	0.353
2	3806	389	9.78	3.62	100	0.371	38.4	36	35.2	0.351
3	5693	547	10.41	3.88	144	0.372	37.2	34.8	34.6	0.35

Table B.8: Results obtained in the shear tests for Sieved API 1.

	Pa	Pa	-	-	Pa	g/cm3	º	º	º	g/cm3
Test	sigma1	Fc	FFc	Ffrho	tau,c	RhoB	phiE	phiLin	phiSf	rho, f
1	2112	1178	1.79	1.03	306	0.575	51.4	34.5	41.9	0.482
2	4112	1503	2.73	1.7	357	0.623	46.8	37.2	40.1	0.495
3	6136	2188	2.8	1.76	524	0.626	46.4	37	39.9	0.469

Table B.9: Results obtained in the shear tests for filler 2C.

	Pa	Pa	-	-	Pa	g/cm3	º	º	º	g/cm3
Test	sigma1	Fc	FFc	Ffrho	tau,c	RhoB	phiE	phiLin	phiSf	rho, f
1	1796	277	6.44	4.04	75	0.627	37.2	33.2	33.2	0.567
2	3498	380	9.19	5.88	101	0.639	36.2	33.5	32.5	0.561
3	5249	477	11.01	7.08	127	0.643	35.8	33.6	32.4	0.571

Table B.10: Results obtained in the shear tests for filler 2B.

	Pa	Pa	-	-	Pa	g/cm3	º	º	º	g/cm3
Test	sigma1	Fc	FFc	Ffrho	tau,c	RhoB	phiE	phiLin	phiSf	rho, f
1	1823	290	6.29	3.97	73	0.631	39.9	36	34.7	0.565
2	3611	425	8.5	5.48	108	0.644	38.5	35.7	34.2	0.565
3	5358	581	9.23	6.01	150	0.652	37.7	35.1	33.7	0.566

Table B.11: Results obtained in the shear tests for binder 1B.

	Pa	Pa	-	-	Pa	g/cm3	º	º	º	g/cm3
Test	sigma1	Fc	FFc	Ffrho	tau,c	RhoB	phiE	phiLin	phiSf	rho, f
1	1985	1343	1.48	0.42	372	0.286	52.4	28.1	40.8	0.221
2	3975	2057	1.93	0.59	530	0.307	48	32.2	39.8	0.211
3	5925	2653	2.23	0.72	685	0.324	45.8	32.7	39	0.225

Table B.12: Results obtained in the shear tests for lubricant 1.

Pa	Pa	-	-	Pa	g/cm3	º	º	º	g/cm3
sigma1	Fc	FFc	Ffrho	tau,c	RhoB	phiE	phiLin	phiSf	rho, f
2095	847	2.47	0.88	220	0.356	44.8	33.3	39.7	0.22
3853	1166	3.3	1.23	302	0.373	41.1	32.8	36.6	0.227
5766	1505	3.83	1.51	396	0.393	39	32	35.7	0.23

Table B.13: Results obtained in the shear tests for filler 4.

Pa	Pa	-	-	Pa	g/cm3	º	º	º	g/cm3
sigma1	Fc	FFc	Ffrho	tau,c	RhoB	phiE	phiLin	phiSf	rho, f
2028	270	7.51	3.51	67	0.467	40.3	37.1	37.1	0.458
3985	459	8.69	4.11	116	0.473	39.2	36.4	36.4	0.457
5881	620	9.48	4.51	160	0.476	38.4	35.9	35.7	0.46

Table B.14: Results obtained in the shear tests for binder 2.

Pa	Pa	-	-	Pa	g/cm3	º	º	º	g/cm3
sigma1	Fc	FFc	Ffrho	tau,c	RhoB	phiE	phiLin	phiSf	rho, f
1721	575	2.99	1.4	171	0.468	37	27.2	32.4	0.35
3400	717	4.74	2.34	210	0.494	33.6	27.8	30.8	0.363
4910	821	5.98	2.95	246	0.493	31.8	27.3	29.2	0.341

Table B.15: Results obtained in the shear tests for disintegrant 1.

Pa	Pa	-	-	Pa	g/cm3	º	º	º	g/cm3
sigma1	Fc	FFc	Ffrho	tau,c	RhoB	phiE	phiLin	phiSf	rho, f
2530	725	3.49	1.72	159	0.493	49	42.3	44.6	0.449
4987	1013	4.92	2.53	217	0.514	47.7	43.1	43.9	0.453
7262	1424	5.1	2.62	314	0.514	46.4	42	43	0.451

Table B.16: Results obtained in the shear tests for API 2.

Pa	Pa	-	-	Pa	g/cm3	º	º	º	g/cm3
sigma1	Fc	FFc	Ffrho	tau,c	RhoB	phiE	phiLin	phiSf	rho, f
2391	2065	1.16	0.37	530	0.318	66.6	31.4	48	0.214
4627	3673	1.26	0.44	897	0.347	63.5	35.1	46.8	0.223
7080	5335	1.33	0.49	1291	0.373	61.5	35.8	47	0.255

Table B.17: Results obtained in the shear tests for Blend 1.

Blend 1	Pa	Pa	-	-	Pa	g/cm3	º	º	º	g/cm3
Test	sigma1	Fc	FFc	Ffrho	tau,c	RhoB	phiE	phiLin	phiSf	rho, f
1	2088	156	13.37	7.22	36	0.54	43	41.4	38.8	0.534
2	4032	224	18.03	9.67	53	0.536	41	39.7	37.4	0.526
3	6036	235	25.69	13.92	56	0.542	40.2	39.4	37.1	0.532

Table B.18: Results obtained in the shear tests for Blend 2.

Blend 2	Pa	Pa	-	-	Pa	g/cm3	º	º	º	g/cm3
Test	sigma1	Fc	FFc	Ffrho	tau,c	RhoB	phiE	phiLin	phiSf	rho, f
1	1964	252	7.8	4.61	60	0.592	41.9	38.9	37.1	0.567
2	4142	284	14.58	8.83	65	0.606	41.7	40.2	38.2	0.586
3	6063	411	14.75	8.84	98	0.6	40.8	39.3	37.4	0.564

Table B.19: Results obtained in the shear tests for Blend 3.

Blend 3	Pa	Pa	-	-	Pa	g/cm3	º	º	º	g/cm3
Test	sigma1	Fc	FFc	Ffrho	tau,c	RhoB	phiE	phiLin	phiSf	rho, f
1	1989	319	6.23	3.82	77	0.613	42.1	38.3	37.4	0.552
2	3910	453	8.63	5.43	109	0.629	41	38.2	36.8	0.557
3	5810	616	9.44	5.96	150	0.632	40.3	37.9	36.4	0.55

Table B.20: Results obtained in the shear tests for Blend 4.

Blend 4	Pa	Pa	-	-	Pa	g/cm3	º	º	º	g/cm3
Test	sigma1	Fc	FFc	Ffrho	tau,c	RhoB	phiE	phiLin	phiSf	rho, f
1	2067	388	5.33	3.42	94	0.642	42.4	37.9	38.3	0.567
2	4001	606	6.6	4.36	147	0.66	41.2	37.6	37.3	0.56
3	5996	808	7.43	4.95	196	0.667	41	37.8	37.3	0.577

Table B.21: Results obtained in the shear tests for Blend 5.

Blend 5	Pa	Pa	-	-	Pa	g/cm3	º	º	º	g/cm3
Test	sigma1	Fc	FFc	Ffrho	tau,c	RhoB	phiE	phiLin	phiSf	rho, f
1	2037	393	5.19	2.83	98	0.545	41.6	36.8	37.7	0.496
2	4000	600	6.67	3.72	148	0.558	40.6	36.9	37.1	0.497
3	5918	844	7.01	3.97	208	0.567	40.4	36.9	36.8	0.494

B.2 Wall friction tests

Table B.22: Results obtained in the wall friction tests for disintegrant 1.

Repetition	1		2		3		4		5	
sigma wall	tau wall	PHIX	tau wall	PHIX	tau wall	PHIX	tau wall	PHIX	tau wall	PHIX
2018	865	23.2	814	22	790	21.4	777	21.1	763	20.7
1518	688	24.4	648	23.1	628	22.5	620	22.2	613	22
1019	501	26.2	475	25	460	24.3	456	24.1	451	23.9
518	277	28.1	268	27.3	262	26.8	262	26.8	258	26.5
268	156	30.3	151	29.4	149	29	143	28.1	147	28.7
193	115	30.8	113	30.4	109	29.6	109	29.6	107	29.1
119	81	34.3	77	33	75	32.4	72	31.1	72	31.1
69	55	38.6	53	37.6	51	36.6	47	34.5	49	35.5

Table B.23: Results obtained in the wall friction tests for filler 3.

		Repetition	1		2		3		4		5	
Cell	Test	sigma wall	tau wall	PHIX	tau wall	PHIX	tau wall	PHIX	tau wall	PHIX	tau wall	PHIX
XS-WM	1	1015	524	27.3	503	26.4	503	26.4	498	26.1	500	26.2
		825	418	26.9	413	26.6	413	26.6	407	26.3	407	26.3
		635	326	27.2	320	26.8	322	26.9	315	26.4	317	26.5
		445	230	27.3	230	27.3	226	27	224	26.8	224	26.8
		256	138	28.3	136	28	136	28	134	27.6	134	27.6
		65	47	35.8	47	35.8	47	35.8	46	35.5	45	34.8
XS-WL0	1	5014	2644	27.8	2628	27.7	2569	27.1	2612	27.5		
		4063	2146	27.8	2126	27.6	2114	27.5	2122	27.6		
		3113	1632	27.7	1592	27.1	1585	27	1608	27.3		
		2163	1118	27.3	1103	27	1095	26.8	1114	27.3		
		1212	628	27.4	613	26.8	620	27.1	620	27.1		
		264	138	27.6	142	28.3	142	28.3	146	29		
	2	7514	4011	28.1	3896	27.4	3975	27.9	4015	28.1	4074	28.5
		6113	3288	28.3	3165	27.4	3213	27.7	3232	27.9	3343	28.7
		4714	2557	28.5	2395	26.9	2450	27.5	2470	27.7	2525	28.2
		3313	1699	27.2	1699	27.2	1699	27.2	1723	27.5	1790	28.4
		1915	1008	27.8	988	27.3	988	27.3	996	27.5	1004	27.7
		514	273	28	277	28.3	277	28.3	277	28.3	277	28.3
	3	10013	5007	26.6	4975	26.4	5003	26.5	5070	26.9	5232	27.6
		8213	4122	26.6	4125	26.7	4050	26.3	4232	27.3	4319	27.7
		6413	3248	26.9	3260	26.9	3138	26.1	3268	27	3410	28
		4613	2375	27.2	2379	27.3	2292	26.4	2324	26.7	2367	27.2
		2814	1486	27.8	1490	27.9	1438	27.1	1438	27.1	1415	26.7
		1014	557	28.8	561	29	537	27.9	514	26.9	514	26.9

Table B.24: Results obtained in the wall friction tests for filler 2A.

		Repetition	1		2	
Cell	Test	sigma wall	tau wall	PHIX	tau wall	PHIX
XS-WM	1	10018	3473	19.1	3620	19.9
		8218	2916	19.5	3047	20.3
		6418	2351	20.1	2458	21
		4618	1782	21.1	1853	21.9
		2818	1185	22.8	1221	23.4
		1018	450	23.9	454	24
	2	7518	2778	20.3	2770	20.2
		6117	2316	20.7	2308	20.7
		4718	1861	21.5	1853	21.4
		3318	1383	22.6	1375	22.5
		1919	826	23.3	806	22.8
		518	253	26	241	25
	3	5019	1913	20.9	1932	21.1
		4069	1600	21.5	1604	21.5
		3119	1272	22.2	1272	22.2
		2168	921	23	921	23
		1218	541	24	541	24
		270	134	26.5	134	26.5
XS-WL0	1	1023	394	21.1	385	20.6
		842	336	21.7	328	21.3
		662	275	22.6	273	22.4
		482	215	24	211	23.7
		302	151	26.5	149	26.2
		123	77	32.2	75	31.6
	2	782	332	23	320	22.3
		636	279	23.7	270	23
		501	232	24.8	226	24.3
		367	179	26	175	25.6
		232	123	27.9	123	27.9
		97	64	33.5	64	33.5
	3	521	245	25.2	237	24.5
		431	211	26.1	205	25.5
		341	173	26.9	168	26.2
		252	136	28.3	132	27.7
		162	96	30.7	92	29.7
		72	53	36.3	51	35.3

Table B.25: Results obtained in the wall friction tests for filler 1A.

		Repetition	1		2	
Cell	Test	sigma wall	tau wall	PHIX	tau wall	PHIX
XS-WM	1	10008	5121	27.1	5042	26.7
		8208	4212	27.2	4173	26.9
		6409	3331	27.5	3307	27.3
		4609	2438	27.9	2442	27.9
		2809	1541	28.8	1541	28.8
		1009	593	30.4	507	30.6
	2	7509	3778	26.7	3730	26.4
		6108	3106	27	3055	26.6
		4709	2418	27.2	2399	27
		3308	1735	27.7	1735	27.7
		1910	1055	28.9	1051	28.8
		509	300	30.5	300	30.5
	3	5010	2486	26.4	2375	25.4
		4060	2023	26.5	1940	25.5
		3110	1573	26.8	1513	26
		2159	1126	27.5	1087	26.7
		1209	660	28.6	644	28.1
		261	154	30.6	154	30.6
XS-WL0	1	1011	558	28.9	552	28.6
		830	466	29.3	456	28.8
		651	364	29.2	364	29.2
		471	264	29.3	268	29.6
		291	170	30.2	170	30.2
		111	74	33.4	72	32.8
	2	762	430	29.4	420	28.9
		626	354	29.5	349	29.1
		491	285	30.1	277	29.4
		356	207	30.2	204	29.8
		221	132	30.8	130	30.4
		86	60	34.9	58	34.1
	3	510	298	30.3	288	29.5
		421	247	30.4	241	29.8
		331	194	30.4	190	29.9
		241	143	30.7	143	30.7
		151	96	32.5	94	32
		61	47	37.6	45	36.5

Table B.26: Results obtained in the wall friction tests for binder 1A.

		Repetition	1		2	
Cell	Test	sigma wall	tau wall	PHIX	tau wall	PHIX
XS-WM	1	10010	5607	29.3	5502	29
		8210	4714	29.9	4687	29.7
		6410	3782	30.5	3746	30.3
		4610	2802	31.3	2778	31.1
		2810	1766	32.2	1754	32
		1010	672	33.6	656	33
	2	7510	4284	29.7	4137	28.9
		6109	3572	30.3	3442	29.4
		4710	2829	31	2727	30.1
		3309	2047	31.7	1976	30.8
		1911	1209	32.3	1170	31.5
		510	300	30.5	296	30.2
	3	5010	2576	27.2	2596	27.4
		4060	2130	27.7	2154	27.9
		3110	1672	28.3	1687	28.5
		2159	1193	28.9	1209	29.3
		1209	695	29.9	699	30.1
		261	158	31.2	158	31.2
XS-WL0	1	1014	547	28.3	532	27.7
		833	456	28.7	445	28.1
		653	368	29.4	360	28.9
		473	271	29.8	268	29.5
		294	173	30.6	170	30
		114	75	33.5	70	31.5
	2	763	415	28.5	405	28
		627	347	29	337	28.3
		492	277	29.4	271	28.9
		357	204	29.7	200	29.2
		223	130	30.3	128	29.9
		88	57	32.8	55	31.9
	3	512	288	29.4	279	28.6
		422	241	29.8	236	29.2
		332	192	30.1	187	29.3
		242	143	30.6	139	29.9
		152	92	31.3	90	30.7
		62	43	34.8	43	34.8

Table B.27: Results obtained in the wall friction tests for API 1.

		Repetition	1		2		3		4		5	
Cell	Test	sigma wall	tau wall	PHIX	tau wall	PHIX	tau wall	PHIX	tau wall	PHIX	tau wall	PHIX
XS-WM	1	10015	5635	29.4	5694	29.6	5667	29.5	5682	29.6	5667	29.5
		8215	4604	29.3	4631	29.4	4615	29.3	4608	29.3	4612	29.3
		6415	3568	29.1	3556	29	3545	28.9	3537	28.9	3533	28.8
		4615	2521	28.6	2513	28.6	2501	28.5	2486	28.3	2478	28.2
		2815	1502	28.1	1490	27.9	1470	27.6	1466	27.5	1466	27.5
		1015	530	27.5	518	27	510	26.7	510	26.7	518	27
	2	7515	4327	29.9	4287	29.7	4264	29.6	4244	29.5	4232	29.4
		6114	3517	29.9	3481	29.7	3458	29.5	3434	29.3	3418	29.2
		4716	2695	29.7	2655	29.4	2636	29.2	2624	29.1	2608	28.9
		3315	1869	29.4	1841	29.1	1830	28.9	1810	28.6	1810	28.6
		1916	1067	29.1	1047	28.7	1039	28.5	1027	28.2	1023	28.1
		515	292	29.6	288	29.2	277	28.2	277	28.2	273	27.9
	3	5016	2893	30	2829	29.4	2798	29.1	2766	28.9	2758	28.8
		4066	2300	29.5	2284	29.3	2248	28.9	2233	28.8	2221	28.6
		3116	1743	29.2	1727	29	1707	28.7	1687	28.4	1679	28.3
		2165	1205	29.1	1189	28.8	1178	28.5	1166	28.3	1162	28.2
		1215	676	29.1	668	28.8	656	28.4	648	28.1	644	27.9
		267	166	31.9	162	31.3	158	30.6	154	30	154	30
XS-WL0	1	1020	628	31.6	594	30.2	581	29.7	573	29.3	569	29.2
		839	503	31	490	30.3	483	29.9	477	29.6	473	29.4
		659	401	31.4	388	30.5	385	30.3	379	29.9	375	29.6
		479	302	32.2	290	31.2	287	30.9	283	30.5	279	30.2
		300	205	34.4	194	33	190	32.4	189	32.2	185	31.7
		120	109	42.4	100	39.8	96	28.7	94	38.2	94	38.2
	2	771	483	32.1	460	30.8	451	30.3	447	30.1	443	29.9
		634	394	31.8	381	31	375	30.6	373	30.5	369	30.2
		500	315	32.2	307	31.6	302	31.1	300	31	298	30.8
		365	241	33.5	232	32.4	228	32	228	32	224	31.6
		230	168	36.1	160	34.9	158	34.5	156	34.2	155	33.9
		95	96	45.3	89	42.9	87	42.3	85	41.7	85	41.7
	3	519	349	33.9	330	32.4	324	32	319	31.5	315	31.2
		429	287	33.7	279	33	275	32.7	268	31.9	264	31.6
		340	234	34.5	228	33.9	224	33.4	221	33	213	32.1
		250	183	36.2	179	35.6	175	35.1	170	34.2	166	33.6
		160	134	39.9	130	39.1	126	38.3	123	37.5	119	36.6
		70	83	49.9	81	49.2	79	48.5	75	47.1	72	45.7

Table B.28: Results obtained in the wall friction tests for Sieved API 1.

Repetition	1		2		3		4		5	
sigma wall	tau wall	PHIX	tau wall	PHIX	tau wall	PHIX	tau wall	PHIX	tau wall	PHIX
2018	1157	29.8	1116	28.9	1095	28.5	1076	28.1	1073	28
1519	856	29.4	850	29.2	829	28.6	816	28.3	812	28.1
1019	577	29.5	579	29.6	567	29.1	545	28.1	549	28.3
518	313	31.1	309	30.8	300	30	281	28.4	283	28.6
269	179	33.7	173	32.8	160	30.8	153	29.6	155	29.9
193	136	35.1	130	33.9	121	32	115	30.7	115	30.7
119	96	38.9	92	37.7	83	34.8	79	33.6	81	34.2
69	70	45.3	64	42.8	60	41.1	57	39.3	57	39.3

Table B.29: Results obtained in the wall friction tests for filler 1B.

	Repetition	1		2		3		4		5	
Test	sigma wall	tau wall	PHIX	tau wall	PHIX	tau wall	PHIX	tau wall	PHIX	tau wall	PHIX
1	1013	513	26.9	507	26.6	503	26.4	501	26.3	492	25.9
	832	430	27.3	424	27	418	26.7	417	26.6	409	26.2
	652	341	27.6	337	27.4	334	27.1	332	27	330	26.8
	472	253	28.1	251	28	245	27.4	249	27.8	243	27.2
	292	162	29	158	28.4	156	28.1	160	28.7	156	28.1
	113	68	31	70	31.7	68	31	68	31	68	31
2	763	392	27.2	386	26.9	383	26.6	385	26.8	383	26.6
	626	330	27.8	322	27.2	320	27.1	322	27.2	320	27.1
	492	264	28.2	260	27.9	258	27.7	256	27.5	254	27.4
	357	194	28.5	194	28.5	192	28.3	190	28.1	190	28.1
	222	128	30	126	29.6	124	29.3	123	28.9	123	28.9
	87	58	33.8	58	33.8	58	33.8	57	32.9	57	32.9
3	511	266	27.5	258	26.8	258	26.8	256	26.6	256	26.6
	422	224	28	219	27.4	217	27.2	219	27.4	215	27
	332	177	28.1	175	27.9	175	27.9	175	27.9	173	27.6
	242	134	29	132	28.6	132	28.6	132	28.6	132	28.6
	152	90	30.8	89	30.2	89	30.2	87	29.7	87	29.7
	62	43	34.9	43	34.9	43	34.9	43	34.9	45	36

Table B.30: Results obtained in the wall friction tests for filler 1C.

	Repetition	1		2		3		4		5	
Test	sigma wall	tau wall	PHIX	tau wall	PHIX	tau wall	PHIX	tau wall	PHIX	tau wall	PHIX
1	1013	441	23.5	435	23.3	437	23.3	439	23.4	437	23.3
	832	368	23.8	368	23.8	369	23.9	368	23.8	368	23.8
	652	294	24.3	292	24.1	294	24.3	296	24.4	292	24.1
	473	221	25	217	24.6	219	24.8	219	24.8	219	24.8
	293	141	25.8	141	25.8	141	25.8	141	25.8	143	26.1
	113	62	28.8	64	29.5	64	29.5	62	28.8	62	28.8
2	762	339	24	330	23.4	336	23.8	334	23.6	332	23.5
	626	283	24.3	283	24.3	283	24.3	279	24	279	24
	492	226	24.7	224	24.5	224	24.5	224	24.5	224	24.5
	357	168	25.2	168	25.2	168	25.2	166	24.9	166	24.9
	222	111	26.6	109	26.2	111	26.6	109	26.2	109	26.2
	87	51	30.3	53	31.2	51	30.3	49	29.4	51	30.3
3	512	241	25.2	236	24.7	230	24.2	226	23.8	226	23.8
	422	202	25.6	198	25.1	196	24.9	194	24.7	190	24.3
	332	162	26	160	25.8	156	25.2	156	25.2	155	25
	242	123	26.9	121	26.5	119	26.1	119	26.1	119	26.1
	152	81	28	79	27.5	81	28	79	27.5	79	27.5
	62	41	33.6	38	31.2	40	32.4	40	32.4	40	32.4

Table B.31: Results obtained in the wall friction tests for filler 2C.

Repetition	1		2		3		4		5	
sigma wall	tau wall	PHIX	tau wall	PHIX	tau wall	PHIX	tau wall	PHIX	tau wall	PHIX
2020	805	21.7	803	21.7	809	21.8	814	22	824	22.2
1521	624	22.3	628	22.4	633	22.6	633	22.6	641	22.9
1021	435	23.1	437	23.2	443	23.5	443	23.5	447	23.6
520	228	23.7	234	24.2	234	24.2	236	24.4	239	24.7
271	130	25.7	128	25.3	130	25.7	128	25.3	132	26
195	96	26.2	94	25.8	96	26.2	96	26.2	96	26.2
121	62	27.2	62	27.2	64	27.9	64	27.9	64	27.9
96	51	27.9	53	28.8	51	27.9	53	28.8	53	28.8

Table B.32: Results obtained in the wall friction tests for filler 2B.

Repetition	1		2		3		4		5	
sigma wall	tau wall	PHIX	tau wall	PHIX	tau wall	PHIX	tau wall	PHIX	tau wall	PHIX
2020	794	21.4	780	21.1	773	20.9	778	21.1	780	21.1
1521	616	22.1	605	21.7	599	21.5	609	21.8	609	21.8
1021	430	22.8	426	22.6	426	22.6	430	22.8	432	22.9
520	237	24.5	239	24.7	239	24.7	241	24.9	243	25
271	136	26.6	136	26.6	136	26.6	132	26	136	26.6
195	98	26.7	98	26.7	100	27.1	98	26.7	102	27.5
121	68	29.2	68	29.2	68	29.2	68	29.2	68	29.2
71	43	31.4	46	32.7	45	32.5	45	32.5	44	31.5

Table B.33: Results obtained in the wall friction tests for binder 1B.

Repetition	1		2		3		4		5	
sigma wall	tau wall	PHIX	tau wall	PHIX	tau wall	PHIX	tau wall	PHIX	tau wall	PHIX
2009	1140	29.6	1097	28.6	1080	28.3	1082	28.3	1078	28.2
1509	824	28.6	818	28.5	811	28.2	816	28.4	814	28.4
1010	550	28.6	549	28.5	545	28.4	550	28.6	550	28.6
509	287	29.4	288	29.6	285	29.2	285	29.2	287	29.4
259	155	30.8	156	31.1	156	31.1	149	29.9	155	30.8
184	115	32.1	117	32.5	119	32.9	107	30.3	115	32.1
110	77	35.2	79	35.8	81	36.5	70	32.5	77	35.2
59	51	40.6	53	41.6	55	42.6	45	37.3	51	40.6

Table B.34: Results obtained in the wall friction tests for lubricant 1.

Repetition	1		2		3		4		5	
sigma wall	tau wall	PHIX	tau wall	PHIX	tau wall	PHIX	tau wall	PHIX	tau wall	PHIX
2009	456	12.8	469	13.2	484	13.6	469	13.2	469	13.2
1509	373	13.9	381	14.2	396	14.7	381	14.2	383	14.2
1010	283	15.6	290	16	300	16.5	288	15.9	292	16.1
509	177	19.2	181	19.6	185	20	181	19.6	181	19.6
259	109	22.9	109	22.9	111	23.2	111	23.2	109	22.9
184	89	25.8	85	24.8	87	25.3	85	24.8	85	24.8
110	62	29.6	60	28.8	58	28.1	60	28.8	58	28.1
59	41	34.9	40	33.7	38	32.4	40	33.7	38	32.4

Table B.35: Results obtained in the wall friction tests for API 2.

Repetition	1			2		3		4		5	
Test	sigma wall	tau wall	PHIX	tau wall	PHIX	tau wall	PHIX	tau wall	PHIX	tau wall	PHIX
1	1008	720	35.5	665	33.4	656	33	648	32.7	647	32.7
	827	556	33.9	541	33.2	535	32.9	530	32.6	530	32.6
	647	430	33.6	422	33.1	418	32.9	415	32.6	415	32.6
	468	309	33.5	305	33.1	302	32.8	300	32.7	300	32.7
	288	192	33.7	189	33.2	185	32.7	187	32.9	187	32.9
	108	81	36.8	75	34.9	75	34.9	75	34.9	75	34.9
2	759	518	34.3	498	33.3	494	33.1	488	32.8	490	32.9
	623	418	33.9	405	33.1	403	32.9	400	32.7	400	32.7
	488	324	33.6	319	33.1	315	32.8	313	32.7	311	32.5
	353	234	33.5	228	32.9	226	32.6	224	32.4	224	32.4
	218	145	33.6	151	32.9	139	32.6	138	32.2	138	32.2
	83	60	35.8	58	35	55	33.2	55	33.2	57	34.1
3	508	351	34.6	341	33.9	339	33.8	337	33.6	334	33.3
	418	307	36.3	285	34.3	281	33.9	275	33.4	273	33.2
	328	241	36.3	224	34.4	222	34.1	217	33.5	215	33.2
	238	172	35.8	166	34.9	164	34.6	160	33.9	158	33.6
	148	111	36.9	109	36.4	106	35.5	102	34.5	102	34.5
	48	53	42.1	51	42.2	49	40	47	38.9	45	37.8

Table B.36: Results obtained in the wall friction tests for filler 4.

Repetition	1		2		3		4		5	
sigma wall	tau wall	PHIX	tau wall	PHIX	tau wall	PHIX	tau wall	PHIX	tau wall	PHIX
2017	884	23.7	884	23.7	871	23.4	884	23.7	877	23.5
1517	664	23.6	675	24	667	23.7	684	24.3	673	23.9
1018	449	23.8	454	24.1	454	24.1	464	24.5	462	24.4
517	237	24.7	241	25	239	24.9	247	25.5	241	25
267	134	26.6	134	26.6	130	26	134	26.6	130	26
192	98	27.1	98	27.1	96	26.6	98	27.1	98	27.1
118	66	29.3	66	29.3	64	28.6	64	28.6	64	28.6
68	45	33.8	41	31.6	41	31.6	43	32.7	43	32.7

Table B.37: Results obtained in the wall friction tests for binder 2.

Repetition	1		2		3		4		5	
sigma wall	tau wall	PHIX	tau wall	PHIX	tau wall	PHIX	tau wall	PHIX	tau wall	PHIX
2014	690	18.9	714	19.5	718	19.6	716	19.6	716	19.6
1514	539	19.6	560	20.3	565	20.5	567	20.5	565	20.5
1015	381	20.6	401	21.6	405	21.8	409	22	409	22
514	224	23.6	236	24.6	239	25	243	25.3	245	25.5
264	138	27.5	147	29.1	149	29.4	151	29.7	151	29.7
189	109	30.1	115	31.3	117	31.8	117	31.8	117	31.8
115	81	35.2	81	35.2	81	35.2	81	35.2	81	35.2
65	55	40.2	57	41.2	55	40.2	55	40.2	55	40.2

Table B.38: Results obtained in the wall friction tests for Blend 1.

	Repetition 1		Repetition 2		Repetition 3		Repetition 4		Repetition 5	
sigma wall	tau wall	PHIX	tau wall	PHIX	tau wall	PHIX	tau wall	PHIX	tau wall	PHIX
2020	907	24.2	860	23.1	846	22.7	837	22.5	822	22.1
1520	690	24.4	662	23.5	650	23.2	639	22.8	620	22.2
1020	477	25	464	24.4	456	24.1	452	23.9	439	23.3
520	258	26.4	253	25.9	253	25.9	249	25.6	245	25.2
270	149	28.9	143	28	143	28	141	27.6	139	27.3
195	111	29.8	109	29.3	107	28.9	107	28.9	107	28.9
121	77	32.7	75	32	74	31.4	70	30.1	74	31.4
70	49	34.9	49	34.9	49	34.9	47	33.8	47	33.8

Table B.39: Results obtained in the wall friction tests for Blend 2.

Repetition	1		2		3		4		5	
sigma wall	tau wall	PHIX	tau wall	PHIX	tau wall	PHIX	tau wall	PHIX	tau wall	PHIX
2021	618	17	647	17.7	620	17.1	601	16.6	633	17.4
1521	500	18.2	505	18.4	488	17.8	469	17.1	479	17.5
1022	377	20.3	375	20.2	362	19.5	347	18.8	354	19.1
521	237	24.5	234	24.2	226	23.5	228	23.7	226	23.5
271	139	27.2	141	27.6	139	27.2	138	26.9	138	26.9
196	106	28.4	107	28.8	106	28.4	106	28.4	107	28.8
122	74	31.2	75	31.8	72	30.5	74	31.2	75	31.8
71	49	34.5	49	34.5	47	33.4	50	35.1	49	34.5

Table B.40: Results obtained in the wall friction tests for Blend 3.

Repetition	1		2		3		4		5	
sigma wall	tau wall	PHIX	tau wall	PHIX	tau wall	PHIX	tau wall	PHIX	tau wall	PHIX
2021	895	23.9	867	23.2	858	23	846	22.7	841	22.6
1521	675	23.9	660	23.4	652	23.2	647	23	639	22.8
1022	471	24.8	460	24.2	456	24.1	451	23.8	451	23.8
521	256	26.2	253	25.9	253	25.9	251	25.7	249	25.5
271	145	28.1	141	27.5	141	27.5	141	27.5	141	27.5
196	109	29.2	107	28.7	106	28.3	106	28.3	106	28.3
122	75	31.7	74	31.1	72	30.4	72	30.4	72	30.4
72	51	35.4	49	34.3	47	33.3	47	33.3	47	33.3

Table B.41: Results obtained in the wall friction tests for Blend 4.

Repetition	1		2		3		4		5	
sigma wall	tau wall	PHIX	tau wall	PHIX	tau wall	PHIX	tau wall	PHIX	tau wall	PHIX
2022	956	25.3	937	24.9	926	24.6	918	24.4	916	24.4
1523	728	25.5	716	25.2	711	25	707	24.9	705	24.8
1023	488	25.5	492	25.7	492	25.7	488	25.5	484	25.3
522	262	26.6	262	26.6	258	26.3	258	26.3	258	26.3
272	151	29	145	28	143	27.7	141	27.4	141	27.4
197	111	29.4	109	29	107	28.6	107	28.6	106	28.2
123	77	32.1	75	31.5	75	31.5	74	30.8	72	30.2
73	55	36.9	53	35.9	51	34.9	51	34.9	49	33.9

Table B.42: Results obtained in the wall friction tests for Blend 5.

Repeition	1		2		3		4		5	
sigma wall	tau wall	PHIX	tau wall	PHIX	tau wall	PHIX	tau wall	PHIX	tau wall	PHIX
2017	950	25.2	942	25	937	24.9	929	24.7	927	24.7
1518	728	25.6	722	25.4	724	25.5	718	25.3	716	25.3
1018	498	26	500	26.1	505	26.4	501	26.2	500	26.1
517	266	27.2	266	27.2	268	27.4	264	27	266	27.2
268	143	28.2	143	28.2	143	28.2	141	27.8	141	27.8
192	106	28.8	104	28.3	104	28.3	104	28.3	104	28.3
118	70	30.5	68	29.8	68	29.8	66	29.2	66	29.2
68	43	32.5	43	32.5	41	31.4	41	31.4	41	31.4

C

Addendum to Principal Component Analysis

This appendix contains the original PCA scores and loadings plots obtained with the first model that took into account 21 observations and 30 variables.

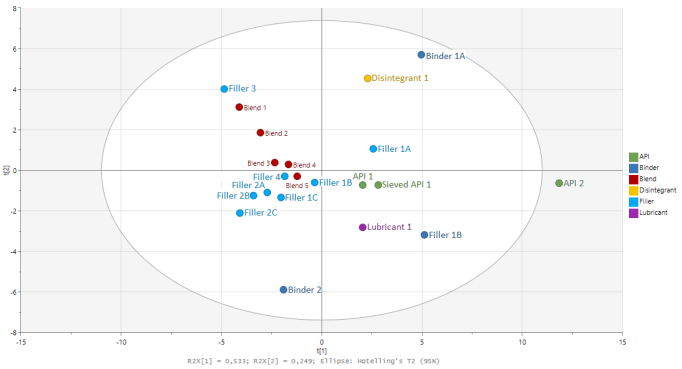

Figure C.1: Scores plot obtained with the original PCA model generated with 21 observations and 30 variables.

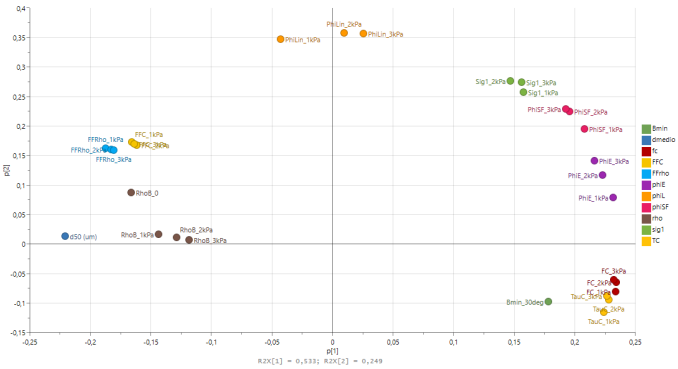

Figure C.2: Loadings plot obtained with the original PCA model generated with 21 observations and 30 variables.

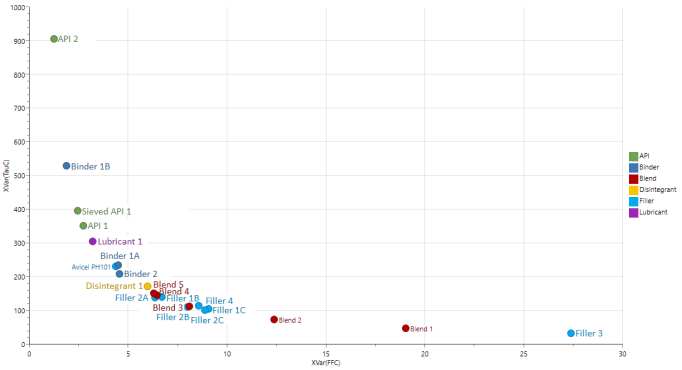

Figure C.3: Correlation between τ_c and FFC.

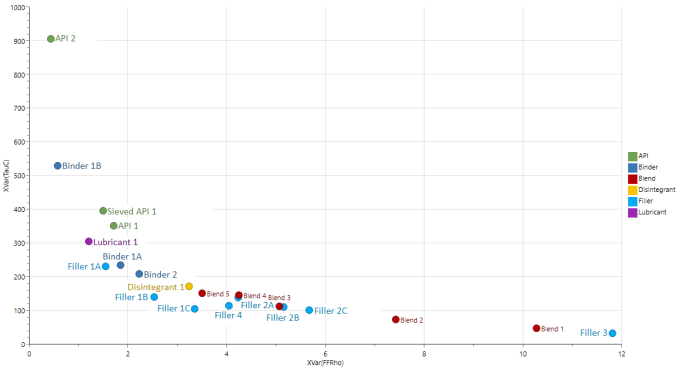

Figure C.4: Correlation between τ_c and FFρ.

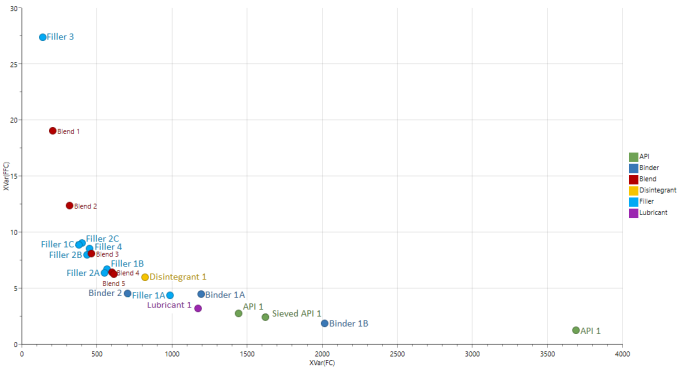

Figure C.5: Correlation between σ_c (FC) and FFC.

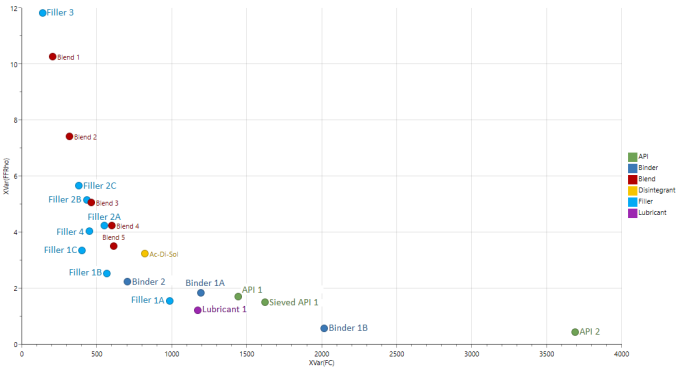

Figure C.6: Correlation between σ_c (FC) and FFρ.

D

Addendum to Warren-Spring equation validation

This chapter contains results of the calculations made by fitting the Warren-Spring equation to the powders described in Chapter 3.

Table D.1: Results obtained by fitting the Warren-Spring equation to the experimental data. Results in Pa, except for FFC, which is dimensionless.

Powder	Filler 1A						Filler 3					
Cell	XS-Mr			XS-SV3			XS-Mr			XS-SV3		
Pre-shear tension (kPa)	1	2	3	1	2	3	1	2	3	1	2	3
RST-XS.s												
tau_c	154.00	220.00	318.00	83.00	130.00	227.00	24.00	28.00	45.00	15.00	27.00	39.00
sigma_c	639.00	960.00	1364.00	333.00	537.00	901.00	102.00	120.00	190.00	58.00	104.00	148.00
sigma_1	2235.00	4534.00	6692.00	1923.00	3960.00	5864.00	1993.00	4104.00	6025.00	1726.00	3584.00	5495.00
FFC	3.50	4.72	4.91	5.78	7.38	6.51	19.46	34.11	31.72	29.71	34.44	37.12
sigma_B	~100	~150	~200	~75	~100	~200	~20	~10	~10	~10	~10	~10
sigma_A	~700	~1400	~2200	~700	~1400	~2400	~700	~1300	~2000	~650	~1400	~2400
Warren-Spring Reasoning 1												
tau_c	148.71	186.35	306.26	71.46	102.87	210.48	19.10	8.78	15.55	0.80	1.55	29.66
T	183.71	164.37	340.42	91.35	102.79	254.92	22.08	9.83	18.25	1.04	2.10	41.85
n	1.00	1.11	1.03	1.00	1.08	1.04	1.00	1.00	1.00	1.00	1.00	1.00
sigma_c	623.39	890.25	1340.75	293.24	462.87	864.29	83.54	39.22	67.33	3.24	6.15	114.73
sigma_1	2231.93	4525.08	6686.60	1922.54	3958.46	5859.05	1995.44	4100.20	6021.35	1723.72	3584.89	5499.68
FFC	3.58	5.08	4.99	6.56	8.55	6.78	23.89	104.53	89.42	532.37	582.91	47.94
sigma_B	115.58	137.30	233.28	56.28	78.07	167.30	14.44	6.54	11.83	0.63	1.25	24.20
M_A	1299.03	2645.42	3926.14	1154.77	2386.86	3563.36	1197.56	2456.84	3645.61	1071.76	2248.20	3469.99
sigma_A	712.07	1465.51	2171.38	681.74	1443.46	2220.33	675.60	1362.00	2104.73	675.72	1454.21	2297.04
Warren-Spring Reasoning 2												
sigma_1	2220.33	4524.86	6686.60	1919.86	3905.88	5806.93	1994.84	4099.95	6014.12	1721.99	3593.25	5399.67
FFC	3.56	5.08	4.99	6.55	8.44	6.72	23.88	104.53	89.31	531.84	582.65	47.94
sigma_A	712.07	1454.87	2170.91	710.07	1595.15	2403.91	689.02	1350.02	2021.47	700.06	1421.95	2300.00
M_A	1290.14	2645.26	3926.14	1152.54	2344.16	3521.19	1197.07	2456.65	3639.67	1070.20	2246.82	3469.98

Table D.2: Results obtained by fitting the Warren-Spring equation to the experimental data (Continuation).Results in Pa, except for FFC, which is dimensionless.

Powder	Binder 1A						API 1					
Cell	XS-Mr			XS-SV3			XS-Mr			XS-SV3		
Pre-shear tension (kPa)	1	2	3	1	2	3	1	2	3	1	2	3
RST-XS.s												
tau_c	159.00	241.00	307.00	69.00	154.00	218.00	215.00	336.00	470.00	185.00	322.00	443.00
sigma_c	801.00	1227.00	1550.00	313.00	655.00	917.00	886.00	1422.00	1942.00	713.00	1275.00	1768.00
sigma_1	2866.00	5717.00	8186.00	2231.00	4388.00	6617.00	2089.00	4253.00	6156.00	1878.00	3855.00	5738.00
FFC	3.58	4.66	5.28	7.13	6.70	7.21	2.36	2.99	3.17	2.63	3.02	3.25
sigma_B	~100	~200	~300	~75	~100	~200	~200	~300	~400	~200	~300	~400
sigma_A	~700	~1500	~2100	~750	~1400	~2400	~800	~1500	~2150	~800	~1550	~2200
Warren-Spring Reasoning 1												
tau_c	151.15	93.52	181.99	25.91	141.64	176.26	50.00	128.24	239.85	45.78	210.66	236.84
T	131.05	34.75	100.74	14.10	154.75	170.51	7.52	34.33	92.26	8.71	108.00	100.09
n	1.04	1.28	1.18	1.20	1.04	1.09	1.68	1.55	1.47	1.65	1.44	1.27
sigma_c	782.74	752.59	1163.62	164.38	623.98	808.66	591.47	1054.10	1567.80	454.84	1139.20	1444.30
sigma_1	2863.87	5702.40	8159.29	2220.88	4385.83	6612.52	2074.34	4235.93	6135.76	1871.77	3844.41	5718.78
FFC	3.66	7.58	8.18	13.51	7.03	8.18	3.51	4.02	3.91	4.12	3.38	3.96
sigma_B	102.79	50.97	132.23	16.20	107.61	132.23	29.68	82.90	169.37	29.12	162.44	173.58
M_A	1595.30	3218.88	4617.80	1308.85	2606.40	3961.01	1187.08	2458.48	3595.30	1102.86	2270.65	3391.04
sigma_A	678.54	1552.74	2169.96	744.96	1483.85	2343.79	722.43	1511.92	2249.46	732.19	1464.40	2206.26
Warren-Spring Reasoning 2												
sigma_1	2853.01	5701.50	8118.38	2198.94	4385.11	6600.35	2073.87	4235.83	6135.49	1870.89	3841.76	5718.65
FFC	3.64	7.58	6.98	13.38	7.03	8.16	3.51	4.02	3.91	4.11	3.37	3.96
sigma_A	724.13	1533.71	2319.40	809.33	1501.98	2425.60	707.56	1503.72	2266.06	750.92	1507.71	2218.56
M_A	1587.85	3218.28	4589.60	1292.46	2605.86	3952.07	1186.68	2458.41	3595.08	1102.08	2268.39	3390.93

Table D.3: Results obtained by fitting the Warren-Spring equation to the experimental data (end).Results in Pa, except for FFC, which is dimensionless.

Powder	Filler 2A					
Cell	XS-Mr			XS-SV3		
Pre-shear tension (kPa)	1	2	3	1	2	3
RST-XS.s						
tau_c	99.00	132.00	182.00	71.00	85.00	139.00
sigma_c	394.00	530.00	727.00	260.00	309.00	505.00
sigma_1	1866.00	3653.00	5418.00	1675.00	3230.00	4981.00
FFC	4.74	6.89	7.45	6.45	10.46	9.86
sigma_B	~75	~125	~200	~75	~100	~150
sigma_A	~700	~1400	~2100	~750	~1500	~2200
Warren-Spring Reasoning 1						
tau_c	65.12	65.75	123.84	59.96	25.08	133.42
T	55.10	48.10	116.57	55.11	16.31	208.82
n	1.17	1.19	1.12	1.12	1.21	1.00
sigma_c	306.71	337.44	564.08	205.81	448.44	387.13
sigma_1	1862.28	3647.44	5408.75	1673.56	3334.50	4980.92
FFC	6.07	10.81	9.59	8.13	7.44	10.23
sigma_B	49.19	47.34	94.16	40.30	99.84	112.44
M_A	1118.58	2223.66	3303.44	1047.74	2105.32	3164.62
sigma_A	692.39	1427.28	2099.18	719.49	1484.35	2186.71
Warren-Spring Reasoning 2						
sigma_1	1862.05	3647.13	5408.74	1672.86	3334.06	4979.22
FFC	6.07	10.81	9.59	8.13	7.43	10.22
sigma_A	701.87	1427.28	2101.14	702.69	1502.17	2143.09
M_A	1118.38	2223.38	3303.44	1047.09	2104.91	3163.06